

## PDF hosted at the Radboud Repository of the Radboud University Nijmegen

The following full text is a publisher's version.

For additional information about this publication click this link.

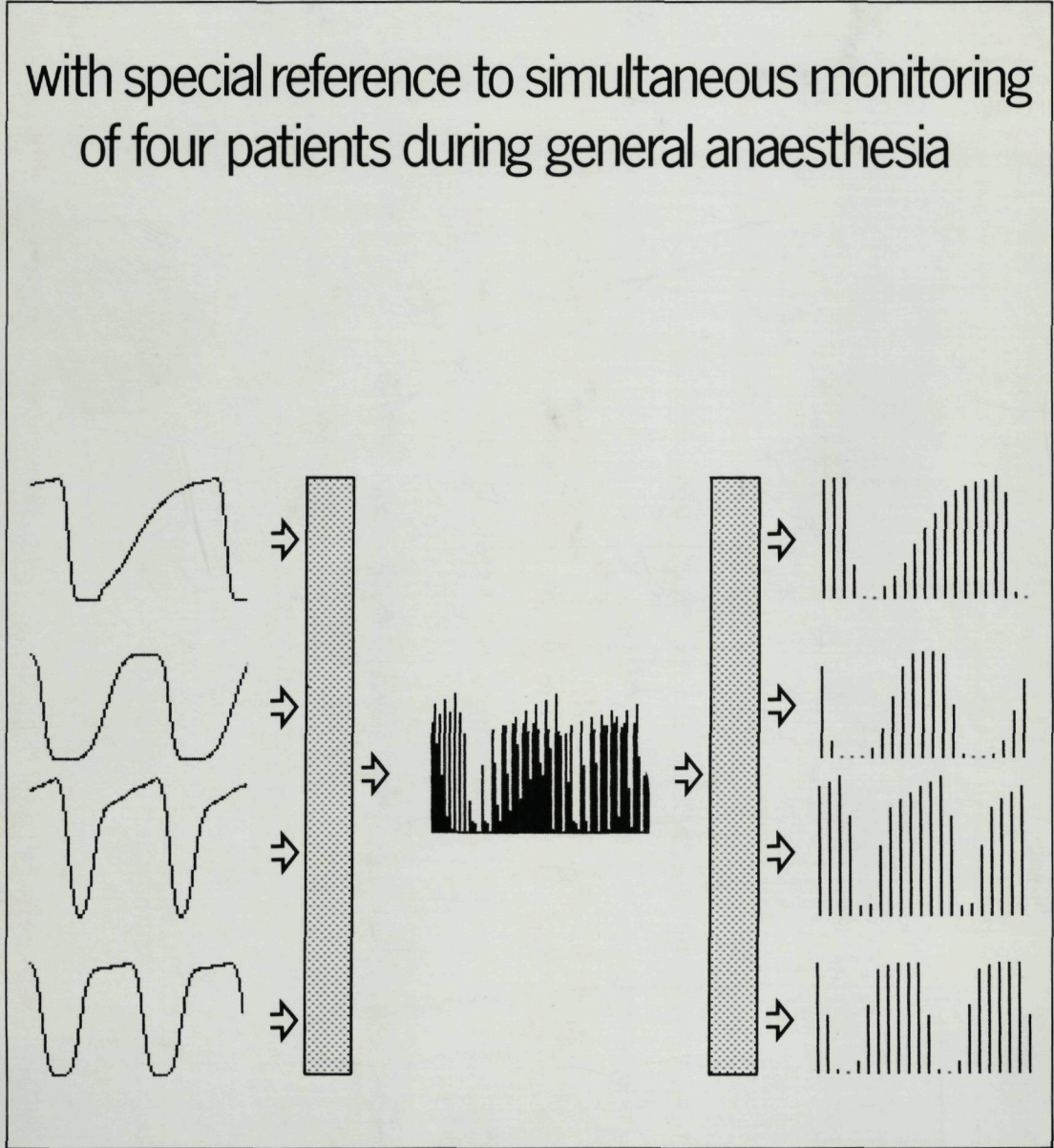
<http://hdl.handle.net/2066/148392>

Please be advised that this information was generated on 2017-12-05 and may be subject to change.

2974

# THE USE OF LONG SAMPLING TUBES IN RESPIRATORY MASS SPECTROMETRY

with special reference to simultaneous monitoring  
of four patients during general anaesthesia



J.G.C. LEROU



**THE USE OF LONG SAMPLING TUBES  
IN RESPIRATORY MASS SPECTROMETRY**

**with special reference to simultaneous monitoring  
of four patients during general anaesthesia**





**THE USE OF LONG SAMPLING TUBES  
IN RESPIRATORY MASS SPECTROMETRY**

**with special reference to simultaneous monitoring  
of four patients during general anaesthesia**

**PROEFSCHRIFT**

**TER VERKRIJGING VAN DE GRAAD VAN  
DOCTOR IN DE GENEESKUNDE AAN DE  
KATHOLIEKE UNIVERSITEIT TE NIJMEGEN,  
OP GEZAG VAN DE RECTOR MAGNIFICUS  
PROF. DR J.H.G.I. GIESBERS,  
VOLGENS BESLUIT VAN HET  
COLLEGE VAN DEKANEN IN HET  
OPENBAAR TE VERDEDIGEN OP  
VRIJDAG 4 MEI 1984  
DES NAMIDDAGS TE 4 UUR**

**DOOR**

**JOZEF GOMMAIRE CAMILLE LEROU  
GEBOREN TE BRUGGE (BELGIË)**

**1984**

**DRUK: STICHTING STUDENTENPERS NIJMEGEN**

**Promotor: Prof. Dr H.H. Beneken Kolmer**  
**Co-referent: Dr J. van Egmond**

*To Mieke, Michiel, and Pieter-Paul,  
who made this book.*



# CONTENTS

Acknowledgements . . . . .	xi
Principal symbols and abbreviations . . . . .	xii
Conventions . . . . .	xiv
Chapter 1: Introduction and outline of the study . . . . .	1
1.1 Introduction . . . . .	1
1.2 Outline of the study . . . . .	5

## PART I

Chapter 2: Physicochemical background of mass spectroscopy . . .	11
2.1 The Rutherford-Bohr atom model . . . . .	12
2.2 Ionization and fragmentation . . . . .	13
2.3 Force and momentum . . . . .	14
2.4 The motion of ions in electric and magnetic fields . . . .	15
2.4.1 A single positive ion moving in an electrostatic field . . . . .	15
2.4.2 A single positive ion moving in a magnetic field . .	19
2.4.3 An ion beam moving in a magnetic field . . . . .	20
2.4.4 Direction focusing . . . . .	23
2.4.5 An ion beam moving in a combination field . . . . .	26
2.4.6 A single positive ion moving in a quadrupole field .	28
Chapter 3: Operation of a mass spectrometer . . . . .	33
3.1 Introduction . . . . .	33
3.2 Vacuum and inlet system . . . . .	34
3.2.1 Requirements . . . . .	34
3.2.2 Description of the gas handling system . . . . .	35
3.2.3 Fulfillment of the requirements . . . . .	41

3.3 Ionization and ion beam formation . . . . .	42
3.3.1 Construction and operation of an electron impact source . . . . .	42
3.3.2 Ion beam source features . . . . .	44
3.4 Ion separation: the quadrupole mass filter . . . . .	46
3.5 Ion detection system . . . . .	50
3.5.1 Measuring system . . . . .	50
3.5.2 Recording modes . . . . .	50
3.6 Mass spectrometer performance . . . . .	51
3.7 History and types of mass spectrometers . . . . .	52
3.7.1 The parabola apparatus . . . . .	52
3.7.2 Aston's mass spectrograph . . . . .	53
3.7.3 Magnetic field mass spectrometers . . . . .	54
3.7.4 Dynamic mass spectrometers . . . . .	55
3.7.5 Double focusing mass spectrometers . . . . .	55
 Chapter 4: Respiratory mass spectrometry and anaesthesia . . . .	 57
4.1 Output signal stability . . . . .	57
4.2 Spectrum overlap . . . . .	60

## PART II

Chapter 5: The equipment used . . . . .	67
5.1 Description of the Centronic 200 MGA . . . . .	67
5.1.1 General . . . . .	67
5.1.2 Inlet and vacuum unit . . . . .	70
5.1.3 Quadrupole head unit . . . . .	71
5.1.4 Control units . . . . .	72
5.2 Description of the rest of the equipment . . . . .	73
5.2.1 The chart recorder . . . . .	73
5.2.2 The XY-recorder . . . . .	73
5.2.3 The Minc computer and the tape recorder . . . . .	73
5.2.4 The bubble flowmeter . . . . .	73
5.2.5 The step change device . . . . .	74
5.3 Calibration procedure . . . . .	76

5.4 Evaluation of the Centronic 200 MGA . . . . .	77
5.4.1 Static accuracy . . . . .	77
5.4.2 Dynamic accuracy . . . . .	82
5.4.3 Performance of the anaesthetics module . . . . .	83
5.4.4 Viscosity changes . . . . .	86
5.4.5 Resolving power . . . . .	86
 Chapter 6: Performance of long sampling tubes: theory . . . . .	 87
6.1 Introduction . . . . .	87
6.2 Process model for tubes with uniform diameter . . . . .	89
6.2.1 Hagen-Poiseuille's law for fluids (liquids or gases)	89
6.2.2 General formulae . . . . .	93
6.2.3 Atmospheric inlet, vacuum outlet conditions . . . . .	98
6.2.4 Calculation of performance parameters . . . . .	100
6.2.5 Discussion . . . . .	101
6.3 Process model for combined tubes . . . . .	108
6.3.1 Calculation of geometry or flow . . . . .	108
6.3.2 General formulae . . . . .	109
6.3.3 Calculation of performance parameters . . . . .	110
6.3.4 Discussion . . . . .	111
 Chapter 7: Performance of long sampling tubes: experiments . . . . .	 119
7.1 Experimental study in the laboratory . . . . .	119
7.1.1 Materials and methods . . . . .	120
7.1.2 Results . . . . .	123
7.1.2.1 Centronic inlet capillary . . . . .	124
7.1.2.2 Polyethylene tubes . . . . .	126
7.1.2.3 Various materials . . . . .	136
7.1.2.4 Nylon . . . . .	139
7.1.3 General discussion . . . . .	150
7.2 Experimental study in the operating theatre . . . . .	152
7.2.1 Long versus short inlet line . . . . .	152
7.2.2 Clinical use of long sampling tubes . . . . .	153



Chapter 8: Simultaneous monitoring of four patients . . . . .	159
8.1 Sampling theory . . . . .	159
8.2 System design . . . . .	163
8.2.1 The pneumatic sampling system . . . . .	163
8.2.2 The valve control unit . . . . .	163
8.2.3 Sample and hold circuits . . . . .	163
8.3 System evaluation . . . . .	164
8.3.1 Respiratory input signal . . . . .	164
8.3.2 Separate vacuum source . . . . .	165
8.3.3 Switching artifact . . . . .	166
8.3.4 Sampling rate . . . . .	168
8.4 Discussion . . . . .	170
8.5 Clinical applications . . . . .	174
8.6 Conclusions . . . . .	176
 Chapter 9: Future development: multi-part inlet line . . . . .	 177
9.1 Optimum radii for a tube with two parts . . . . .	177
9.2 Optimum radii for a tube with more than two parts . . . . .	181
 Summary . . . . .	 187
 Samenvatting . . . . .	 191
 References . . . . .	 195
 Curriculum vitae . . . . .	 201

This thesis was prepared in the Lung Function Laboratory (head: Prof. Dr H.H. Beneken Kolmer) of the Institute for Anaesthesiology (head: Prof. Dr J.F. Crul) of the Catholic University of Nijmegen, the Netherlands.

## ACKNOWLEDGEMENTS

I thank all people who helped me in the course of this study, but I wish to mention some of them by name.

I am indebted to my colleagues for allowing me the opportunity to do this work, to Dr J. Ponte who triggered the development of the sampling system for simultaneous monitoring, and to Prof. Dr Ir C.A. Cramers and Dr Ir P.A. Leclercq (Eindhoven University of Technology) for their invaluable contribution in developing the process model presented. The hospitality and cooperation of the Staff of the Department of Obstetrics and Gynaecology, and the nurses of the operating theatres of this department are gratefully acknowledged.

This study would have been impossible without the skilfull contributions of Messrs H. van der Vegt (electronics) and G. Toenders (mechanical constructions). Technical help was also provided by the other members of the Technical Department (head: W. Theunissen, ing.): Messrs W. van de Wijdeven and W. Kleinhans.

Mr C. Nicolassen, assisted by Mr A. van Uden, prepared the drawings. Glossy prints were made by the Department of Photography (head: Mr A. Reynen). I praise their work. I also thank the staff of the Medical Library (head: Mr E. de Graaff) for assembling the literature.

My gratitude goes also to Miss M. van Duren for entering most of the manuscript text into the document files for the SCRIPT program, and to Mr F. van der Heijden who solved special problems with this document-composition program. His help allowed me to prepare a "camera-ready copy" from which the manuscript could be printed directly.

Finally, I wish to mention the help of Miss I. Baltussen, Mr T. Janssen, Mrs C. Kroon-Leeflang, Miss H.J.M. van der Pluijm, Miss B. Ringnalda, Mrs C. Robertson-Vermeulen, Miss E. Scheltinga, Mr J. van de Weyer, and Mr C. van Zantvoort.

# PRINCIPAL SYMBOLS AND ABBREVIATIONS

Only symbols used several times are listed.

Symbols	Dimensions (in <i>lmti</i> )	Names
<i>a</i>	<i>l</i>	radial coordinate
<i>a</i> , <i>a<sub>x</sub></i> , <i>a<sub>y</sub></i> , <i>a<sub>z</sub></i>	<i>lt<sup>-2</sup></i>	acceleration, acceleration in x, y, z direction
ac		alternating current
A		parameter depending on U in Mathieu equation
B	<i>mt<sup>-2</sup>i<sup>-1</sup></i>	magnetic flux density (magnetic induction)
D	<i>l<sup>2</sup>t<sup>-1</sup></i>	diffusion coefficient
<i>D<sub>B</sub></i> , <i>D<sub>i</sub></i> , <i>D<sub>o</sub></i> , $\bar{D}$	<i>l<sup>2</sup>t<sup>-1</sup></i>	diffusion coefficient (at atmospheric, inlet, outlet, average pressure)
dc		direct current
E	<i>lmt<sup>-3</sup>i<sup>-1</sup></i>	electric field strength
<i>E<sub>x</sub></i> , <i>E<sub>y</sub></i> , <i>E<sub>z</sub></i>	<i>lmt<sup>-3</sup>i<sup>-1</sup></i>	electric field strength (x, y, z direction)
ENF		enflurane
<i>f</i>		Gidding's correction factor
<i>f<sub>co</sub></i>	<i>t<sup>-1</sup></i>	cut off frequency
<i>f<sub>s</sub></i>	<i>t<sup>-1</sup></i>	sampling rate
<i>F<sub>A</sub></i> , <i>F<sub>E'</sub></i> , <i>F<sub>I</sub></i>		fractional gas concentration (alveolar, end-expiratory, inspiratory)
<i>F<sub>B</sub></i>	<i>l<sup>3</sup>t<sup>-1</sup></i>	sample flow at atmospheric pressure
H	<i>l</i>	relative band broadening
HAL		halothane
I, <i>I<sub>e</sub></i> , <i>I<sub>i</sub></i>	<i>l</i>	current, free electron current, ion current
i.d.	<i>l</i>	internal diameter
ISO		isoflurane
l, <i>ℓ</i>	<i>l</i>	length of first part of combined tube
L	<i>l</i>	total tube length

m	<i>m</i>	mass
p	$lmt^{-1}$	momentum
$P_B$	$l^{-1}mt^{-2}$	atmospheric pressure
$P_{H_2O}$	$l^{-1}mt^{-2}$	water vapour pressure
$P_i, P_o, \bar{P}$	$l^{-1}mt^{-2}$	pressure (inlet, outlet, average)
$P_1, P_\ell$	$l^{-1}mt^{-2}$	pressure at junction of combined tube
$P_x$	$l^{-1}mt^{-2}$	pressure at distance x
P		$P_i/P_o$
P'		$P_1/P_o$ or $P_\ell/P_o$
q	<i>ti</i>	electric charge
Q		parameter depending on $V_{ac}$ in Mathieu equation
r	<i>l</i>	radius
$r_0$	<i>l</i>	radius of quadrupole field
$r_1, r_2$	<i>l</i>	radii of first and second part of combined tube
$r_m$	<i>l</i>	radius of ion trajectory in magnetic field
R		resolving power
s	<i>l</i>	distance
t	<i>t</i>	time
$t_M$	<i>t</i>	residence time
$t_r$	<i>t</i>	10% to 90% response time
U	$l^2mt^{-3}i^{-1}$	voltage (dc)
$\Delta U$	$l^2mt^{-3}i^{-1}$	accelerating voltage
v	$lt^{-1}$	velocity
$\bar{v}$	$lt^{-1}$	mean velocity
$\bar{v}_1, \bar{v}_o$	$lt^{-1}$	mean linear gas velocity (inlet, outlet)
$\bar{v}_x, \bar{v}_x'$	$lt^{-1}$	mean linear gas velocity at distance x, x'
$\bar{v}$	$lt^{-1}$	average linear gas velocity
$\bar{v}_1, \bar{v}_2$	$lt^{-1}$	average linear gas velocity in first and second part of a combined tube
$V_{ac}$	$l^2mt^{-3}i^{-1}$	peak amplitude of ac voltage
x, x', y, z	<i>l</i>	space coordinates
x'', y'', z''	$lt^{-2}$	second time derivatives of x, y, z
y	<i>l</i>	length of second part of combined tube

$z$	$l$	length
$Z$		ratio of inlet and outlet pressure of whole tube
$Z_i$		Z of tube part i
$\eta$	$l^{-1}mt^{-1}$	dynamic viscosity coefficient
$\nu$	$t^{-1}$	frequency
$\sigma$	$t$	apparent or measured band broadening
$\Phi$	$l^2mt^{-3}i^{-1}$	potential
$\Phi_0$	$l^2mt^{-3}i^{-1}$	potential applied to a rod
$\omega$	$t^{-1}$	pulsation ( $2\pi\nu$ )

## CONVENTIONS

1. The square root of a mathematical expression will be denoted by the sign  $\sqrt{\quad}$  followed by the expression in brackets.

Example:  $\sqrt{(2m\Delta U)}$

2. When "gases" are mentioned in the text, "gases and vapours" are meant. For a definition of the terms "gas" and "vapour" the reader is referred to Radford (Radford, 1964).

# CHAPTER 1

## INTRODUCTION AND OUTLINE OF THE STUDY

### 1.1 INTRODUCTION

Analysis of respiratory gases during anaesthesia can serve one or more purposes. They are:

1. to control the fractional gas concentrations in the respiratory air of the patient,
2. to assess the metabolic, cardiovascular, and respiratory function of the patient,
3. to evaluate the relation of the end-tidal concentration of anaesthetic gases to the "depth of anaesthesia".

These purposes can be ideally achieved if the following requirements are met:

1. there should be a simultaneous and continuous analysis of  $O_2$ ,  $CO_2$ ,  $N_2$ , anaesthetics in use (e.g.  $N_2O$ , volatiles), and tracer gases (e.g. Ar),
2. the method(s) used should be:
  - a. fast: the period elapsed between sampling and result should be as short as possible,
  - b. accurate: statically and dynamically (the dynamic accuracy should allow distortion-free recording of a single breath curve),
  - c. simple: in calibration and use,
  - d. inexpensive: to purchase and to maintain,
3. the result should be automatically recorded, i.e. an electrical output signal is required.

The methods used for the analysis of gases are commonly divided into either chemical or physical, although this distinction is sometimes difficult to make (Mapleson, 1962; Sykes, Vickers and Hull, 1981). The methods based on chemical processes do not generally allow rapid, continuous analysis, whereas physical methods do. For the latter, the underlying principle used during the measurement is a more or less specific physical property of the gas being analysed. These physical properties are listed in table 1.1 (Lilly, 1950; Cotes, 1979).

Table 1.1: Physical properties used in gas analysis

---

1. Absorption of radiation	6. Flame conductivity
2. Current or voltage	7. Viscosity
- polarographic potential	8. Mass
- fuel cell	9. Paramagnetism
- pH sensitive electrode	10. Photo-ionization
- collector electrodes	11. Refractive index
3. Density	12. Solubility
4. Differential adsorption	13. Sound transmission
(gas chromatography)	14. Thermal conductivity
5. Emission of radiation	

---

Listed properties are in most cases not unique for an individual gas, and the methods involved are called non-specific. Gas concentration measurements based upon a non-specific method will possibly be disturbed by interference of other gases in the mixture. The methods based on a (virtually) unique physical attribute of a gas are termed specific.

The various applications of the physical principles, which allow continuous recording of the entire contour of a gas concentration during a respiratory cycle (i.e. the "respired waveform"), are shown in table 1.2. Only O<sub>2</sub>, CO<sub>2</sub>, N<sub>2</sub>, N<sub>2</sub>O, Ar, and halothane, which is taken as an example for the volatile anaesthetics, are considered. Table 1.3 shows that the use of N<sub>2</sub>O and halothane enlarges the problem of interfering gases.

Table 1.2: Breath-by-breath gas analysis

*Physical principles allowing to record an entire respired waveform.*

Principle	Gases	References
I.R. absorption	CO <sub>2</sub>	Smalhout, 1967 Hill et al., 1968
U.V. absorption	halothane	Tatnall et al., 1978
Polarography	O <sub>2</sub>	Kreuzer et al., 1960 Beneken Kolmer, 1967
Fuel cell	O <sub>2</sub>	Sodal et al., 1968
Collector electrode	O <sub>2</sub> , CO <sub>2</sub>	Nitta et al., 1969
U.V. emission	N <sub>2</sub>	Daniels et al., 1975
Mass-charge ratio	all	Fowler, 1969
Paramagnetism	O <sub>2</sub>	Pauling et al., 1946 Conway et al., 1973
Sound transmission	CO <sub>2</sub>	Stott, 1957
Thermal conductivity	CO <sub>2</sub>	Serra et al., 1963 Jessop, 1966
	O <sub>2</sub>	Serra et al., 1963

For the simultaneous analysis of the gases given above, a range of analysers would be necessary with the following disadvantages: different response times, phase shift between the results, large total sample flow, and bulky equipment. However, there is one instrument that allows simultaneous analysis of a number of different gases. This instrument is called a "mass spectrometer", or more specifically "respiratory mass spectrometer" to stress its use in the analysis of respiratory gas mixtures. It allows simultaneous, continuous, fast, accurate, and automatically recorded analysis. However, it is expensive and not very simple to use.

A solution to the problem of cost is to share one respiratory mass spectrometer between several patients. This idea was worked out for intensive care units (Potter, 1976; Riker and Habermann, 1976; Crawford McAslan, 1976; Gothard et al., 1980) and operating theatres (Ozanne et al., 1981; Gillbe, Heneghan and Branthwaite,



Table 1.3: Breath-by-breath gas analysis

*Gases interfering with the analysis of the gases listed in table 1.2. Remarks are given between brackets.*

Principle	Interferences/remarks	References
I.R. absorption	Ar, O <sub>2</sub> , N <sub>2</sub>	Ammann et al., 1968
	halothane	Hill et al., 1967
	N <sub>2</sub> O	Burton, 1969
	H <sub>2</sub> O: negligible	Cooper, 1957
U.V. absorption	none	Tatnall et al., 1978
Polarography	halothane	Severinghaus et al., 1971
	N <sub>2</sub> O	Albery et al., 1978
Fuel cell	halothane	Elliott et al., 1966
	(explosion hazard)	Wilson et al., 1972
Collector electrode	H <sub>2</sub> O, N <sub>2</sub>	
	anaesthetic vapours	Bushmann, 1975
U.V. emission	CO <sub>2</sub> , H <sub>2</sub> O	Cotes, 1979
Mass-charge ratio	this study	
Paramagnetism	(not usable	
	with IPPV)	Conway et al., 1973
Sound transmission	anaesthetic gases	Stott, 1957
Thermal conductivity	N <sub>2</sub> O, Ar	Sykes et al., 1981

1981; Spence and Davis, 1981). In this set-up, the mass spectrometer is located near the operation theatres, while long sampling tubes suck off the sample gas from the anaesthetic circuit of each patient being monitored. The length of the tubes depends on the distance between the mass spectrometer and the operating theatres; distances of 60 m have been reported (Link and Eyrich, 1982). A valve box sequentially directs the sample flow from the operating theatres to the mass spectrometer (see fig.1.1).

This thesis deals with problems which stem from the use of a single mass spectrometer shared by several patients.

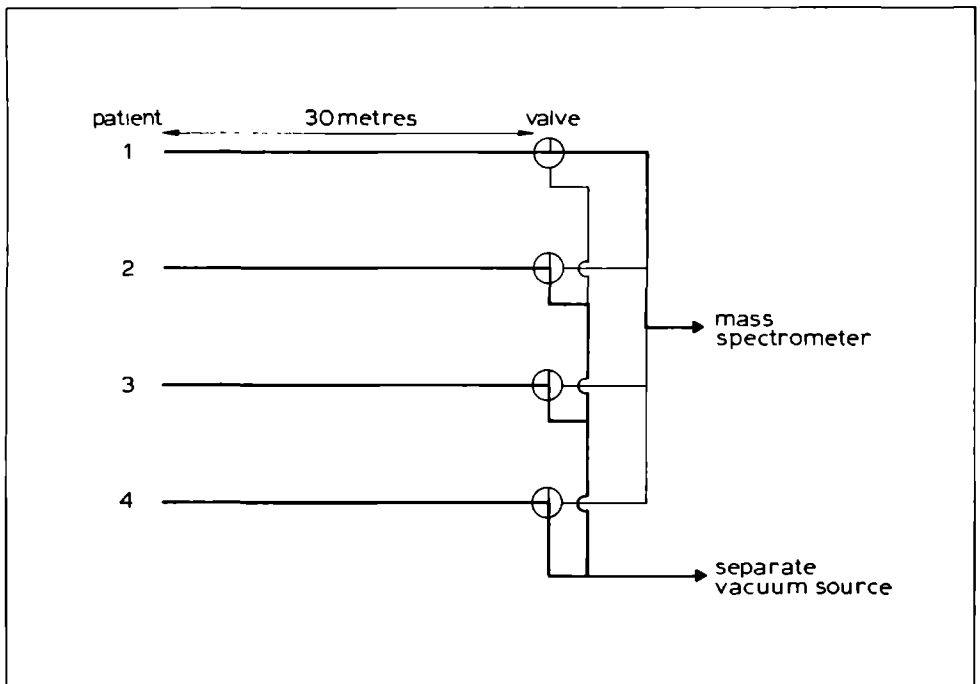


*Fig.1.1: Scheme of a sampling system for four patients sharing one mass spectrometer. On the diagram line no.1 is sampled, while a separate vacuum source is drawing off gas from the other lines. Thus current information is fed to the mass spectrometer when the system switches from line no.1 to line no.2.*

## 1.2 OUTLINE OF THE STUDY

The remote operation of a respiratory mass spectrometer, which sequentially analyses the respiratory gases of several patients, has several implications. Firstly, the sample gas needs time to travel down the long tube (= transit time, or delay time, or lag time), i.e. the method becomes less fast. Secondly, the long tubes distort the respired waveforms, i.e. the method becomes less accurate. Thirdly, a dead period is introduced between the successive sampling periods on each line. So the anaesthetist sharing the monitoring facility has no information about his patient during considerable periods of time.

None of the authors referred above discussed in detail the relationships between sample flow, transit time, and distortion of respired waveforms. They did not recognize the necessity to search for a "compromise" between these three factors, which are determined by the geometry of long sampling tubes, whereas distortion, in addition, is influenced by the tube material. Only one report treated the problem of the dead period caused by the combination of a centrally located mass spectrometer and a data acquisition system (Ozanne et al., 1981).

Therefore this study has two purposes. They are:

1. to select a long sampling tube offering a "compromise" between distortion of respired waveforms, sample flow, and transit time,
2. to search for a sampling system which provides simultaneous monitoring of four patients with one mass spectrometer.

In 1965, Fowler, who introduced the mass spectrometer into clinical practice, wrote about the new generation of mass spectrometers which still had to be built:

"At the same time, like all mass spectrometers, these are complex physical instruments requiring of the user knowledgeable operation and maintenance in every day use, and a full understanding of the design principles if they are to be successfully applied to new problems. They are not 'black boxes' for casual use by housemen..." (Fowler, 1965).

Although manufacturers have achieved much in the meantime to facilitate the clinical use of mass spectrometers, it was felt at the start of the present study that Fowler's words had to be taken seriously.

Therefore the two purposes of this study are worked out in six main objectives. They are:

1. to review the principles of a respiratory mass spectrometer, and the problems arising from its use during general anaesthesia (chapters 2, 3, and 4),

2. to evaluate the performance of the Centronic 200 MGA mass spectrometer which incorporates facilities to solve some of these problems (chapter 5),
3. to work out a mathematical model describing the relationships between sample flow, transit time, and distortion of respiratory signals on one hand, and the geometry of ideal long sampling tubes on the other (chapter 6),
4. to select a long sampling tube which by experimental observation not only approximates the theoretically predicted distortion (for a given geometry), but also can be used easily in clinical practice (chapter 7),
5. to design and test a sampling system which shows the principles and possibilities of simultaneous monitoring of four patients (chapter 8),
6. to search for future developments which could improve the obtained results (chapter 9).

Chapters 2 to 4 are united in Part I, and chapters 5 to 9 in Part II.



---

## PART I

---

### Chapter 2: Physicochemical background of mass spectroscopy

- 2.1 The Rutherford-Bohr atom model
- 2.2 Ionization and fragmentation
- 2.3 Force and momentum
- 2.4 The motion of ions in electric and magnetic fields

### Chapter 3: Operation of a mass spectrometer

- 3.1 Introduction
- 3.2 Vacuum and inlet system
- 3.3 Ionization and ion beam formation
- 3.4 Ion separation: the quadrupole mass filter
- 3.5 Ion detection system
- 3.6 Mass spectrometer performance
- 3.7 History and types of mass spectrometers

### Chapter 4: Respiratory mass spectrometry and anaesthesia

- 4.1 Output signal stability
- 4.2 Spectrum overlap



## CHAPTER 2

### PHYSICOCHEMICAL BACKGROUND OF MASS SPECTROSCOPY

A *mass spectroscope* is an instrument which separates charged particles according to their mass-charge ratio. Mass spectroscopes can deal with gaseous, liquid, or solid samples. In this study only gaseous samples will be considered.

Mass spectroscopy is based on physicochemical principles. For the sake of simplicity, this chapter will first describe this physicochemical background, although much about it, e.g. atomic structure and the existence of isotopes, was discovered thanks to the progress in the field of mass spectroscopy.

It is useful to define here the four components of a mass spectroscope. They are:

1. a sample system,
2. an ion source,
3. an ion separator system,
4. an ion detector system.

These four components will be treated in detail in chapter 3.

Mass spectroscopes can be classified either as mass spectrographs or as mass spectrometers, depending on the type of ion detector system in use:

- *mass spectrographs* have a photographic plate as detector,
- *mass spectrometers* have an electrical detector system.

Therefore only the mass spectrometer produces an electrical output signal. This classification will be illustrated in section 3.7. In the present study the mass spectrometer will be mainly dealt with, because this type of mass spectroscopy is used in the continuous analysis of anaesthetic gas mixtures.



## 2.1 THE RUTHERFORD-BOHR ATOM MODEL

For the purpose of this study, atomic structure can be satisfactorily described by the classical Rutherford-Bohr atom model. According to it, an atom is pictured as a miniature solar system with a positively charged nucleus surrounded by a cloud of negatively charged electrons orbiting the nucleus. These electrons can link atoms to form molecules. The nucleus itself contains positively charged protons and electrically neutral neutrons. The atom as a whole is electrically neutral; its structure is guaranteed by a balance of nuclear forces.

All these particles, i.e. the protons, neutrons, and electrons have a mass and a charge listed in table 2.1. Not only SI-units for mass and charge, i.e. kg and C(oulomb) are shown, but also physical atomic units, i.e. atomic mass units (u), and electron units (e). These units have the following conversions:

$$1 \text{ u} = 1/12 \text{ mass of a neutral } ^{12}\text{C-atom} = 1.6605655 \times 10^{-27} \text{ kg,}$$

$$1 \text{ e} = 0.16021892 \times 10^{-18} \text{ C(oulomb).}$$

Table 2.1: Mass and charge of a proton, neutron, and electron  
*The SI units (kg and C), and atomic units (u and e) are shown  
 (From: Physical Letters, 111B, April 1982)*

	mass		charge	
	kg	u	C	e
proton	$1.672648 \times 10^{-27}$	1.007276	$0.16021892 \times 10^{-18}$	+1
neutron	$1.674954 \times 10^{-27}$	1.008665	0	0
electron	$0.91095 \times 10^{-30}$	$548.6 \times 10^{-6}$	$-0.16021892 \times 10^{-18}$	-1

Table 2.1 shows that protons and neutrons have about the same mass, whereas electrons have a negligible mass. Thus atomic mass depends mainly on the total number of protons and neutrons. For a given

atom, say carbon, the number of protons equals the number of electrons: carbon contains 6 protons and 6 electrons. However, the number of neutrons in an atom may vary: these atomic variants are called "isotopes". Carbon has two naturally occurring stable isotopes:  $^{12}\text{C}$  and  $^{13}\text{C}$ , containing 6 and 7 neutrons, respectively. Isotopic atomic masses, expressed in u, are extremely close to whole numbers. The nearest whole number to an isotopic atomic mass is called the *mass number* of an isotope (this number equals the total number of protons and neutrons). For example, the  $^{13}\text{C}$  isotope of carbon with an atomic mass = 13.00335 u has a mass number = 13. An average atomic "weight" of an element can be calculated from the exact masses of its isotopes and their relative abundances: "carbon" has an atomic weight of 12.01115 u (Handbook of Chemistry and Physics, 1970).

## 2.2 IONIZATION AND FRAGMENTATION

Highly energized particles can be used to damage the described atomic structure. For instance, bombarding atoms with free electrons removes electrons from their orbits. An electron being removed, the atom has a surplus positive charge and is called a positive *ion*. The process of creating an ion is called *ionization*, and the minimum energy cost for it is called "ionization potential". With this "potential", the accelerating potential for the bombarding electrons is meant. Ionization potential may be a wrong term in fact, because it stands for an amount of energy; "ionization energy" may be a better term. More than one orbiting electron can be removed at the same time, provided enough energy is delivered to the atom.

Just as with atoms, molecules can be ionized, but when sufficient energy is supplied, molecules may undergo fragmentation into charged and neutral particles. Polyatomic molecules, e.g. volatile anaesthetics, undergo decomposition in many fragments.

Using SI units, the mass-charge ratio of an ion is expressed in kg per C(oulomb). However, in mass spectroscopy mass-charge ratios are usually given in atomic units. The mass  $m$  is given as  $n$  atomic mass units (u), and the charge  $q$  as  $n'$  electron units (e). So the

mass-charge ratio  $m/q$ , expressed in  $u/e$ , equals  $n/n'$ , but usage has led to dropping the expression  $u/e$ . Under certain conditions, the ratio may be rounded off to the nearest whole number.

EXAMPLE: a  $^{12}C^{16}O_2^{++}$  ion has a mass of 43.98982 u and a charge of +2e; its mass-charge ratio is  $21.99491 \approx 22$  (u/e).

This  $m/q$  ratio has to be converted into SI units, if the  $m/q$  ratio has to be introduced into equations containing coherent SI units. Using the above mentioned proportions between u and kg on one hand, and between e and C on the other, the following conversion factor is found:  $1 u/e = 10.364353 \times 10^{-9} \text{ kg.C}^{-1}$ .

EXAMPLE: the  $m/q$  ratio of the same ion is  $227.96301 \times 10^{-9} \text{ kg.C}^{-1}$

In a mass spectroscope the ionization process is realized in the *ion source*. Further manipulation of these ions is possible by the action of electric and/or magnetic fields in the *ion separator system*, where the charged particles are separated according to their  $m/q$  ratio. The influence of these fields upon moving ions is treated in section 2.4. Separated ions are detected by the mass spectrometer as "mass peaks", or as "mass lines" by the mass spectrograph. The "collection" of these peaks or lines is called the "mass spectrum" of a substance (for further discussion of these terms see section 3.5).

## 2.3 FORCE AND MOMENTUM

The relationship between a force  $F$  applied to an object with mass  $m$ , and the resulting acceleration  $a$  is given by the second law of Newton. The momentum  $p$  of an object is the product of its mass and its velocity  $v$ . These relationships may be summarized as follows:

$$F = ma = m \frac{dv}{dt} = \frac{d(mv)}{dt} = \frac{dp}{dt} \quad (2.1)$$

## 2.4 THE MOTION OF IONS IN ELECTRIC AND MAGNETIC FIELDS

The motion of a single ion through electric and magnetic fields can be described easily, but in mass spectroscopy more particles have to be considered at the same time. In fact, the ions produced in the ion source are accelerated and focused into an ion beam, which is further analysed. Two factors are important for the behaviour of the beam ions in the electric and magnetic fields:

- The kinetic energy acquired by the ions in the ion source. Ideally all ions should acquire the same energy, i.e. the ion beam should be "mono-energetic".
- The thickness and angular divergence of the ion beam. Ideally the beam should be infinitesimally narrow and have no divergence.

In practice the ions of an ion beam show a certain energy spread, and the beam not only has a certain thickness but also is slightly divergent.

Instead of a very general treatment, some special cases of the motion of ions in electric and magnetic fields will be discussed. These cases are readily applicable to mass spectroscopy.

### 2.4.1 A single positive ion moving in an electrostatic field

#### 2.4.1.1 Field parallel to the direction of motion

A uniform electrostatic field is situated between two plates, which are at distance  $s$  from each other, and are at the potentials  $U_1$  and  $U_2$ , respectively, with  $U_1 > U_2$  and  $\Delta U = U_1 - U_2$ . The field strength is given as:

$$E = \frac{U_1 - U_2}{s} = \frac{\Delta U}{s} \quad (2.2)$$

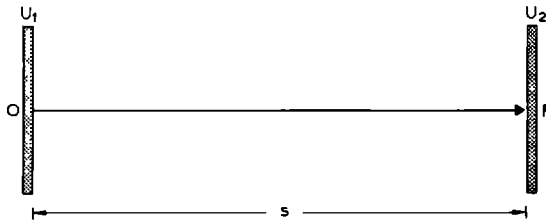


Fig.2.1: Motion of a positive ion in an electrostatic field parallel to the direction of motion. The field is generated between two plates with potential  $U_1$  and  $U_2$ .

In an electric field, an ion with mass  $m$  and charge  $q$  is subject to a force with a magnitude  $qE$  or:

$$qE = ma \tag{2.3}$$

A positive ion with mass  $m$  and charge  $q$  enters the field at O, or is created at O, where the ion is supposed to have no kinetic energy of its own. At O, the ion has the potential energy  $qU_1$ . If it moves under the influence of the electrostatic field to P (see fig.2.1), its potential energy decreases to  $qU_2$ . The decrease in potential energy is turned totally into kinetic energy if no energy is lost during motion, e.g. by collisions with other particles. Thus the following relation is obtained:

$$q(U_1 - U_2) = \frac{m(v_2^2 - v_1^2)}{2} = q\Delta U \tag{2.4}$$

where  $v_1$  and  $v_2$  are the velocities of the ion at O and P, respectively. Since it was supposed that the ion had no kinetic energy at O, eq.2.4 reduces to :

$$q\Delta U = \frac{mv_2^2}{2} \tag{2.5}$$

indicating that lighter ions will move faster at the field exit than heavier ions, and that the kinetic energy of ions emerging from the field depends on the accelerating voltage  $\Delta U$ . Accordingly, such an electrostatic field can be called "electrostatic accelerator".

EXAMPLE: Suppose a  $N_2O^+$  ion with a mass-charge ratio rounded off to 44 (u/e) is created at O, where  $U_1 = 3000$  Volt. If  $U_2 = 0$  V, and  $s = 0.065$  m, then the velocity of the ion at the exit of the electrostatic accelerator is given as (eq.2.5):

$$v_2 = \sqrt{ 2 \frac{3000}{44} \times \frac{1}{10.364353 \times 10^{-9}} } = 114.70390 \times 10^3 \text{ m.s}^{-1}$$

### 2.4.1.2 Field perpendicular to the direction of motion

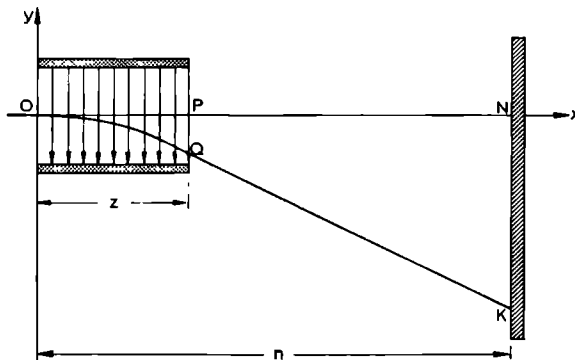


Fig.2.2: Motion of an ion in an electrostatic field perpendicular to the direction of motion. An ion with mass  $m$  and charge  $q$  enters the field at O, leaves it at Q and hits a photographic plate at K.

The same field as above is supposed to have a length  $z$ , and to be perpendicular to the direction of motion of the ion (see fig.2.2). The ion enters the field in O, which is chosen as the origin of the x-y axes. The ion is moving with a constant velocity  $v$  along the x-axis, i.e. there is no acceleration in the x-direction.

The trajectory of the ion through the field can be calculated as follows. The equations of motion are:

$$x = vt \tag{2.6}$$

$$y = \frac{a_y t^2}{2} \tag{2.7}$$

where  $a_y$  is the acceleration in the  $y$ - direction. Combining eqs.2.3, 2.6, 2.7, and eliminating  $t$  yields:

$$y = \frac{q E x^2}{m 2 v^2} \tag{2.8}$$

Eq.2.8 defines the trajectory of the ion through the field as a parabolic path, with the top of the parabola in 0. After emerging from the field, the trajectory of the ion becomes a straight line tangent to the parabola at the exit point Q, since the electric field is no longer acting on the ion.

Suppose that, after emerging from the field and travelling along a straight line, the ion hits at point K a photographic plate placed normal to the direction of motion at point N, which has the coordinates  $n,0$ . The  $x$ -coordinate of K equals  $n$  and the  $y$ -coordinate is given as:

$$NK = -x \frac{q E}{m v^2} x \frac{z(2n-z)}{2} \tag{2.9}$$

indicating that an ion with greater kinetic energy will be less deflected than an ion with smaller kinetic energy. In other words, this electrostatic field selects ions according to their energy or acts as an "energy selector".

## 2.4.2 A single positive ion moving in a magnetic field

Suppose a positive ion enters at O (see fig.2.3) a uniform magnetic field, which has sharp boundaries and is perpendicular to the plane of drawing. Point O is the origin of the x-y axes.

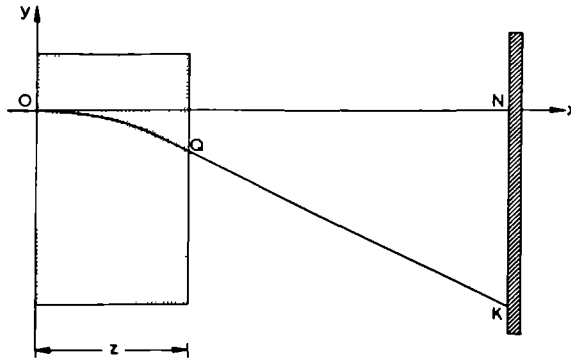


**Fig.2.3:** *Motion of an ion in a magnetic field perpendicular to the plane of drawing. The ion enters the field at O and hits a photographic plate at K.*

If  $v$  is the (constant) velocity of the ion, and if  $B$  is the magnetic induction of the field, the force on the ion exerted by the magnetic field is given as:

$$F_m = qvB \quad (2.10)$$

The magnetic force is always at right angles to the direction of motion, changing the direction of the ion but not its speed. The straight line motion of the ion is bent into a circular path. The magnetic force equals the centripetal force on the ion. This is expressed by:

$$qvB = \frac{mv^2}{r_m} \quad (2.11)$$



where  $r_m$  is the radius of the circular path. Substituting  $mv$  by  $p$  in eq.2.11, and manipulating algebraically yield:

$$r_m = \frac{p}{qB} \quad (2.12)$$

If  $q = +1e$ , i.e. the ion is singly charged, eq.2.12 reduces to:

$$r_m = p \times B^{-1} \quad (2.13)$$

Eq.2.13 shows that, in a given magnetic field,  $r_m$  is proportional to the momentum of a singly charged ion.

Suppose the magnetic field has a width  $z$ , and a photographic plate is placed perpendicular to the direction of motion at point N with the coordinates  $(n,0)$ . The ion leaves the field at Q and, since the magnetic force is no longer acting on the ion, follows a straight line, tangent to the circle (with radius  $r_m$ ) in Q. The ion hits the plate at point K. Its x-coordinate is  $n$ , whereas its y-coordinate is approximately given as:

$$NK = - \frac{q}{m} \times \frac{B}{v} \times \frac{z(2n-z)}{2} \quad (2.14)$$

indicating that an ion with a greater momentum will be less deflected than an ion with a smaller momentum.

### 2.4.3 An ion beam moving in a magnetic field

An infinitely narrow, nondivergent ion beam is delivered by a combination of an ion source and an electrostatic accelerator. The beam ions enter a uniform magnetic field, which has sharp boundaries and is perpendicular to the direction of motion: see fig.2.4. Within the magnetic field, the ion beam is dispersed into a number of discrete beams, each beam following a circular pathway. Three different situations are presented now to evaluate the factors influencing

the radius  $r_m$  of the circular pathway. This evaluation will clarify some current terms.

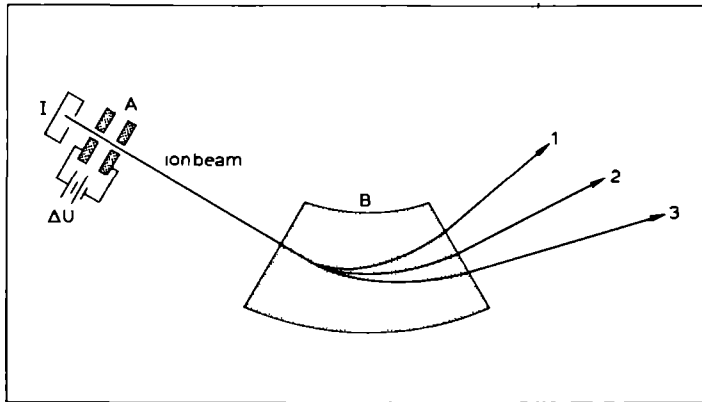


**Fig.2.4:** *An infinitely narrow, nondivergent ion beam, delivered by the combination of an ion source (I) and an electrostatic accelerator (A), enters a magnetic field. The accelerating voltage is  $\Delta U$ . The composite beam is split into discrete beams (Redrawn from Kerwin (McDowell, 1963), by courtesy of McGraw-Hill Book Co.).*

**First case:** The ions of the beam sent into the field have equal charge  $q = +1e$ , but possess different momenta  $p$ .

Eq.2.13 shows that, in a uniform magnetic field with a fixed magnetic induction  $B$ , an infinitely narrow beam of singly charged ions of various masses and velocities will be dispersed into a number of discrete beams following circular trajectories with radii proportional to the momenta of the ions. Thus a discrete beam consists of ions with the same momentum. The magnetic field is said to act as a "momentum analyser" or "momentum spectrometer", or to give a "momentum spectrum". If the ions have the same mass, they must have different velocities. The dispersion occurs according to their velocities and is termed "velocity dispersion".

**Second case:** The beam ions have equal charge  $q = +1e$  and equal energy, i.e. the beam is mono-energetic.

Eq.2.5 can be used to calculate the energy delivered to the ions by the accelerator, if the initial energy of the ions in the ion source is negligible. A mono-energetic beam consists of ions with the same energy or, in other words, every ion is accelerated by the same potential difference in the electrostatic accelerator. Combining eqs.2.5 and 2.11, and eliminating the velocity of the ions, the radius of a discrete beam is given as:

$$r_m = \frac{1}{B} \sqrt{(2m\Delta U)} \quad (2.15)$$

indicating that under the given circumstances  $r_m$  is proportional to  $\sqrt{m}$ . Thus the magnetic field acts as a pure "mass analyser", the ion beam is said to undergo "mass dispersion", and the momentum spectrum becomes a "mass spectrum".

Third case: The ions have different charges, but equal energy.

The same calculation as in the second case yields:

$$r_m = \frac{1}{B} \sqrt{(2 \frac{m}{q} \Delta U)} \quad (2.16)$$

indicating that the composite ion beam disperses into discrete ion beams, according to the mass-charge ratio of the constituting ions. Double-charged ions behave as single-charged ions of half the mass. Eq.2.16 is generally known as the "mass spectrometer equation", because it governs ion motion in magnetic field mass spectrometers (see section 3.7.3).

EXAMPLE: Suppose a double-charged argon ion with a mass rounded off to 40 u is accelerated by a potential difference of 3000 V, and

enters a magnetic field of 0.1 Tesla. The radius of the ion trajectory is given as:

$$r_m = \frac{1}{0.1} \sqrt{2 \times \frac{40}{2} \times 3000 \times 10.364353 \times 10^{-9}} = 0.35266 \text{ m}$$

The dispersing action of a magnetic field, which is to be used in a mass spectrometer, must achieve "effective separation" of ions with identical mass-charge ratios. The importance of this feature is stressed in the next section.

#### 2.4.4 Direction focusing

##### 2.4.4.1 Direction focusing in a uniform magnetic field

The ideal model of fig.2.4 is troubled by the angular divergence of the ion beam which is always present in practice. Fig.2.5 shows how a slightly divergent mono-energetic ion beam is deflected by a given magnetic field. It should be understood that the divergent beam contains many of the ion beams as described in the foregoing section. Fig.2.5 shows that ions of the same mass-charge ratio, but belonging to different "rays" of the divergent beam, don't focus properly. Thus, no "effective separation" is obtained since it is not feasible to measure the abundance of the individual ion species.

It is possible, however, to design a magnetic field which effects at the same time mass dispersion and direction focusing, i.e. ions having the same mass-charge ratio, but belonging to different "rays" of a slightly divergent ion beam, are focused in one point (see fig.2.5). Direction focusing is required for effective separation of the ions in a mass spectrometer. In practice, magnetic field shapes only approximate this ideal focusing field and some amount of defocusing always exists at the point where the ions with the same mass-charge ratio should focus. For a mathematical treatment of the refocusing properties of magnetic fields, the interested reader is referred to textbooks (Barnard, 1953; Brunnee and Voshage, 1964).

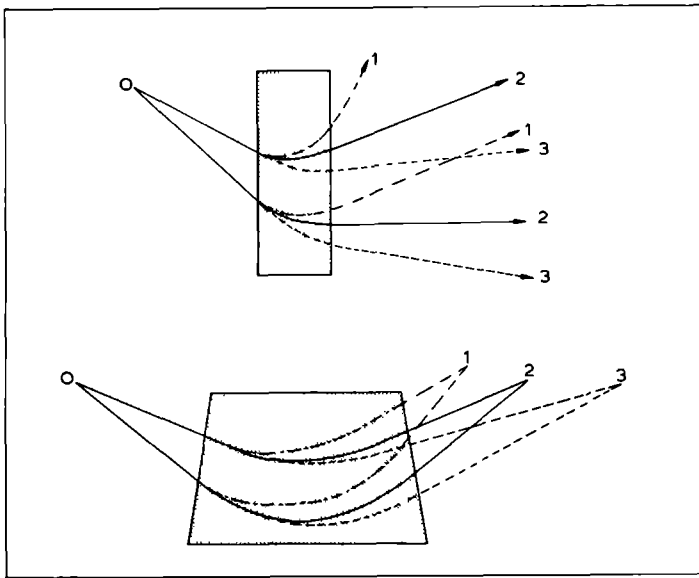


Fig.2.5: Dispersion of a mono-energetic divergent ion beam in a nonfocusing (top) and in a focusing (bottom) magnetic field (schematically). The beam is created at O and contains ions with three different mass-charge ratios (1, 2, and 3). No effective separation is obtained in the nonfocusing field. In the focusing field, however, ions with identical  $m/q$  are focused in one point although they belong to different "rays" of the divergent beam.

#### 2.4.4.2 Direction focusing in a radial electrostatic field

An electrostatic field is created between two coaxial sector-shaped cylindrical electrodes, and is supposed to have sharp boundaries. The distance  $d_e$  between the electrodes is much smaller than their mean radius  $a_e$  ( $d_e \ll a_e$ ) (see fig.2.6). The direction perpendicular to the plane of drawing is not considered as motion in that direction is neglected. The field is created in such a manner that the cylindrical surface with radius  $r = a_e$  is the zero-potential surface ( $U_r = 0$ ).

Suppose a *single ion* enters the field perpendicular to the field boundary at  $r = a_e$ . No energy is lost as  $U_r$  is zero at that surface.

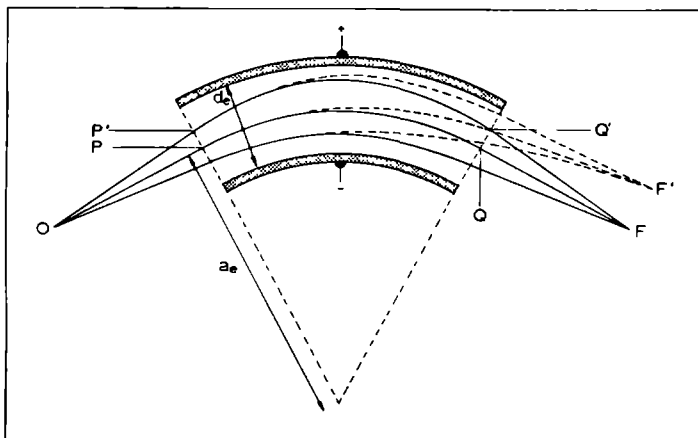


Fig.2.6: *Direction focusing and velocity dispersion in a radial electrostatic field. Ions of different rays of the ion beam are focused in F or F', according to their velocities. Ions with the higher velocity focus in F'.*

If this ion also has a velocity  $v_0$  (or possesses an energy), such that the electrostatic force equals the centripetal force, the ion describes a circular path along OPQF.

If an *ion beam* enters the field instead of a single ion, three cases, relevant for further discussion, can be distinguished:

**First case:** a mono-energetic beam with small angular divergence, composed of ions with identical mass-charge ratio.

An ion, which has O as point of origin and enters the field at P' (with the same velocity  $v_0$ ), will lose kinetic energy since it is approaching the more positive electrode. This ion will move along OP'Q'F. The reverse is true for an ion entering the field below P ( $r < a_e$ ). It can be proven that all ions starting at O are focused in one point F. Accordingly "direction focusing" is established. It can even be shown that ions with slightly different masses (but with the same energy) focus in the same point. Thus a radial electrostatic field has no mass dispersion properties.

Second case: a very narrow, nondivergent beam of ions with identical mass-charge ratio but heterogeneous in energy, enters the field normal to the field boundary at the central ray.

The heterogeneity in energy means that the ions will enter the field at P with different velocities. Ions with velocity  $v_0$  will move along the circular path OPQF. Ions with other velocities will have a radial displacement when emerging from the field. The ion beam is said to have undergone "velocity dispersion". At the exit boundary, the nondivergent ion beam has turned into a divergent beam.

Third case: a slightly divergent beam of ions with small differences in mass and heterogeneous in energy, will undergo direction focusing (as in the first case) and velocity dispersion (as in the second case) at the same time. The ions are "focused" on a line through F and F'.

In conclusion, this field doesn't have any value with respect to mass dispersion. However, the combination with a magnetic field can lead to a very useful instrument: the double focusing mass spectroscope (see section 2.4.5.2 and 3.7.5).

## 2.4.5 An ion beam moving in a combination field

It is supposed that the ion beam is very narrow and that the fields are perpendicular to the direction of motion.

### 2.4.5.1 Parallel and simultaneously acting fields

A nondivergent ion beam, which contains ions moving with a velocity  $v$ , enters a combination of an electrostatic and magnetic field as shown in fig.2.7. The ions will be influenced at the same time by both fields. The deviation caused by each field has been calculated already for an electrostatic field strength  $E$  and a magnetic induction  $B$ . Suppose that the fields are influencing the ions over a distance  $z$ , and that the ions hit a photographic plate placed at a distance  $n$  from the point of ion entry. If the fields are inactive,

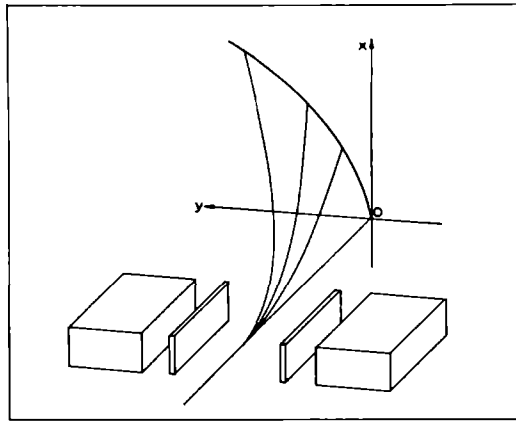


**Fig.2.7:** Behaviour of an ion beam in a combined electric and magnetic field, which are parallel and acting simultaneously.

the ions hit the plate in point O, which is chosen as the origin of the xy-axes. The deviation caused by the electrostatic and magnetic field occurs in the y- and x-direction, respectively.

Using eqs.2.9 and 2.14, and denoting the deviation in the x- and y-direction by  $x'$  and  $y'$ , respectively, elimination of  $v$  yields:

$$y' = \frac{m E}{q B^2} \frac{2}{z(2n-z)} x'^2 \tag{2.17}$$

Eq.2.17 is the equation of a parabola through the origin O and symmetrical to the y-axis. If a mixture of ions varying in mass-charge ratios and velocities is sent into the combination, a number of parabolas is created. Each parabola has its own characteristic  $m/q$  value, whereas each point on a parabola represents a specific velocity. Ions with the highest speed are located nearest to the origin O. If there is a small velocity spread between ions, only a small segment of a parabola will be formed. The properties of this field arrangement were used by Thomson in his "parabola apparatus" described in section 3.7.1.



### 2.4.5.2 Consecutive magnetic and electrostatic field

*Velocity focusing:* ions, entering a magnetic field with different velocities, undergo "velocity dispersion" (see the first case in section 2.4.3). The same holds for an electrostatic field (see the second case in section 2.4.4.2). If the consecutive action of an electrostatic and a magnetic field is used, it is possible to counterbalance exactly the velocity dispersion produced in the first field by that in the second field. This velocity focusing effect was first used in Aston's mass spectrograph illustrated in section 3.7.2.

*Double focusing:* a combination of an electric and magnetic field can also be applied to obtain direction and velocity focusing. Velocity focusing is produced as in Aston's mass spectrograph. Direction focusing is also attained by the combination, and mass dispersion is produced by the magnetic field. A double focusing instrument is shown in the section on the history of mass spectroscopes.

### 2.4.6 A single positive ion moving in a quadrupole field

The geometry and the electrical design of a quadrupole field, which is generated by four parallel rod-shaped electrodes, is illustrated in fig.2.8. The rods are arranged symmetrically along the z-axis of the x,y,z Cartesian coordinates. The cross section of each rod is hyperbolic. Opposite rods are separated by a distance  $2r_0$  and are electrically connected. Adjacent rods are at opposite potentials  $\phi_0$  and  $-\phi_0$ . Therefore the z-axis is at zero potential.

In the x-y plane, the potential is given as:

$$\phi = \frac{\phi_0}{r_0^2} (x^2 - y^2) \quad (2.18)$$

Eq.2.18 and fig.2.8 show that the equipotentials are rectangular hyperbolas with a four-fold symmetry about the z-axis. The field strengths in the three directions are (Paul and Raether, 1955):

$$E_x = + \frac{2\phi_0}{r_0^2} x \quad (2.19)$$

$$E_y = - \frac{2\phi_0}{r_0^2} y \quad (2.20)$$

$$E_z = 0 \quad (2.21)$$

Eqs.2.19 and 2.20 show that the field strength in the quadrupole field depends linearly on the coordinates. An ion with charge  $q$ , which is shot with a certain velocity in the  $z$ -direction into the field, is subjected to the forces  $qE_x$  and  $qE_y$ . There is no force acting upon the ion in the  $z$ -direction, since  $E_z = 0$ .

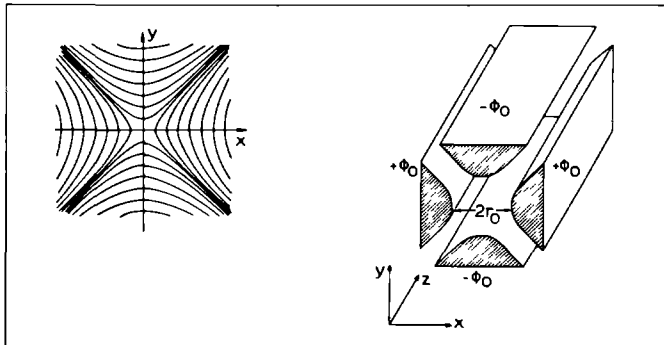


**Fig.2.8:** *The four hyperbolic rods generating a quadrupole field are shown on the right. On the left, the equipotential lines are illustrated (After Dawson (1976), by courtesy of Elsevier Scientific Publishing Co.).*

Combining eqs.2.3, 2.19, 2.20, and 2.21 yields the equations of motion for the ion in the field:

$$x'' + \frac{q \ 2\phi_0}{m \ r_0^2} x = 0 \quad (2.22)$$

$$y'' - \frac{q \ 2\phi_0}{m \ r_0^2} y = 0 \quad (2.23)$$

$$z'' = 0 \quad (2.24)$$

where  $x''$ ,  $y''$ , and  $z''$  are the second time derivatives of the  $x$ ,  $y$ , and  $z$  coordinates, i.e. the accelerations in the  $x$ ,  $y$ , and  $z$  directions. Eqs.2.22 and 2.23 describe the motion in the  $xz$  and  $yz$  planes respectively, whereas eq.2.24 indicates that there is a motion with constant velocity (no acceleration) in the  $z$ -direction. These equations also indicate that ion motion will be influenced by the time dependency of the potential  $\phi_0$  applied to the electrodes. Three forms of time dependency of  $\phi_0$  are discussed, but only the form needed further in the study will be explored in more detail.

Firstly, suppose  $\phi_0$  is a constant potential  $U$ . In the  $xz$  plane, the positive ion will be forced towards the  $z$ -axis with a force which is growing with increasing distance from the  $z$ -axis (see eq.2.19). The ion will acquire an oscillating but "stable" trajectory between the  $x$ -electrodes. A "stable" trajectory is temporarily defined as a trajectory with an amplitude which remains finite as the distance along the  $z$ -axis approaches infinity. The amplitude of an "unstable" trajectory, however, increases without limit. In fact, in the  $yz$  plane, the positive ion is attracted towards one of the electrodes at the potential  $-U$  and will have an unstable trajectory. Eventually the ion will hit an electrode.

Secondly, suppose  $\phi_0$  is a periodic function of time:  $V_{ac} \cos \omega t$ , where  $V_{ac}$  is the peak amplitude and  $\omega = 2\pi\nu$ , where  $\nu$  is the frequency of the periodic function. Since the potentials at the electrodes are alternating in sign, the ion is alternately attracted to or repulsed by the same electrode. A complex trajectory results from this electrical arrangement.

Thirdly, suppose  $\Phi_0$  is a combination of a direct and an alternating component, given as  $U+V_{ac} \cos \omega t$ , whereas  $V_{ac}$  is larger than  $U$ . Thus ions are subject to the combined electrical forces as described in the first two cases, and ion trajectories will be very complex again. This is illustrated in fig.2.9.

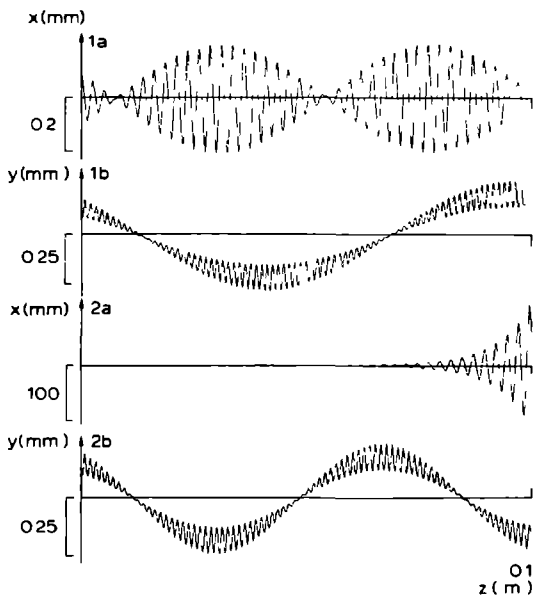


**Fig.2.9: Ion trajectories projected on the xz plane (a), and on the yz plane (b) for an ion with  $m/q = 44.0$  (1a, 1b), and with  $m/q = 43.8$  (2a, 2b) in a quadrupole field with the same field conditions ( $r_0 = 3 \text{ mm}$ ). The ion with  $m/q = 44.0$  has a stable trajectory in both planes. The ion with  $m/q = 43.8$  has an unstable trajectory in the xz plane. Trajectories were calculated by a program SIMQUA using the equations of ion motion 2.25 and 2.26.**

Instead of a qualitative description, a quantitative discussion of ion trajectories is given. Substitution of  $U+V_{ac} \cos \omega t$  for  $\Phi_0$  in the eqs.2.22 and 2.23 yields the equations of ion motion through the quadrupole field:

$$x'' + \frac{q}{m r_0^2} (U + V_{ac} \cos \omega t) x = 0 \quad (2.25)$$

$$y'' - \frac{q}{m r_0^2} (U + V_{ac} \cos \omega t) y = 0 \quad (2.26)$$

It is useful to define the following three dimensionless parameters (Paul, Reinhard and von Zahn, 1958):

$$\xi = \frac{\omega t}{2} \quad (2.27)$$

$$A = \frac{q}{m r_0^2} \frac{8 U}{\omega^2} \quad (2.28)$$

$$Q = \frac{q}{m r_0^2} \frac{4 V_{ac}}{\omega^2} \quad (2.29)$$

By means of these three parameters, eqs. 2.25 and 2.26 can be transformed into differential equations equivalent to the Mathieu equations, the solutions of which are known. These solutions yield the trajectories as shown in fig. 2.9. The Mathieu equations have two types of solutions, for a stable or an unstable ion trajectory. Thus a quadrupole field can be used for ion selection, since only ions with stable trajectories pass through the quadrupole field. The type of solution only depends on the value of A and Q. Further mathematical analysis, helpful in the description of the quadrupole field as an ion selector, will be given in section 3.4.

## CHAPTER 3

### OPERATION OF A MASS SPECTROMETER

The operation of an effectively functioning mass spectrometer is based on a systematic application of the theoretical background described in the foregoing chapter. This chapter reviews the four principal components that can be recognized in any mass spectrometer (fig.3.1), some of its performance characteristics, and the main types of the instrument. Attention will be focused upon the quadrupole mass analyser.

#### 3.1 INTRODUCTION

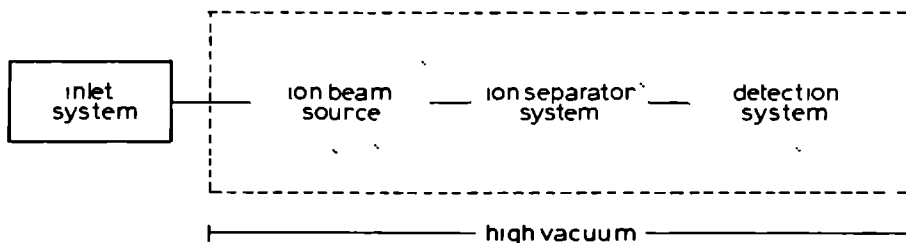


**Fig.3.1:** *The four components of a mass spectrometer: vacuum and inlet system, ion beam source, ion separator system, and detection system.*

A sample is taken from the gas mixture, which has to be analysed, via a sample or inlet system. The sample is introduced in the ion source, where the neutral gas molecules are ionized and possibly fragmented. The ions are accelerated, focused into an ion beam, and shot into the ion separator (or "mass analyser") system, where ions are separated according to their mass-charge ratio. Finally, the ions with identical mass-charge ratio are detected by an electrical

measuring system as "mass peaks" which form the "mass spectrum" of the gas or gas mixture.

The processes of ionization, ion acceleration, separation and detection take place in high vacuum, in order to keep the chance of ion collisions minimal (see fig.3.1).

## 3.2 VACUUM AND INLET SYSTEM

On one hand, the reliable operation of a mass spectrometer requires a vacuum level of about 1 mPa for reasons to be given below; on the other hand, a respiratory mass spectrometer must draw off its gas sample at atmospheric pressure, roughly 100 kPa. Thus, besides a *high vacuum system* to produce the vacuum level for normal operation, an *inlet system* is needed to suck off continuously a gas sample, to transport it to the ionizer system and to reduce at the same time the sample pressure by eight decades. The combination of the high vacuum system and the inlet system will be termed the *gas handling system* of the mass spectrometer.

A high vacuum level, i.e. 10 to 0.1 mPa, is required to guarantee the proportionality between the partial pressure of a gas and its ion current, since ion scattering and space charges are virtually eliminated at low pressures (see section 3.3). The pressure of about 1 mPa also keeps the partial pressures of gases remaining in the ionizing, analysing and detection system to a minimum, i.e. the "background spectrum" is kept minimal (Muysers and Smidt, 1969).

Firstly, the requirements to be met by the gas handling system will be given, secondly the gas handling system generally used in respiratory mass spectrometers will be described, and lastly, it will be verified how the described system satisfies the requirements.

### 3.2.1 Requirements

The following primary requirements are to be fulfilled by the gas handling system of a respiratory mass spectrometer:

1. a constant operating pressure of 0.1 to 1 mPa in the analysing section,
2. continuous sampling at atmospheric pressure,
3. constant partial pressure ratios during gas transport,
4. a linear relationship between the ion beam intensity of one component and its partial gas pressure, regardless of molecular weight and viscosity,
5. no "interference" between sample components, i.e. the measurement of one component should not be influenced by the presence of another component in a gas mixture.

Other requirements are:

1. a relatively high gas pressure within the stream of free electrons in order to have a high ion current (see section 3.3),
2. "fast" transmission of a change in gas composition at the sample point,
3. air cooling of the vacuum pumps and oil traps (baffles). The use of water, compressed air, liquid nitrogen or dry ice should be avoided.

### 3.2.2 Description of the gas handling system

A gas handling system, meeting most of these requirements, is shown schematically in fig.3.2. After an overview of the gas handling system, its components will be treated individually.

*The inlet system:* a gas sample is drawn in continuously at atmospheric pressure ( $p_1$ ) through a flexible capillary tube by means of a rotatory pump (sample transport pump). The pressure drop ( $p_1 \rightarrow p_2$ ) along the capillary is the first pressure reduction between the atmosphere and the high vacuum. The design of the components, i.e. pumping speed and tube geometry, ensures a viscous gas flow between the sampling point and the mouth of the pump.

At an intermediate point of the inlet system, i.e. at the sample chamber, the gas sample is at an intermediate pressure  $p_2$  (about 1 to 3 kPa). The pressure gap between sample chamber and ionization chamber ( $p_4 \approx 1$  mPa) is bridged by a "leak" (molecular leak or



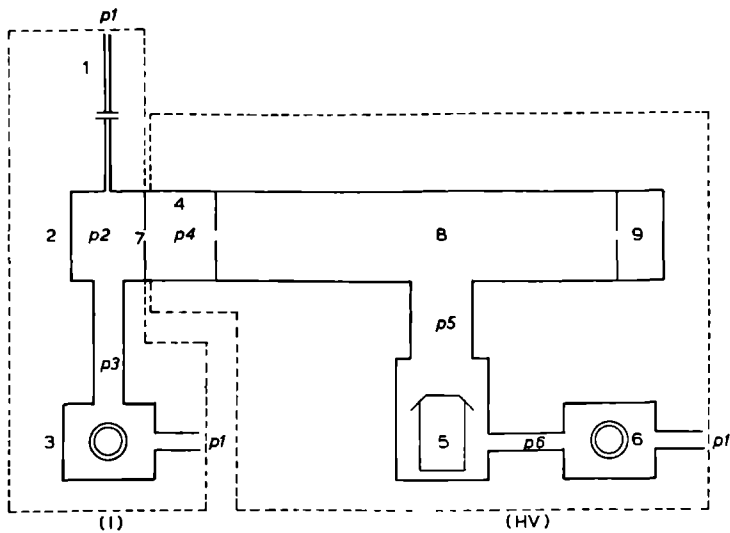


Fig.3.2: Diagram of the gas handling system of a respiratory mass spectrometer: inlet system (I) and high vacuum system (HV). The other components shown are: flexible inlet capillary (1), sample chamber (2), rotatory pumps (3,6), ionization chamber (4), vapour stream pump (5), molecular leak (7), analyser system (8), and electrical measuring system (9). The pressures are:  $p_1$  = atmospheric pressure, and  $p_2$  to  $p_6$  = pressures at the various points.

porous leak), where molecular flow conditions prevail. The gas molecules are introduced as a molecular beam into the ionizing region. Most of the sample, however, is removed by the rotatory pump and discarded to the atmosphere.

*The high vacuum system:* the pumping speed of a high vacuum pump (vapour stream pump or another) and the conductances within the system are arranged to achieve the required pressure of about 1 to 0.1 mPa. The mean free path of ions at this kind of pressure guarantees molecular flow conditions where the probability of intermolecular collisions is low.

### 3.2.2.1 The inlet system

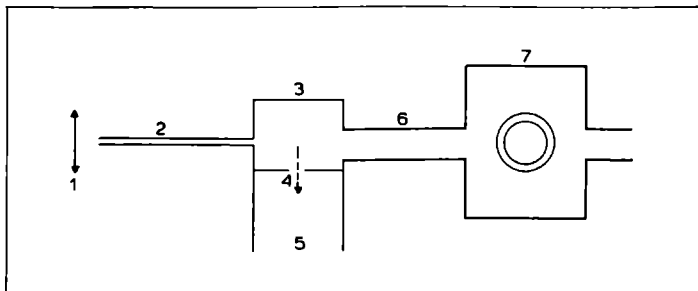


Fig.3.3: *The inlet system: respiratory gas mixture (1), inlet capillary (2), sample chamber (3), molecular leak (4), high vacuum system (5), connecting tube (6), sample transport pump (7).*

Fig.3.3 illustrates that part of the inlet system consists of a pump (7), a connecting tube (6) and a chamber (3), which is supposed to be evacuated until a constant pressure of about 1 to 3 kPa is reached. However, the chamber has two "leaks". One "leak" is functioning as a gas source, i.e. the inlet capillary (2), the other "leak" acts as a gas sink, i.e. the molecular leak (4) to the high vacuum system (5). After a period of pumping, an equilibrium situation is reached and a constant sample chamber pressure is established, which is determined by the ratio of the sample flow and the effective pumping speed (neglecting the very small leak to the high vacuum system). This is illustrated in fig.3.4. The constant sample chamber pressure guarantees a constant gas flow into the high vacuum system which is one of the conditions for a stable overall sensitivity of the instrument.

The sample is drawn in by a mechanical pump (rotatory oil sealed pump). This pump conveys gases by one or more stages of compression. Each stage consists of a rotor turning excentrically in a stator or cylinder. During operation, gas tightness between rotor and cylinder wall is ensured by oil sealing, and e.g. by spring loaded vanes (blades) in the rotor. A typical sample gas flow through the

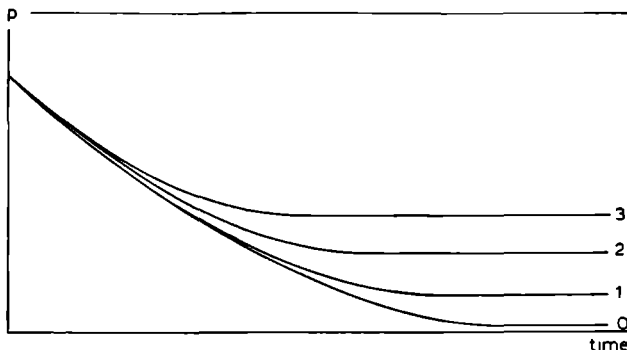


Fig.3.4: *Pressure of the sample chamber as a function of time. At curve 0 the sample flow is zero; curves 1 to 3 illustrate the influence of increasing sample flows.*

inlet capillary of a respiratory mass spectrometer is  $40 \text{ liter.Pa.s}^{-1}$ , i.e. a sample flow of about  $24 \text{ ml.min}^{-1}$  at atmospheric pressure (Buckingham and Dennis, 1975).

It was already mentioned that the design of the inlet system should ensure viscous flow throughout the system. This requirement must be fulfilled for sample gas mixtures with viscosities varying within a wide range, if inert tracer gas (e.g. argon) is to be used in the course of respiratory investigations. If this requirement is not met, the change in gas viscosity will result in a change in gas flow into the high vacuum system. Changing the flow into the ion source will lead to faulty measurement (Fowler, 1969).

### 3.2.2.2 The molecular leak

The leak between sample chamber and ionization chamber on one hand separates, on the other hand bridges the viscous flow and the molecular flow regime. In order to minimize gas flow in the transition regime, the pressure has to drop as abruptly as possible over the leak. If the flow through the leak is essentially molecular, it is called "molecular leak".

A molecular leak can be made of an orifice in a thin diaphragm (e.g. a gold blade), or can consist of a porous material. The mean free path of the gas molecules has to exceed largely the dimensions of the leak. This requirement leads for a thin diaphragm to a rather low pressure in the sample chamber, resulting in viscosity effects as described earlier. The use of a sintered porous leak, which consists of compressed carbide granules, makes an upstream pressure of 1 to 3 kPa possible, since the pore size is very small. Only a small part ( $4 \times 10^{-3}$  liter.Pa.s<sup>-1</sup>) of the total throughput of the inlet system (40 liter.Pa.s<sup>-1</sup>) passes through the leak (Buckingham and Dennis, 1975).

### 3.2.2.3 High vacuum system

Firstly, the high vacuum system should produce a stable vacuum level of 1 to 0.1 mPa; secondly, the system should ensure a wash out of the ionization chamber (and molecular leak) with a small time constant after a change of incoming gas. A fast clearance of the ionization chamber after a change of incoming gas is ensured by a small ratio of the volume of the ionization chamber and the effective pumping speed at working pressure (Fowler, 1969).

The high vacuum is produced by a series combination of a high vacuum pump and a fore-vacuum pump, the latter being of the same type as a sample transport pump. Several types of high vacuum pumps exist, but "vapour stream" pumps are very widely used. These pumps entrain and transport gases by momentum transfer. In the past, the diffusion of the gas into the pump vapour has been thought to be the most important step in pump operation. Accordingly, these pumps were and are usually called "diffusion pumps".

A vapour stream pump consists of a cylinder, closed at its base (see fig.3.5). The area facing the bottom forms the inlet side and is connected with the system to be evacuated. The outlet is at the side of the lower portion of the cylinder. A heater is fitted in the pump bottom, while the pump body is cooled with air or a coolant. The vapour stream, created by heating a liquid (mostly silicone oil) in the bottom, rises in a chimney situated within the pump body. Vapour molecules emerge from the chimney by one or more annular jet

"nozzles", which are designed to form high velocity vapour streams in the direction of the cylinder wall and bottom. According to the number of nozzles, the pump is of the single- or multi-stage type. The vapour condenses at the cooled cylinder wall, drains to the bottom and is revaporized. The pumping mechanism originates from the gas-vapour interactions. At the inlet side, gas molecules are entrained by the vapour stream and are given a momentum in the outlet direction during gas-vapour intermolecular collisions. The downward motion of the gas molecules crowds them together, resulting in a compression at a pressure sufficient for normal operation of the fore-vacuum pump.

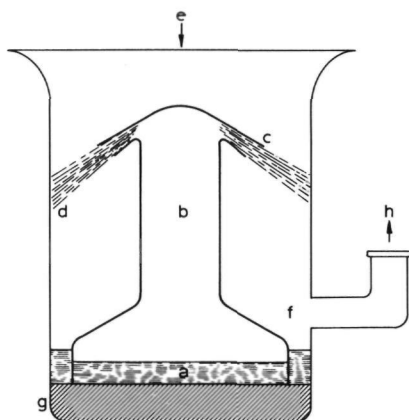


Fig.3.5: Cross section of a single-stage vapour stream pump: boiling pump liquid (a), vapour chimney (b), nozzle (c), vapour stream (d), inlet (e), backing space (f), heater (g), backing pump flange (h).

Provisions must be made to prevent backstreaming of vaporized pump fluid into the vacuum system, e.g. by insertion of a cooled baffle. Vapour hitting this baffle returns to the pump as a liquid after condensation.

### 3.2.3 Fulfillment of the requirements

It is concluded from the foregoing that most of the requirements, given in section 3.2.1, can be met by the described gas handling system. However, the fulfillment of some requirements needs some further discussion.

Constant partial pressure ratios during gas transport (requirement 3) are guaranteed in the inlet system as long as viscous flow exists, since transport phenomena in this regime are mass independent. Gross variation in sample viscosity already has been cited as a problem. Gross variation in inlet system resistance, e.g. by particle deposition, is a similar problem. Another problem is created by the sampling of mixtures containing condensable vapours, e.g. water vapour, and will be discussed in chapter 4.

Constant partial pressure ratios in the ionization chamber can be checked as follows. A gas enters and leaves the ionization chamber in the molecular flow regime. So, mass discrimination effects cancel each other (Brunnee and Voshage, 1964): mathematical proof, by calculating the relationship between the sample chamber pressure  $p_2$  and the ionization chamber pressure  $p_4$  was provided by Honig (1945). It follows to a good approximation:

$$p_4 = p_2 \frac{G_i}{G_o} \quad (3.1)$$

where  $G_i$  and  $G_o$  represent the conductances of the molecular leak and the ionization chamber exit hole, respectively. Since  $G_i$  and  $G_o$  are mass dependent in the same way, their ratio is not. Thus, ionization chamber gas pressure is mass independent. Since this condition holds for every gas species in a mixture, no interference between sample components may be expected (requirement 5).

The proportionality of ion beam intensities to the partial gas pressures of the sample components is treated in the next section on the ion beam source.

### 3.3 IONIZATION AND ION BEAM FORMATION

Neutral sample molecules have to be ionized (in an "ion source") before they can be accelerated or separated by electric or magnetic fields. Once created, the ions are instantaneously drawn out from the ion source, accelerated by an electrostatic accelerator, and focused into an ion beam. Therefore these processes are treated in the same section. In respiratory mass spectrometry, positive ions created in an electron impact source are used.

An ideal ion source should have following basic features:

1. the delivered ion beam is mono-energetic,
2. the delivered ion beam has an intensity sufficient for the detection system in use,
3. the ion beam intensity is linearly related to partial sample gas pressure,
4. the ion beam is stable,
5. the ion beam shows no divergence,
6. there is no production of background ions,
7. no memory effects are present between successive samples.

These features and some important points for their realization will be discussed in section 3.3.2.

#### 3.3.1 Construction and operation of an electron impact source

The neutral sample molecules are ionized by collision with electrons (see section 2.2). This type of ion source has following components:

- a source of electrons with sufficient energy (electron beam source),
- an ionization chamber,
- an ion accelerator and focusing system.

These three components as a whole may be better called "ion beam source" instead of "ion source". Its construction and operation are shown schematically in fig.3.6. The components are described in the same order as listed above.

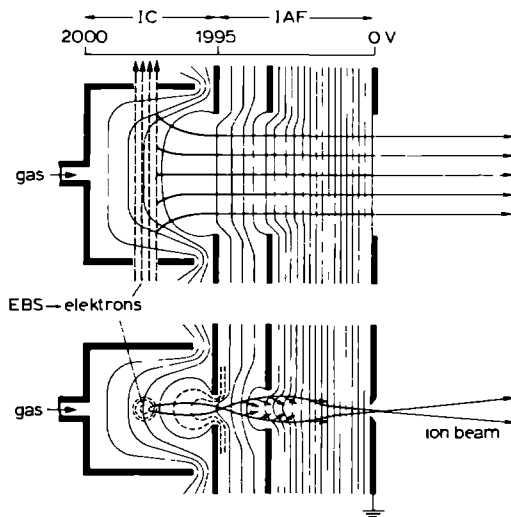


Fig.3.6: Schematic view in two cross sections of an ion beam source: electron beam source (EBS), ionization chamber (IC), ion accelerator and focusing system (IAF), of which the equipotentials are shown (After Brunnee and Voshage (1964), by courtesy of Verlag K. Thiemeig KG).

1. The electrons are emitted by a heated filament and are accelerated by a potential difference between the filament and another electrode. The filament can be called "cathode" and the electrons are said to be "energized". Energized electrons pass through the ionization chamber, i.e. the space where the ionization process takes place, and are collected by a trap, which is at a slightly higher potential than the ionization chamber in order to trap secondary electrons.

2. Continuous pumping sucks the sample gas through the ionization chamber where a total gas pressure of 10 mPa to 100  $\mu$ Pa is reached. On their way to the analyser system, neutral sample molecules are bombarded by the energized electrons which traverse the ionization chamber perpendicular to the path of the sample molecules. The dimensions of the chamber determine the effective electron path length, i.e. that part of the electron path available for interaction with neutral molecules.



3. Part of the ions actually created is extracted from the ionization chamber, accelerated, and focused into an ion beam by a set of plates (see fig.3.6). The ionization chamber is at the highest (e.g. 2000 V), the draw-out plate at a slightly lower potential (e.g. 1995 V), providing an extraction potential of a few volt. After extraction, the ions are accelerated by an "electrostatic accelerator" (described in section 2.4.1.1).

The current of a particular ion, emerging from the ion source, can be expressed as (Brunnee and Voshage, 1964):

$$I_i = I_e \times p_g \times l \times s \times K_e \quad (3.2)$$

where  $I_i$  = current of a particular ion emerging from the ion source

$I_e$  = electron current

$p_g$  = partial gas pressure in the ionization chamber

$l$  = effective electron path length

$s$  = differential ionization

$K_e$  = extraction coefficient

The differential ionization  $s$  is a function of electron energy, and is defined as: the number of ions, created by one electron with a given energy, travelling one metre through a gas at one Pascal. The extraction coefficient  $K_e$  is the fraction of ions drawn out from the source.

### 3.3.2 Ion beam source features

The basic features of an ideal ion beam source are now dealt with in the same order as listed above.

1. The energy homogeneity of the ion beam depends on electron beam divergence, and on the potential gradient in the ionization chamber (see fig.3.6). In other words,  $\Delta U$  in eq.2.5 will be equal for all ions if they are created in the same equipotential plane. On the contrary, if the ions are created along different equipotentials, their energies will differ accordingly. A weak magnetic field may be used to restrict the electron beam dimensions.

2. The ion beam intensity can be varied by adjusting the parameters in eq.3.2. These parameters may be briefly considered under five headings. (1) The electron current  $I_e$  should be limited (about 100  $\mu$ A) because higher electron currents build up space charges, disturbing electric and/or magnetic fields. (2) Ionization chamber pressure  $p_g$  should not exceed 10 mPa for three reasons. Firstly, a high vacuum is needed in the analyser part of the mass spectrometer. Secondly, too many ions exert positive ion charge effects on the electron beam, and thirdly a higher  $p_g$  increases the probability for reactions between ions and neutral sample molecules. (3) Enlarging the effective electron path length will increase the clearance time of the ionization chamber, as well as the ion beam divergence. (4) Electron energy can be varied to optimize differential ionization. Ionization only starts at a certain electron energy level. The potential difference needed to attain this level is called "appearance potential", because ions will "appear" as mass peaks in the mass spectrum from that potential difference on. Differential ionization reaches a maximum for a certain electron energy level (about 70 eV for most molecules). (5) The extraction coefficient  $K_e$  depends on the size of the exit aperture, and the extracting potential difference.

3. A linear relationship between the ion current of a particular gas and its partial gas pressure is expressed by eq.3.2. However, linearity is lost with high ion currents by the production of space and surface charges, disturbing extraction and acceleration potentials. The extraction potential should therefore be chosen in a range, where small potential variations minimally affect the ion current (Brunnee and Voshage, 1964).

4. If all (instrumental and external) factors remain constant, not only the ion current should be stationary, but also the relative occurrence of the different species in the beam.

4a. Ion current stability can only be achieved by time stability of all factors in eq.3.2.

4b. Ion beam composition is influenced by electron energy. Varying electron energy results in varying relative occurrence of

single- and multiple-charged ions, and of ionized fragments of polyatomic molecules. In other words, stable electron energy is needed for a stable mass spectrum, which is the basis for accurate quantitative measurements. Ion beam composition and the resulting mass spectrum further depends on the temperature in the ionization chamber. Temperature should be constant.

5. A divergent ion beam not only lowers resolving power (see section 3.6), but also reduces ion beam intensity. The double focusing principle offers solutions for this problem.

6. Production of background ions can be kept to a minimum by providing a high ratio of sample gases to residual gases. The surface of all materials used in the construction of the ion source, should be free of all contamination which could augment the background spectrum.

7. Memory effects depend on gas species: e.g.  $\text{CO}_2$  adheres to metal surfaces (Hunter, Stacy, and Hitchcock, 1949).

### 3.4 ION SEPARATION: THE QUADRUPOLE MASS FILTER

Mass spectrometers can be classified according to the type of ion separator system in use. The main types of mass spectrometers will not be reviewed in this section, but in a recall of history in section 3.7, for two reasons. On one hand, the physical background behind their mode of operation already has been discussed and will be illustrated with historically important instruments. On the other hand, attention will now be focused upon the type of mass spectrometer used in this study, i.e. the quadrupole mass spectrometer. This type of instrument was introduced by Paul and Steinwedel (1953), who described their device as "Ein neues Massenspektrometer ohne Magnetfeld".

Operation of a real quadrupole depends on generating a stable trajectory for ions with a given mass-charge ratio. Ions with a stable trajectory emerge from the field and can be detected, while ions

with unstable trajectories collide with a rod, discharge, and are lost for detection. In that way, ions with a given mass-charge ratio can be filtered out, and the quadrupole field is said to act as a "mass filter" (see fig.3.7).

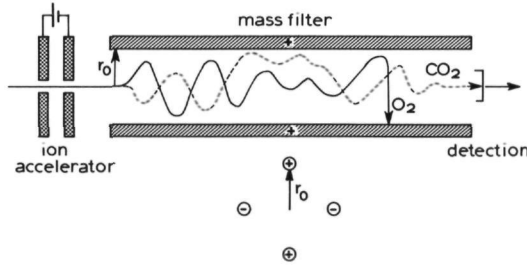


Fig.3.7: *Operating principle of the quadrupole mass filter:  $CO_2$  has a stable trajectory and is detected, whereas  $O_2$  collides with a rod and is lost for detection. Ion motion is illustrated in only one plane.*

The nature of ion motion, stable or unstable, depends on the types of solution of the Mathieu equations, which in their turn depend only on the values of  $A$  and  $Q$  (defined in eqs.2.28 and 2.29). Thus, discussion of the possible values of  $A$  and  $Q$  will show the requirements for stable trajectories. Values of  $A$  and  $Q$  can be plotted in a "stability diagram", which was transformed into a very useful form for a quadrupole mass filter by Paul et al. (1958). Paul's diagram is given in fig.3.8 and shows a field with three boundaries determined by the solutions of the Mathieu equations. Points lying within this field give stable solutions; points lying outside this field give unstable solutions.

The  $A$  and  $Q$  coordinates for different ions can be calculated from eqs.2.28 and 2.29. The coordinates determine the "working points" for the ions. Eqs.2.28 and 2.29 show that working points depend on one hand on the mass-charge ratio of the ion, and on the other on the field conditions:  $r_0$ ,  $U$ ,  $V_{ac}$ ,  $\omega$ . If the field conditions are kept identical, ions with the same  $m/q$  have the same working points.

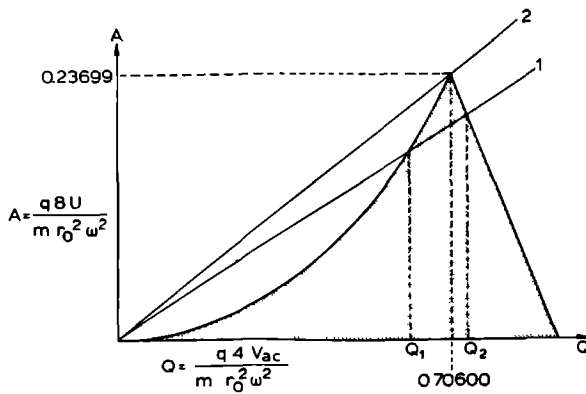


Fig.3.8: Paul's stability diagram. The stability region is shaded. Two scan lines are shown: (1) defining a certain mass interval between  $Q_1$  and  $Q_2$ ; (2) going through the apex.

Under these circumstances, working points of ions with different  $m/q$  lie on a straight line (through the origin) with the following equation:

$$V_{ac} A - 2UQ = 0 \tag{3.3}$$

Eq.3.3 is found by dividing eq.2.28 by eq.2.29, and does not depend on  $m/q$ . In other words, all points on the line are working points of ions with different mass-charge ratio. The slope of the straight line has the value  $2U/V_{ac}$ . Since only ions with working points within the stability region have stable trajectories, a stable mass interval is created between  $Q_1$  and  $Q_2$ , which are the intersecting points of the straight line and the stability region boundaries (see fig.3.8). The stable mass interval can be minimised by adjusting the  $2U/V_{ac}$  ratio, i.e. the slope. This property leads to the expression "scan line".

If the scan line passes through the stability region, just below its apex, only ions with identical mass-charge ratio will have stable trajectories. Thus the mass filter properties of the quadrupole field can be adjusted until only ions with the same mass-charge

ratio traverse the field. The mass of singly charged positive ions, emerging from the mass filter, can be determined as follows.

The apex of the stability region has the coordinates  $A = 0.23699$  and  $Q = 0.70600$  (Paul, Reinhard and von Zahn, 1958). The scan line slope, which can be calculated from eq.3.3, is 0.336. Accordingly, the ratio  $U/V_{ac}$  equals 0.168. The mass  $m$  (in  $u$ ) of the singly charged positive ion emerging from the mass filter is found by substituting  $Q$  and  $\omega$  by 0.70600 and  $2\pi\nu$ , respectively, in eq.2.29. This leads to:

$$m = 13.85 \times 10^6 \frac{V_{ac}}{\nu^2 r_0^2} \quad (3.4)$$

indicating that the mass of the ions emerging from the field can be changed by varying  $V_{ac}$ , i.e. mass scanning is realized. For instance, if  $V_{ac} = 164.7$  V,  $\nu = 2.4$  MHz, and  $r_0 = 3$  mm, then  $m = 44.003 \approx 44$  u.

The  $U/V_{ac}$  ratio, however, has to be kept constant at 0.168 to keep the scan line going through the stability region apex. Thus,  $U$  has to vary too. The potential amplitudes  $U$  and  $V_{ac}$  can be varied up to about 100 times per second, resulting in a quasi-continuous scanning of several  $m/q$  values (see also the section 3.5.2.2 on "selected ion monitoring mode").

The discussion above reveals one of the attractive features of the quadrupole, i.e. variable resolving power. Adjustment of the  $U/V_{ac}$  ratio changes the scan line slope and controls the mass number pass band. If the pass band is wide, adjacent mass numbers are stable, and resolving power is poor. Maximal resolving power is reached as the scan line approaches the apex (a definition of "resolving power" is given in section 3.6).

Illustrations of typical ion trajectories were given in fig.2.9.

## 3.5 ION DETECTION SYSTEM

### 3.5.1 Measuring system

Mass spectrometers have an electrical measuring system to detect the ion beams emerging from the ion separator system. The ions hit a collector (a plate or a Faraday cup), and discharge via a resistor to earth. The potential difference created over the resistor is measured by an electronic amplifier. An electron multiplier (E.M.) is often used in respiratory mass spectrometry as a tool to amplify the initial current. The E.M. creates a current gain in the range of  $0.1 \times 10^6$  to  $10 \times 10^6$ .

### 3.5.2 Recording modes

The detected ion currents can be recorded in two ways, which yield the two operating modes of a respiratory mass spectrometer.

#### 3.5.2.1 Spectrum mode

Suppose a gas or gas mixture is sampled by a quadrupole mass spectrometer, while the ac voltage is linearly altered from its minimum to its maximum value. This linearly increasing voltage is called ramp voltage. According to the voltage setting, ions with a certain mass-charge ratio are detected. The relative abundances of the various ions are obtained when the output current is recorded as a function of the ramp voltage. This result forms the "mass spectrum", which is defined as the pattern of ion beam intensities against  $m/q$  values for a specific sample. An actual mass spectrum of  $N_2O$  is shown in fig.3.9.

#### 3.5.2.2 Selected ion monitoring mode

Instead of using a ramp voltage, a number of voltage steps may be applied to the quadrupole rods. At each step, only the current of ions with a specific  $m/q$  value is measured. A sequence of eight voltage steps creates a series of eight output signals, each being

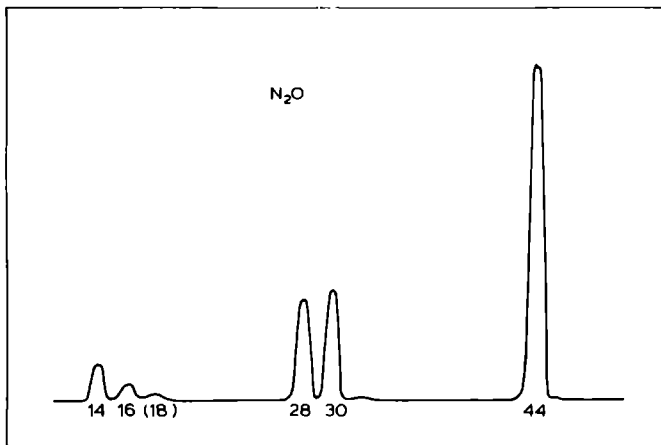


Fig.3.9: *Mass spectrum of N<sub>2</sub>O (from a cylinder for anaesthetic purposes) obtained with the quadrupole mass spectrometer Centronic 200 MGA (Redrawn from original recording).*

proportional to one of the selected ion species. If the voltage series is applied at a high frequency, e.g. 50 Hz, a virtually continuous measurement of eight ions is realized.

### 3.6 MASS SPECTROMETER PERFORMANCE

The *mass range* is the range of  $m/q$  values of the ions which can be detected by a mass spectrometer. This range depends upon the mass spectrometer design. Instruments can be built with a relatively small mass range, e.g. 2 to 50 u, or with a relatively wide range, e.g. 2 to 1000 u.

*Resolving power*: no universally accepted definition for resolving power is found in the literature. A possible definition may be given as follows. The width of an arbitrary peak in the mass spectrum is measured at 5% of the total peak height. If the  $m/q$  value of the arbitrary peak is  $M$ , and the measured peak width is  $\Delta M$ , then the resolving power is given as:  $R = M/\Delta M$ , where  $R$  is dimensionless. Since more ions are lost in a stronger resolving mass analyser, any



improvement in resolving power will reduce the sensitivity of the instrument.

### 3.7 HISTORY AND TYPES OF MASS SPECTROSCOPES

In the previous sections, attention was focused upon the quadrupole mass analyser. With history as a guide, other important types of mass spectrometers will be dealt with. No detailed description of the instruments will be given, since the discussion of the physico-chemical principles behind mass spectroscopy is felt to be sufficient to understand the operation of the described mass spectrometers. Additional information can be found in text books (Brunnee and Voshage, 1964; McDowell, 1963; Blauth, 1965).

#### 3.7.1 The parabola apparatus

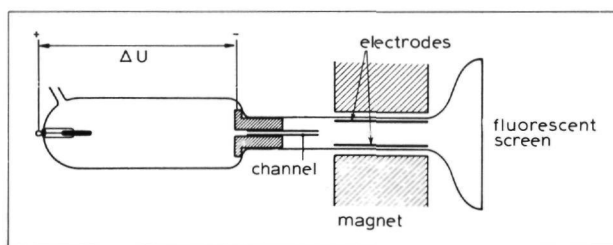
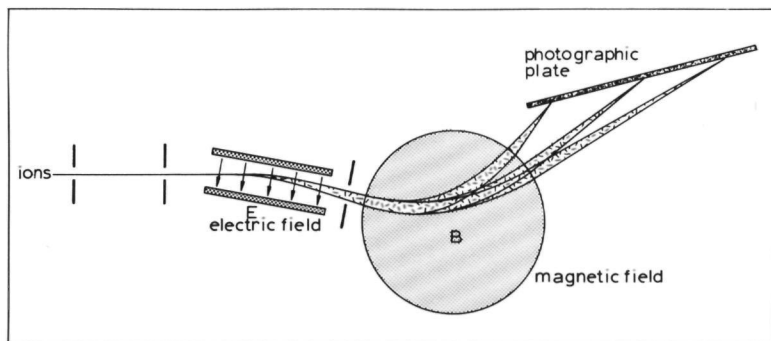


Fig.3.10: Thomson's parabola apparatus. The high voltage ( $\Delta U$ ) discharge tube is shown at the left. (After Farmer (McDowell, 1963), by courtesy of McGraw-Hill Book Company).

Thomson's apparatus is shown in fig.3.10. The gas under study was introduced into a low pressure, high voltage discharge tube, where the molecules were ionized and accelerated. The ion beam, strongly collimated by its passage through the channel in the cathode, was subjected to the simultaneous action of a magnetic and an electric field. A fluorescent screen or a photographic plate placed at a distance from the field acted as a detector. The behaviour of the ions

in the fields was already discussed. The parabola apparatus led to the discovery in 1912 of two neon isotopes.

### 3.7.2 Aston's mass spectrograph



*Fig.3.11: Diagram of Aston's first mass spectrograph. The electric field disperses the ions of the collimated initial beam according to their velocities, but independent of their  $m/q$  values. The magnetic field reverses this dispersion (velocity focusing), and at the same time separates ions according to their  $m/q$  values.*

A new type of positive ray apparatus was developed by Aston, and was called "mass spectrograph". The first was built in 1919, and two improved versions appeared in 1925 and 1937. Ions, generated in a discharge tube, were sent into a combination of a uniform electric field and a circular uniform magnetic field (fig.3.11). This design offered velocity focusing, whereas direction focusing was less required since angular divergence of the ions was minimized by strong collimation. Aston discovered that most of the elements had isotopes, and was able to calculate their abundances.

### 3.7.3 Magnetic field mass spectrometers

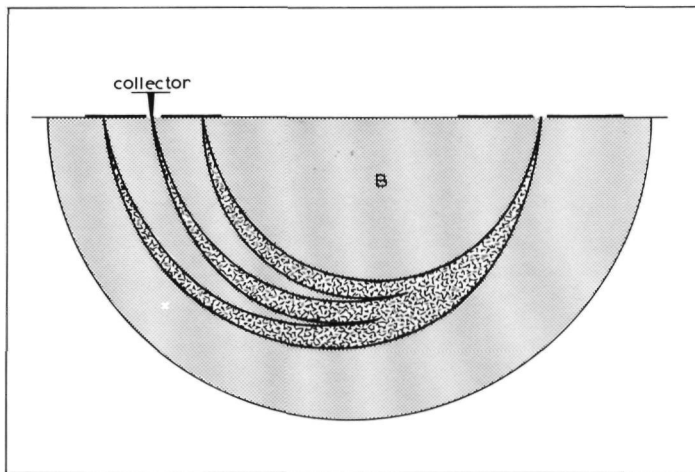


Fig.3.12: *Diagram of a Dempster-type mass spectrometer. An ion beam enters the magnetic field through a slit, and is resolved into three discrete beams. One discrete beam, containing ions with identical  $m/q$  values, reaches the collector via a second slit.*

Whereas Aston introduced the velocity focusing principle, Dempster in 1918 described the first mass spectrometer with direction focusing properties (fig.3.12). The unresolved ion beam, emerging via a slit from the ion beam source, is dispersed by a 180 degree uniform magnetic field. Ions of the discrete beams reach the collector via a second slit, and are detected by an electrical measuring system. The working principle is based on the "mass spectrometer equation" (eq.2.16). In this type of mass spectrometer, ions with different  $m/q$  values are focused on the collector, by varying the accelerating voltage or the magnetic field strength. Alternatively, different collectors are mounted in one instrument for simultaneous measurement of ions with different  $m/q$  values.

### 3.7.4 Dynamic mass spectrometers

The quadrupole mass analyser, described in chapter 2 and this chapter, is only one example of a new generation of mass spectrometers, i.e. the "dynamic mass spectrometers". The interested reader is referred to the book of Blauth (1965).

### 3.7.5 Double focusing mass spectroscopes

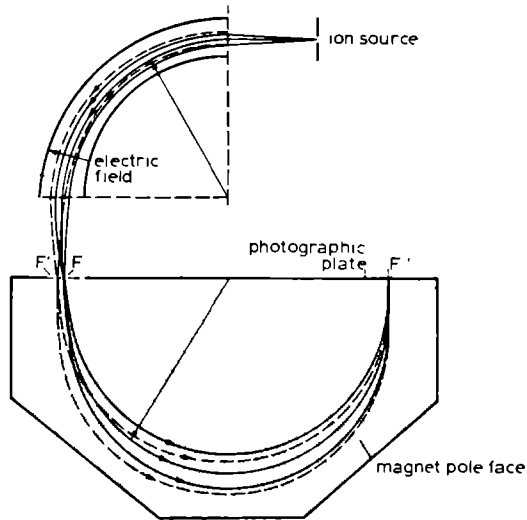


Fig.3.13: *Dempster's double focusing mass spectrograph. The trajectories of ions with a given  $m/q$  value are shown (From Tomlin, 1966, by courtesy of Blackie & Son Limited).*

Several methods improving mass resolving power have been used to compensate for the energy inhomogeneity and angular divergence of an ion beam produced in a real ion beam source. Aston's instrument used velocity focusing, but relied on strong collimation so that the discrete beam intensities were very small. So measurement of ion currents was impossible, and the discrete beams had to be recorded on a photographic plate, which could be exposed to the ion bombardment during a prolonged period.

The double focusing principle, known since 1929, offers high resolution on one hand, and high beam intensities on the other. A design due to Dempster (1935) will illustrate this principle. Fig.3.13 shows that a slightly divergent beam, containing ions of a given  $m/q$  value but with two different velocities, is focused in  $F$  and  $F'$  (compare with fig.2.6). At these points, the ion beams enter a 180 degree magnetic field. Its field strength yields a common focus  $F''$  for all ions of the given  $m/q$  value after deflection. Dempster's instrument yielded double focusing for one  $m/q$  ratio only. Later versions of double focusing mass spectrographs, e.g. the Mattauch-Herzog instrument, offered double focusing at all  $m/q$  values. These high-resolution mass spectrographs are needed, for instance, in the precision determination of atomic masses.

## RESPIRATORY MASS SPECTROMETRY AND ANAESTHESIA

This chapter reviews two types of problems encountered during the analysis of anaesthetic gas mixtures with a respiratory mass spectrometer. Possible solutions are discussed.

## 4.1 OUTPUT SIGNAL STABILITY

In respiratory physiology the composition of a gas mixture is given in terms of fractional concentrations of its components, referred to a dry gas mixture. The sum of the fractional gas concentrations equals unity by definition. Accordingly, gas analysers should preferably provide an output of fractional dry gas concentrations. In the case of a mass spectrometer, this is possible if a number of relationships has *constant* conversion factors. The chain of necessary conversions is illustrated in fig.4.1. These conversion factors may show not only long-term variations, i.e. in the order of minutes to hours, but also short-term variations, i.e. in the order of milliseconds to seconds. These variations generate output signal instability. The conversion factors and their possible variations are discussed further.

The conversion factor  $K_1$  between partial gas pressures at the sample site and partial gas pressures in the ionization chamber, is formed by the conductances of inlet capillary and molecular leak. These conductances may vary as a function of time by the deposition of particles (water droplets, dust, soda lime). The conversion factor  $K_2$  depends on various factors (given in eq.3.2) which can be unstable in relation to time. This was treated in the section on ion beam source features in chapter 3. Factor  $K_3$  may vary as the gain may change in the ion detection and electron multiplying system in the course of time. Variations in these first three conversion factors result in long-term instability.

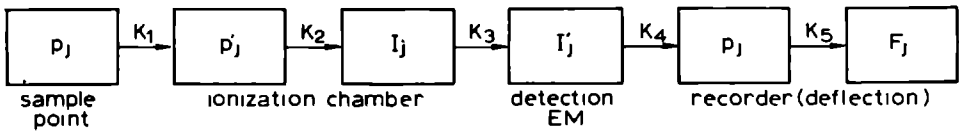


Fig.4.1: *The chain of conversion factors ( $K_j$ ) in respiratory mass spectrometry. The partial pressures of the sample gases are proportionally reduced to lower pressures in the ionization chamber. An ion current proportional to each partial gas pressure is generated and detected (E.M. = electron multiplier). The output signal, which is directly proportional to the partial sample gas pressure, is converted to a fractional dry gas concentration under the conditions given in the text.*

The measured ion currents are converted via conversion factor  $K_4$  to partial pressures, which form the normal output of a respiratory mass spectrometer. The factor  $K_4$  determines the deflection on the recorder and is adjusted during the calibration of the instrument.

The partial pressures measured by the mass spectrometer are related to the fractional dry gas concentrations by the relationship:

$$F_j = \frac{p_j}{p_B - p_{H_2O}} \quad (4.1)$$

where  $F_j$  and  $p_j$  are the fractional dry gas concentration and the partial gas pressure of any component in a gas mixture;  $p_B$  and  $p_{H_2O}$  are the total gas pressure and the water vapour pressure of the mixture, respectively. The conversion of  $p_j$  into  $F_j$ , via the conversion factor  $1/(p_B - p_{H_2O})$ , is only possible if  $p_B$  and  $p_{H_2O}$  are known. If  $p_B$  and  $p_{H_2O}$  are changing in an unknown way during the respiratory cycle, exact breath-by-breath gas analysis in terms of fractional concentrations is impossible. These variations of  $p_B$  and  $p_{H_2O}$  are present during anaesthesia and are of the short-term type. Total gas pressure varies at the sample point by the use of controlled venti-

lation. Water vapour pressure not only fluctuates during the respiratory cycle, but also depends on temperature at the sampling site. Theoretically corrections could be made if  $p_B$ ,  $p_{H_2O}$ , and temperature could be measured continuously. However, the continuous determination of fast changes of water vapour pressure during the respiratory cycle, in phase with other gases, is difficult.

In conclusion, a solution must be found not only to improve long-term stability, but also to exclude short-term effects of changing total gas pressure and water vapour pressure. A possible solution for both problems is offered by the "automatic control system" or "automatic sensitivity control system" (ASC) described by Scheid et al. (1971). Their system is a fast version of the device introduced by Bargeton et al. (1970), who designed a system capable of achieving long-term stability.

Assuming that the sum of all partial pressures at the inlet is constant, it follows that the sum of the signals provided by the mass spectrometer must be constant. Since the fractional dry gas concentrations add up to unity by definition, eq.4.1 is rewritten as:

$$\sum F_j = \frac{\sum p_j}{p_B - p_{H_2O}} = 1 \quad (4.2)$$

By substituting  $K_5$  for  $1/(p_B - p_{H_2O})$ , eq.4.2 may be written as:

$$\sum p_j \times K_5 = 1 = \sum F_j \quad (4.3)$$

indicating that the partial pressure of each component is converted into its fractional dry gas concentration, independently of  $p_B$  and  $p_{H_2O}$  (or without knowing  $K_5$ ), if three conditions are fulfilled. Firstly, the partial pressure of each component must be multiplied by the same factor  $K_5$ ; secondly, the summated values must equal unity, and finally, all components must be present in the summation.

An electronic network capable to fulfill these conditions not only solves the problem of water vapour and varying total inlet pressure, but also provides long-term stability. Any deviation of



the sum of the partial pressures from unity, e.g. by a change in inlet capillary conductance, is suppressed by electronically adjusting the gain of the ion current detector.

## 4.2 SPECTRUM OVERLAP

Anaesthetic gas mixtures may be made up of many components. Each component produces a spectrum of mass peaks, e.g.  $N_2O$  has peaks at  $m/q$  values of 14, 16, 28, 30, and 44. The highest peak in the mass spectrum is called *base peak*, the others are *fragment peaks*. The base peak is not necessarily produced by the *molecular ion*, i.e. the ion formed by the removal of one electron from a molecule. The fragment peaks are produced by the *fragment ions*, i.e. the ions formed by the cleavage of one or more bonds in the molecular ion. For example,  $N_2O^+$  ( $m/q = 44$ ) is the molecular ion of nitrous oxide, and  $NO^+$  ( $m/q = 30$ ) is one of the fragment ions.

Each component may be measured at any of its peaks in the mass spectrum, but the highest signal-to-noise ratio is reached at the base peak which is normally the first choice for the analysis of a certain component. The spectra of the components, generally present in anaesthetic gas mixtures, are listed in table 4.1. It shows that the mass peaks of most of the tabulated components overlap, e.g.  $N_2O$  and  $CO_2$  have identical base peaks at 44, and  $N_2O$  produces a fragment peak at 28, which is the base peak of  $N_2$ . So measurement of most of the components in anaesthetic gas mixtures is complicated by the presence of other components.

The severity of these interference problems depends on the relative concentrations. For instance, suppose  $CO_2$  and  $N_2$  are measured during air breathing on 44 and 28, respectively; the fragment  $CO^+$  ( $m/q = 28$ ) generated by the carbon dioxide will interfere with the measurement of nitrogen. The relative abundance of the  $CO^+$  fragment to  $CO_2^+$  is about 10%. Therefore the measured  $N_2$  fractional concentration (0.73) during expiration ( $CO_2$  fraction  $\approx 0.05$ ) will have a small error (0.7%). The situation will be quite different if  $CO_2$  is measured at 44, while breathing a 2-to-1 nitrous oxide-oxygen mixture. During expiration, the  $CO_2$  signal will be inflated by the con-

Table 4.1: Mass spectra of some gases

*Peaks smaller than 1% of base peaks (\*) are omitted (From: Muysers and Smit, 1969).*

m/q	N <sub>2</sub>	O <sub>2</sub>	CO <sub>2</sub>	N <sub>2</sub> O
12			C <sup>+</sup>	
14	N <sup>+</sup>			N <sup>+</sup>
16		O <sup>+</sup>	O <sup>+</sup>	O <sup>+</sup>
28	N <sub>2</sub> <sup>+</sup> (*)		CO <sup>+</sup>	N <sub>2</sub> <sup>+</sup>
30				NO <sup>+</sup>
32		O <sub>2</sub> <sup>+</sup> (*)		
44			CO <sub>2</sub> <sup>+</sup> (*)	N <sub>2</sub> O <sup>+</sup> (*)

tribution of the high nitrous oxide concentration as both gases have their base peak at 44.

The problem of spectrum overlap can be overcome by measuring gases at m/q values which do not interfere. For instance, if N<sub>2</sub>O is measured by means of NO<sup>+</sup> at 30, CO<sub>2</sub> cannot contribute to the measurement of N<sub>2</sub>O. This solution is not always possible for all gases of interest and mostly yields a poorer signal-to-noise ratio as the fragment peaks are smaller than the base peaks. Analysis of CO<sub>2</sub> on 12 is possible, but the size of this peak is only 5% of the base peak. Moreover, the CO<sub>2</sub> concentration in respiratory gas mixtures is relatively low.

Another solution is provided by the use of a "spectrum overlap eraser" (SOE) (Davis and Spence, 1979). Interfering signals undermine the basic assumption that the sum of all fractional gas concentrations equals unity, and accordingly prevent the ASC to perform properly. The SOE is an electronic system which eliminates the interfering signals on one hand, and allows the use of the ASC system on the other hand. An example will explain the working principle of the SOE. First of all, the ratios between the mass peaks of a gas (e.g. the ratios between the peaks of N<sub>2</sub>O on 14, 16, 28, 30, and 44) are supposed to be constant. If a nitrogen-nitrous oxide mixture is analysed, and if N<sub>2</sub> is measured on 28 and N<sub>2</sub>O on 30, nitrous oxide

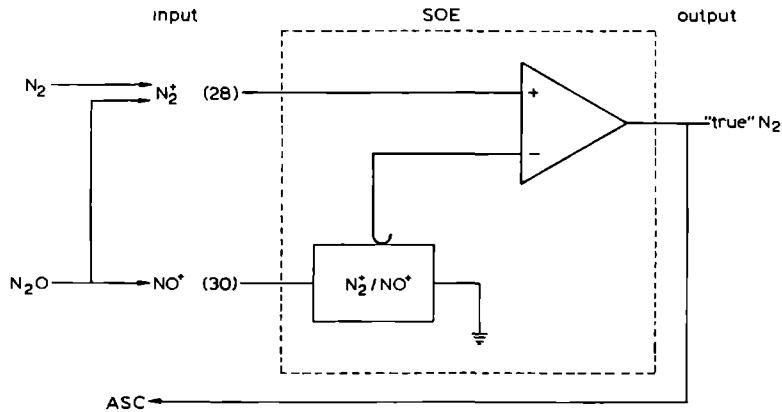


Fig.4.2: Principle of the spectrum overlap eraser (SOE) when  $N_2$  and  $N_2O$  are measured on 28 and 30 respectively. The interfering signal from the  $N_2^+$  fragment of  $N_2O$  is subtracted from the total signal on 28 in the operational amplifier, which yields the true  $N_2$  signal [the latter is returned to the automatic sensitivity system or ASC]. The potentiometer divides the  $NO^+$  signal according to the ratio  $N_2^+/NO^+$  produced by pure  $N_2O$ .

will contribute to the signal of nitrogen. The SOE provides the true amount of nitrogen by subtracting continuously the "interfering signal", caused by the nitrous oxide, from the total signal. The electronic circuit is shown in fig.4.2. The  $NO^+$  signal is fed to a potential divider, which divides the signal according to the ratio of peak 30 to peak 28, produced by pure nitrous oxide. The resulting signal (i.e. the "interfering signal") on one hand, and the total signal measured on 28 on the other, are fed to an operational amplifier where the two incoming signals are subtracted. The final output is the "true"  $N_2$  signal. The described circuitry can be extended for more interfering signals, e.g. from  $CO_2$  and halothane, and can be applied to every gas under study. Thus a logical electronic extension is to build a network with one channel for each gas of interest, e.g.  $N_2$ ,  $O_2$ ,  $CO_2$ , and  $N_2O$ . Each channel may have one input for each interfering signal.

Since the SOE makes electronic links between different channels, it has to be expected that the final output signal of each channel will be influenced by the quality of all input signals on that channel. Thus, calibration errors, nonlinearity, and noise on one channel are more or less transferred to the others. For further details, see chapter 5.

The presence of volatile anaesthetics in an anaesthetic gas mixture enlarges the problem of spectrum overlap, because they are cracked into many fragments interfering with the measurement of nitrogen (on 28), nitrous oxide (on 30), oxygen (on 32), and carbon dioxide (on 44). Moreover, halothane chemically produces  $\text{CO}_2$  inside the mass spectrometer: Graham et al. (1980) showed that  $\text{CO}_2$  production depends on the  $\text{O}_2$  concentration and the filament material. Furthermore, volatile anaesthetics may produce machine deterioration (Graham, Salamonsen, Kay et al., 1980).



---

## PART II

---

### Chapter 5: The equipment used

- 5.1 Description of the Centronic 200 MGA
- 5.2 Description of the rest of the equipment
- 5.3 Calibration procedure
- 5.4 Evaluation of the Centronic 200 MGA

### Chapter 6: Performance of long sampling tubes: theory

- 6.1 Introduction
- 6.2 Process model for tubes with uniform diameter
- 6.3 Process model for combined tubes

### Chapter 7: Performance of long sampling tubes: experiments

- 7.1 Experimental study in the laboratory
- 7.2 Experimental study in the operating theatre

### Chapter 8: Simultaneous monitoring of four patients

- 8.1 Sampling theory
- 8.2 System design
- 8.3 System evaluation
- 8.4 Discussion
- 8.5 Clinical applications
- 8.6 Conclusions

### Chapter 9: Future development: multi-part inlet line

- 9.1 Optimum radii for a tube with two parts
- 9.2 Optimum radii for a tube with more than two parts



## CHAPTER 5

### THE EQUIPMENT USED

This chapter describes the equipment used in the course of the study, the calibration procedure of the mass spectrometer, and the evaluation of the performance of the latter instrument, which was a quadrupole mass spectrometer Centronic 200 MGA Anaesthetic Model (Centronic Limited, Croyden, England).

#### 5.1 DESCRIPTION OF THE CENTRONIC 200 MGA

##### 5.1.1 General

This mass spectrometer is constructed according to the general design described in chapter 3, and incorporates an "anaesthetics module" offering the facilities of a spectrum overlap eraser (SOE) and an automatic sensitivity control system (ASC), described in chapter 4. The instrument is housed in a cabinet 0.62 m wide by 1.1 m high by 0.67 m deep, and weighs approximately 200 kg. It is mounted on four rubber castors which allow to move it easily. Eight gases can be measured (quasi-)simultaneously on eight channels.

All controls are situated at the front side of the instrument and are grouped in four sets: two sets are freely accessible, two sets are situated in a lockable drawer (see fig.5.1).

The top cover controls consist of four push buttons, four indicators, and one digital meter. The instrument is switched on from the off state by depressing the "standby-on" button, which starts the pump down sequence. When the pressure is reduced below 1 mPa, the mass spectrometer can be put into its operating mode by depressing the "operate" button. If the instrument is used regularly, it is kept in the standby position to preserve the high vacuum. Indicators warn for low flow through the inlet capillary ("inlet"), burnt out filament ("filament"), high pressure in the analyser sys-



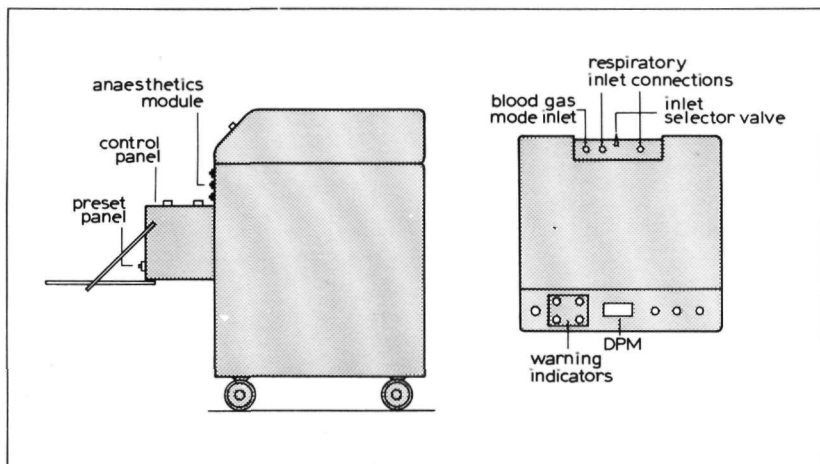


Fig.5.1: Schematic side and top view of the Centronic 200 MGA (DPM = digital panel meter).

tem ("Hi-Vac"), and low signal level ("sensitivity"). Activation of the "Hi-Vac" alarm causes a return to the standby mode. The digital panel meter (DPM) shows the  $m/q$  value of a channel selected on the control panel.

The "control panel" has controls for the overall adjustment of the instrument, and for adjustments of each of the eight channels (see fig.5.2). The overall sensitivity is set by varying the high voltage of the ion detector. Each channel has one control to select an  $m/q$  value (by varying  $V_{ac}$  and  $U$ ) and two controls for coarse and fine gain amplification. The DPM displays the chosen  $m/q$  value when the appropriate channel on the "channel selector" is selected. At the same time an analog meter on the control panel ("tuning indicator") shows the output signal of the selected channel. A toggle switch on the side of the drawer allows a spare filament to be used.

The "preset panel" contains the necessary input and output sockets and controls for spectrum mode purposes. In this situation, a scan unit provides the necessary ramp voltage, and an oscilloscope is connected to the mass spectrometer. Peak shape is optimized by adjusting resolving power and ion energy. Further controls on the

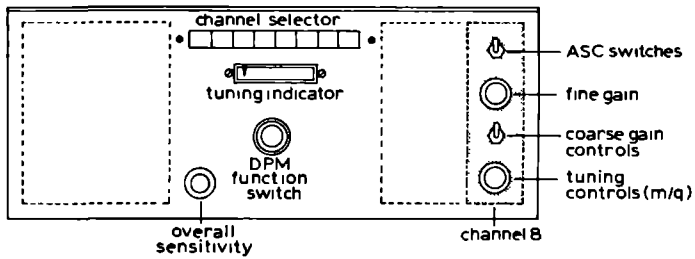


Fig.5.2: The control panel in the lockable drawer. The controls of only one channel are shown (DPM = digital panel meter).

preset panel allow to adjust ion focusing, electron emission, the overall amplification of all channels, and the quadrupole head amplifier zero. The principal operational units of the Centronic 200 (defined in fig.5.3) are now described in more detail.

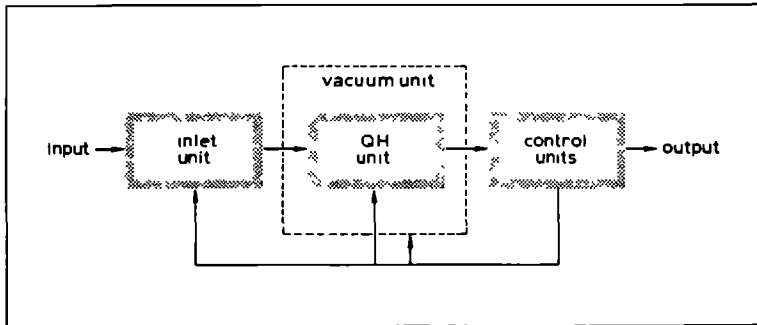
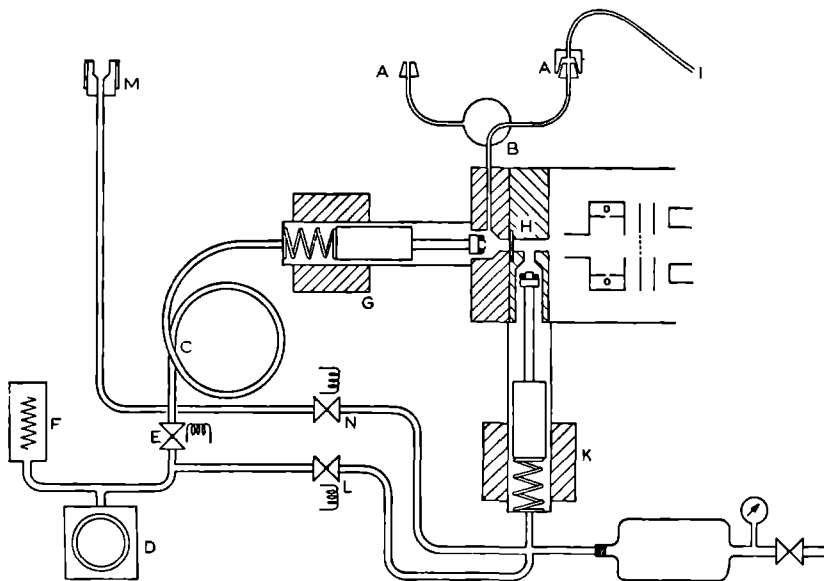


Fig.5.3: The principal units of the Centronic 200 MGA. The quadrupole head unit (QH unit) contains the systems for ion beam formation, mass filtering, and detection.

## 5.1.2 Inlet and vacuum unit



**Fig.5.4:** *Diagram of the inlet system of the Centronic 200 MGA. The blood gas mode inlet (M) is isolated from the rest of the system by three electromagnetic valves (N, L, K) (Copy from manual).*

These units are constructed according to figs.3.2 and 3.3. The flexible inlet capillary (I)<sup>1</sup> has a length of 1.25 m and samples approximately 20 ml.min<sup>-1</sup> (air). Two respiratory inlet terminals (A) are situated at the rear of the instrument for the connection of alternative capillary tubes. A selector valve (B) directs the gas flow to one of the two inlets, or shuts off the inlet system. A stainless steel tube forms the connection between inlet terminal and molecular leak (H). The latter is of the porous type and consists of sintered carbide. The pressure before the molecular leak is in the

<sup>1</sup> The capitals in the text refer to fig.5.4.

order of 1 kPa. The leak is sealed off by an electromagnetic valve (G) in the standby and off position. A large stainless steel tube (C) is fitted between leak and transport pump (D). A second valve (E) isolates this pump from the rest of the inlet system when the instrument is inoperative. Pressure at the inlet mouth of the pump is monitored by a Pirani gauge (F). Detection of too low a flow illuminates the warning indicator "inlet".

The high vacuum system consists of an air-cooled vapour stream pump backed by a fore-vacuum pump. A baffle cooled by a Peltier element is fitted between the analyser system and high-vacuum pump. A foreline oil trap containing activated alumina is placed between the two pumps. Baffle and oil trap prevent migration of vapour molecules or backstreaming of rotatory pump oil, respectively. Pressures in the high vacuum and fore-vacuum are monitored by a Penning and Pirani gauge, respectively.

### 5.1.3 Quadrupole head unit

The *ionizer section* has two identical rhenium filaments (the spare one can be switched on without opening the vacuum system). Electrons are accelerated by a potential difference of about 75 Volts; electron emission current is stabilized. Ions created in the ionizer section are focused and drawn into the analyser section with an energy of about 6 eV.

The *analyser section* consists of four stainless steel rods which are 0.127 m long and have a diameter of  $6 \times 10^{-3}$  m. The ac voltage has a frequency of  $2.4 \times 10^6$  Hz. The dc voltage is in the range from -1 to +180 V, and from +1 to -180 V. The ac/dc amplitude ratio is set by the resolution control. The quadrupole analyser tunes 50 times per second to another m/q value.

The *detection system* consists of an electron multiplier system. The ASC circuit controls the instrument sensitivity by varying the total accelerating voltage in the electron multiplier.

#### 5.1.4 Control units

Electronic circuits control all other units (see fig.5.3). The electronics controls the ionizer operation (filament and stabilization), the generation and timing of the ac and dc driving voltages, and the signal detection and processing.

The *vacuum control unit* has two functions: control of the pump down cycle of the vacuum system, and prevention of contamination of the analyser system by incorrect vapour stream pump operation or power failure.

The *anaesthetics module* consists of a four-channel three-input-per-channel SOE on one hand, and an eight-channel ASC system on the other. Each of the four SOE channels can be switched on or off, and each of the channels has three potentiometers for correction of interfering signals. The channels of the SOE are allocated and corrected as illustrated in table 5.1.

Table 5.1: Allocation of the mass spectrometer channels  
*The first four channels are incorporated in the anaesthetics module. Channel 5 is tuned to a volatile anaesthetic. Each of the first four channels is corrected by two or three of the other channels. Channel 6 to 8 may be tuned to other gases.*

---

channel	tuned m/q value	correction channels
1	28 (N <sub>2</sub> )	3/4/5
2	32 (O <sub>2</sub> )	3/4/5
3	44 (CO <sub>2</sub> )	2/4/5
4	30 (N <sub>2</sub> O)	2/5
5	51 (enflurane)	
6	40 (Ar)	

---

## 5.2 DESCRIPTION OF THE REST OF THE EQUIPMENT

### 5.2.1 The chart recorder

The Gould-Brush 481 Recorder is an analog recorder featuring eight 40 mm (50 divisions) channels, and sensitivities from one millivolt to 10 V per division. A pressurized ink system is used. Frequency response is flat from dc to 40 Hz full scale. This specification given by the manufacturer was checked: frequency response was flat to 50 Hz full scale. Paper speed can be varied in 12 steps from 0.05 to 200 mm.s<sup>-1</sup>; the 100 mm.s<sup>-1</sup> speed proved to be reliable.

### 5.2.2 The XY-recorder

The XY-recorder (Model BD 31 from Kipp & Zonen, Delft, Holland) uses DIN-A 3 graph paper. The recorder also plots signals against time. It has a lower frequency response than the Gould-Brush chart recorder: 0.5 s is needed to reach a deflection of 250 mm on the Y-axis.

### 5.2.3 The Minc computer and the tape recorder

The Minc computer system (PDP 11/23; Digital Equipment Corporation) with Analog-to-Digital Converter of the Lung Function Laboratory (head Prof. Dr H.H. Beneken Kolmer) was used for data acquisition, data analysis, data reduction, calculation, and text editing.

An eight-channel instrumentation recorder (Hewlett Packard 3968A) was used when on-line data acquisition was impossible.

### 5.2.4 The bubble flowmeter

The sample flow through the inlet lines was measured with the bubble meter method. The meter, illustrated in fig.5.5, consists of glass tube with an internal diameter of 26.2 mm. The sample gas is fed into the lower side arm and drawn off via a short length of large bore plastic tubing at the top. By squeezing gently the rubber bulb containing a detergent solution, the soap level is raised. The gas

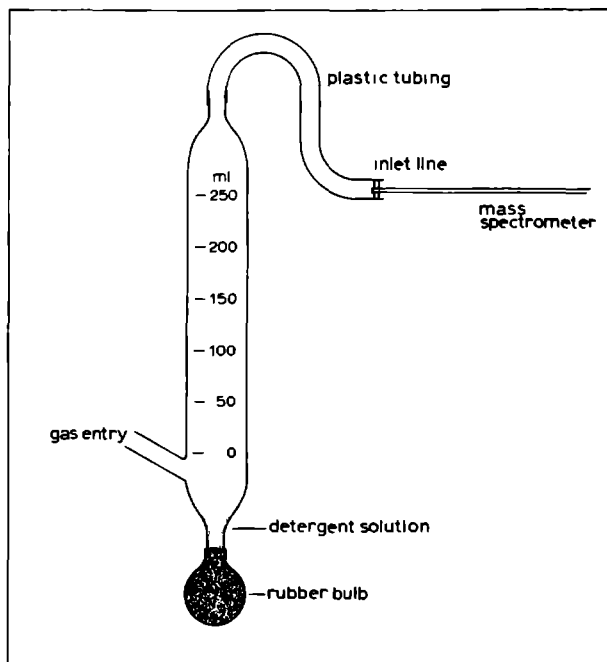


Fig.5.5: *The bubble flowmeter for the measurement of sample flow.*

flow, which urges the soap film (or bubble) up the glass tube, is made visible by the bubble raising in the tube.

The meter was calibrated according to Levy (Levy, 1964). Graph paper attached to the side of the meter shows reference marks. The volume between two marks is 50 ml. Timing the bubble over a known volume yields the sample flow. Gas tightness of the meter components was proved by helium detection.

### 5.2.5 The step change device

The device used to generate stepwise changes in partial gas pressure at the inlet of sampling tubes can be described as follows. It consists of two chambers with a volume of about 6 ml (see fig.5.6). Two independent systems deliver the desired gas mixtures to the gas entry of each of the two chambers, separated by a common wall with a

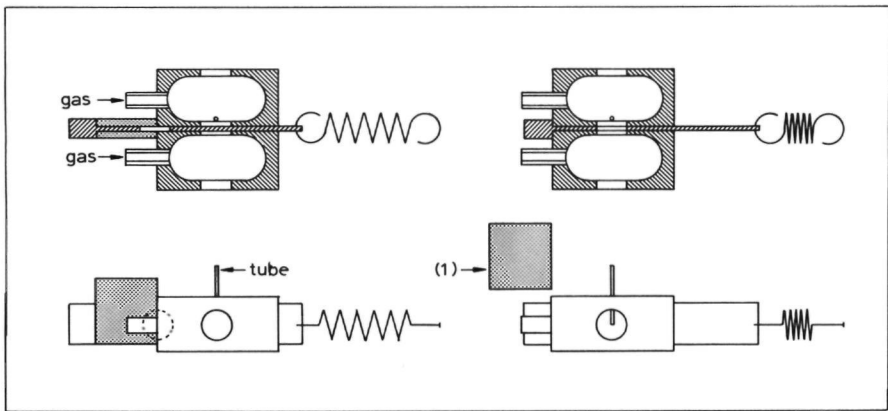


Fig.5.6: *The step change device in two views. Left: start position, right: position of rest. When the brake (1) is removed, the pierced plate slides into its position of rest and the gas flows from one chamber to the other, generating a stepwise change in partial gas pressure at the tip of the tube (Made and drawn by G. Toenders).*

hole. The tip of the sampling tube under study is fixed in front of the middle of this hole. A pierced plate sliding between the chambers prevents in its starting position any gas flow from one chamber to the other. One gas outlet is slightly obstructed to elevate pressure (+ 0.5 kPa) in the chamber where the tip of the tube is not situated. This higher pressure urges the gas through the hole if the pierced plate is in its position of rest. A step change is generated as follows. After removal of the brake, the spring swiftly pulls the plate into its position of rest where the plate operates a micro switch (not shown). The latter activates an electronic circuit generating a pulse signal which is used as trigger signal for data acquisition. Thus this signal defines the moment when the step change is produced.



### 5.3 CALIBRATION PROCEDURE

The output signals of the mass spectrometer are fed to the chart recorder. A suitable sensitivity is selected on each recorder channel, taking into account that the electrical output signal of the mass spectrometer is 10 V for a pure gas. After sampling air for one hour, the instrument is calibrated as follows (halothane is used as an example of a volatile agent). The SOE channels are switched on.

1. The chart recorder channels are set to zero.
2. The quadrupole head amplifier is set to zero.
3. The mass spectrometer channels are tuned as follows:
  - channel 1 to  $m/q = 28$  ( $N_2^+$ ) sampling room air,
  - channel 2 to  $m/q = 32$  ( $O_2^+$ ) sampling room air,
  - channel 3 to  $m/q = 44$  ( $CO_2^+$ ) sampling 100%  $CO_2$ ,
  - channel 4 to  $m/q = 30$  ( $NO^+$ ) sampling 100%  $N_2O$ ,
  - channel 5 to  $m/q = 117$  ( $HC_2F_3Cl^+$ ) sampling 1% halothane,
  - channel 6 to  $m/q = 40$  ( $Ar^+$ ) sampling room air.
4. Sampling room air, following adjustments are made:
  - a. the sensitivity is set for channel 1 to give about 7.5 V,
  - b. the fine gain controls are adjusted to give:
    - 7.82 V for channel 1 ( $N_2$ ),
    - 2.09 V for channel 2 ( $O_2$ ),
    - 0.09 V for channel 6 ( $Ar$ ).
5. Sampling 100%  $CO_2$ , the fine gain on channel 3 is set to give 10 V.
6. Sampling 100%  $N_2O$ , the fine gain on channel 4 is set to 10 V.
7. Sampling 1% halothane in a 1/1 mixture of  $N_2O/O_2$ , the fine gain on channel 5 is set to give 0.1 V.
8. Sampling 100%  $N_2O$ , the signals on channel 1 and 3 are corrected (set to zero).

9. Sampling 100% CO<sub>2</sub>, the signals on channel 1 and 2 are corrected (set to zero).
10. The channels 1 to 6 of the anaesthetics module are switched on.

The calibration procedure is checked with a gas mixture containing 30% N<sub>2</sub>, 30% O<sub>2</sub>, 6% CO<sub>2</sub>, 33% N<sub>2</sub>O, and 1% halothane (L'Air Liquide, Belgium). This calibration is satisfactory for mixtures containing low levels of halothane. Otherwise, 5% halothane should be presented to the inlet, and corrections made.

## 5.4 EVALUATION OF THE CENTRONIC 200 MGA

The Centronic 200 MGA was tested on the following points:

- static accuracy: linearity and stability,
- dynamic accuracy: noise and frequency response,
- performance of the anaesthetics module,
- influence of viscosity changes,
- resolving power.

During these tests the Centronic inlet capillary was used, except for the stability test.

### 5.4.1 Static accuracy

#### 5.4.1.1 Linearity

Two distinct methods were used to evaluate the linearity for N<sub>2</sub>, O<sub>2</sub>, CO<sub>2</sub>, N<sub>2</sub>O, and Ar. For the first method, a number of dry calibrated binary gas mixtures containing N<sub>2</sub> and O<sub>2</sub>, or N<sub>2</sub> and CO<sub>2</sub> (prepared in the Institute of Physiology, Nijmegen, head Prof. Dr F.J. Kreuzer) were fed sequentially to the mass spectrometer. Calibration curves showing the relationship between partial gas pressure and deflection on the recorder, were made for O<sub>2</sub>, N<sub>2</sub>, and CO<sub>2</sub>. The tuned m/q values were 32, 28, and 44, respectively. During all linearity tests the

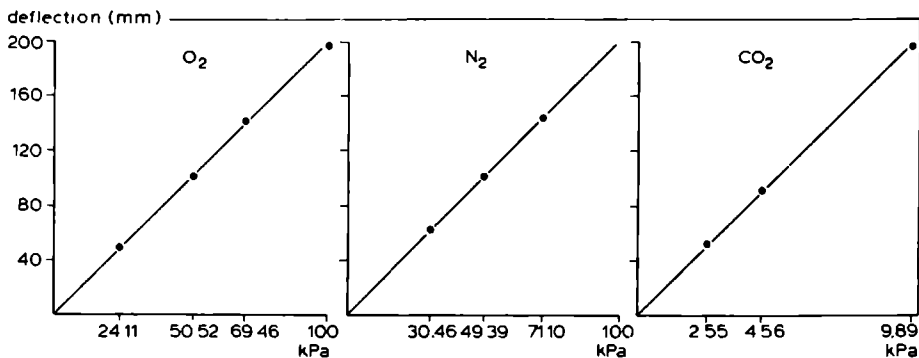


Fig.5.7: Calibration curves for  $N_2$ ,  $O_2$ , and  $CO_2$  obtained with calibrated binary gas mixtures.

ASC system was switched off, since this circuit automatically puts the sum of the two fractional gas concentrations equal to 1. Without the ASC system the mass spectrometer measures partial gas pressures (see chapter 4). The fractional gas concentrations of  $O_2$  and  $CO_2$ , measured by a Scholander apparatus, were converted to partial gas pressures (by means of eq.4.1 where  $p_{H_2O} = 0$  and  $p_B = 100$  kPa, i.e. atmospheric pressure at the time of the measurement). Linearity for  $O_2$  and  $N_2$  was tested over a range from 0 to 100 kPa, and for  $CO_2$  over the range from 0 to 10 kPa. Deflections were noted 30 s after the change to a new gas mixture; between the calibration gas mixtures, room air was sampled during at least 60 s. Fig.5.7 shows that the output signals were nearly linear over the range studied. The greatest deviation from linearity encountered was smaller than 2%.

At the moment of the study, no calibrated binary gas mixtures containing  $N_2O$  or Ar were available. The alternative method used to evaluate linearity is described now. Suppose a dry binary gas mixture containing a component X and a component Y is sampled at atmospheric pressure. The partial pressures of component X and Y are recorded on the x and y-axis, respectively, of an XY-recorder. The sum of the partial gas pressures of the two components is constant and equals atmospheric pressure ( $p_B$ ). The ratio of the two partial

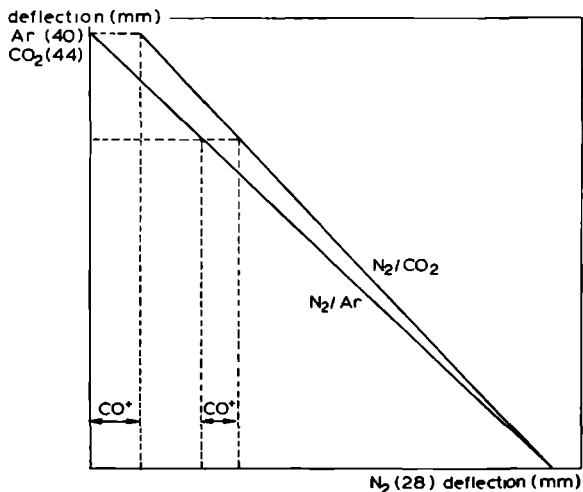


Fig.5.8: Calibration curves for the mixtures  $N_2/CO_2$ , and  $N_2/Ar$  obtained with the alternative method which recorded the continuously varying partial gas pressure of each component of the binary mixtures on one of the two axes of an XY-recorder. The anaesthetics module was switched off. Constant mass spectrum overlap is shown with the  $N_2/CO_2$  mixture.

gas pressures ( $p_X/p_Y$ ) can slowly be changed by turning the rotameters delivering the pure components. If the XY-recording provides a straight line ( $p_X + p_Y = p_B$ ), and there are no interferences on the tuned  $m/q$  values, linearity can be assumed for both components. The following mixtures were used:  $N_2/O_2$ ;  $N_2/Ar$ ;  $N_2/CO_2$ ;  $CO_2/Ar$ ;  $N_2O/N_2$ . The tested range was from 0 to 100 kPa. The tuned  $m/q$  values for  $N_2$ ,  $O_2$ ,  $CO_2$ ,  $N_2O$ , and Ar were 28, 32, 44, 30 ( $NO^+$ ), and 40, respectively. The mixtures  $N_2/O_2$ ,  $N_2/Ar$ , and  $CO_2/Ar$  have no interfering signals on the tuned  $m/q$  values.

However, if the XY-recording provides a straight line and if there are interfering signals on the tuned  $m/q$  values, not only linearity is proven, but a constant ratio of the peaks in the mass spectrum must also be assumed. Fig.5.8 shows the XY-recording of the mixtures  $N_2/CO_2$  and  $N_2/Ar$ , which proved to be essentially

linear. Thus, linearity of  $N_2$ , Ar, and  $CO_2$  must exist and  $CO^+$  must be produced in a constant proportion to  $CO_2^+$ .

All XY-recordings were mathematically analysed as follows. Fifteen points on the "curves" were chosen:

- five points with  $X < 40$  kPa, and  $Y > 60$  kPa,
- five points with  $40 < X < 60$  kPa, and  $40 < Y < 60$  kPa,
- five points with  $X > 60$  kPa, and  $Y < 40$  kPa.

Regression lines were calculated for:

- all points
- points with  $X > 60$  kPa
- points with  $Y > 60$  kPa
- points with  $X < 60$  kPa
- points with  $Y < 60$  kPa

False low values have been reported when sampling gas mixtures with high concentrations of Ar,  $CO_2$ ,  $N_2$ , and  $O_2$  (Gillbe, Heneghan, and Branthwaite, 1981). Therefore, the difference between the slopes of the regression lines fitted through points with  $X$  or  $Y > 60$  kPa on one hand, and through the rest of the points on the other hand, was evaluated as illustrated in fig.5.9.

From the results shown in table 5.2, it is concluded that linearity is well established for the tested gases ( $N_2$ ,  $O_2$ ,  $CO_2$ , Ar, and  $N_2O$ ) in the range from 0 to 100 kPa. This technique provides a method for preparing gas mixtures. To evaluate this, an XY-recording was made with a mixture of  $CO_2/N_2$ . At a certain point the turning of the rotameters was stopped, and a sample of the mixture was taken in a glass syringe. The mass spectrometer reading for  $CO_2$  was 11.47 kPa. A Scholander analysis gave 11.45 kPa ( $p_B = 100$  kPa).

#### 5.4.1.2 Stability

Stability was tested during operation in the operating theatre with the ASC system "on" since the instrument is meant to be used with this system. Every hour the output voltage of the mass spectrometer for  $N_2$  and  $O_2$  was read on a digital voltmeter, while room air was sampled through the same inlet line as used for sampling from the anaesthetic circuit (this line is described in chapter 6). Stability

Table 5.2: Linearity of the Centronic 200 MGA

Values for the intercept A, the slope B and the correlation coefficient (CC) of the regression lines which were fitted through the various groups of points, according to the equation  $y = A+Bx$ . The calculation of  $\Delta x\%$  and  $\Delta y\%$  is illustrated in fig.5.9.

X /Y	Points	A	B	CC	$\Delta x\%$ or $\Delta y\%$
N <sub>2</sub> /O <sub>2</sub>	all	205.9	-1.013	-0.999987	
	N <sub>2</sub> > 60 kPa	208.2	-1.025	-0.999845	-0.08
	N <sub>2</sub> < 60 kPa	206.0	-1.015	-0.999967	
	O <sub>2</sub> > 60 kPa	205.7	-1.000	-0.999833	-0.06
	O <sub>2</sub> < 60 kPa	205.6	-1.011	-0.999976	
CO <sub>2</sub> /Ar	all	207.4	-1.002	-0.999996	
	CO <sub>2</sub> > 60 kPa	209.3	-1.010	-0.999949	+0.03
	CO <sub>2</sub> < 60 kPa	207.1	-0.999	-0.999993	
	Ar > 60 kPa	207.2	-1.005	-0.999952	-0.24
	Ar < 60 kPa	206.7	-0.996	-0.999998	
N <sub>2</sub> O/N <sub>2</sub>	all	205.5	-0.846	-0.999986	
	N <sub>2</sub> O > 60 kPa	207.7	-0.858	-0.999918	+0.34
	N <sub>2</sub> O < 60 kPa	205.4	-0.844	-0.999974	

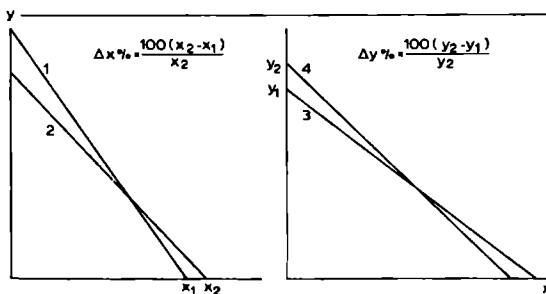


Fig.5.9: Mathematical analysis of the calibration "curves" obtained with the alternative method. Regression lines were fitted through the points with  $X > 60$  kPa (1),  $X < 60$  kPa (2),  $Y > 60$  kPa (3), and  $Y < 60$  kPa (4). Results are listed in table 5.2.

was tested in the operating theatre, because overall stability of the instrument not only depends on the factors described before, but also on the inlet system stability which is challenged by sampling wet respiratory gases. The results ( $N_2$ : 7.80, 7.79, 7.81, 7.83, 7.81 V, and  $O_2$ : 2.08, 2.07, 2.07, 2.05, 2.06 V) show that stability is satisfactory for clinical use (the electrical output signal of the mass spectrometer is 10 V for a pure gas).

#### 5.4.2 Dynamic accuracy

##### 5.4.2.1 Frequency response

The frequency response of a mass spectrometer can be measured by generating a stepwise change in partial gas pressure at the sampling point of the inlet capillary. The resulting electrical output signal as a function of time is termed "step response" and shows two intervals (see fig.5.10):

- (1) *transit time*: the time taken by a gas front to travel down the capillary,
- (2) *response time*: the time necessary for the output voltage to pass from 10% to 90% of the difference between its initial and final value. The response time is related to the highest frequency of the respiratory signal that can be handled by the mass spectrometer.

Using the Centronic 1.2 m inlet capillary, the Centronic 200 MGA had a transit and response time for a stepwise change of  $N_2$  of 0.216 and 0.064 s, respectively. A report of methods and results for other gases will be given in chapter 6.

##### 5.4.2.2 Noise

Noise was within the limits given by the manufacturer when room air was sampled. A lower signal-to-noise ratio was found on the  $CO_2$  channel when  $CO_2$  was measured in  $N_2O$ : see section 5.4.3.

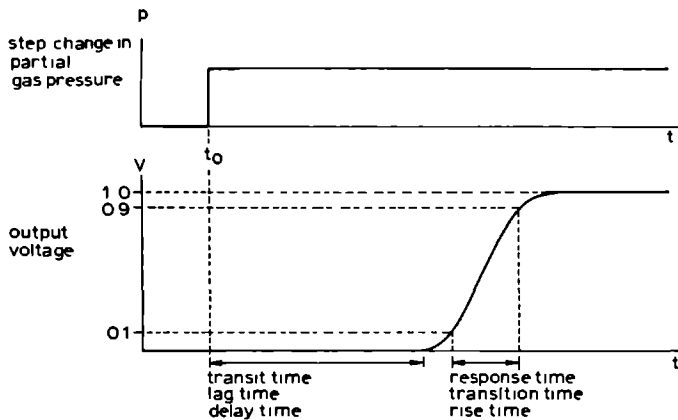


**Fig.5.10:** *Time intervals recognizable in the electrical output signal after a stepwise change in partial gas pressure produced at  $t_0$ . Frequently used synonyms are shown.*

### 5.4.3 Performance of the anaesthetics module

The anaesthetics module may influence both static and dynamic accuracy. Owing to the electronic links of the circuits, errors on one channel are spread over all channels in the summing circuit (ASC) or are transferred completely to one or more channels (SOE). The performance of the module was evaluated on three points: its ability to compensate for varying total pressure at the sample inlet, its influence on static accuracy, and its influence on dynamic accuracy.

#### 5.4.3.1 Compensation of varying inlet pressure

Simultaneous recordings of the total pressure at the sample inlet and of the output signal of one channel are shown in fig.5.11. The total pressure at the sample point was varied while the mass spectrometer was sampling a  $N_2/O_2$  mixture.



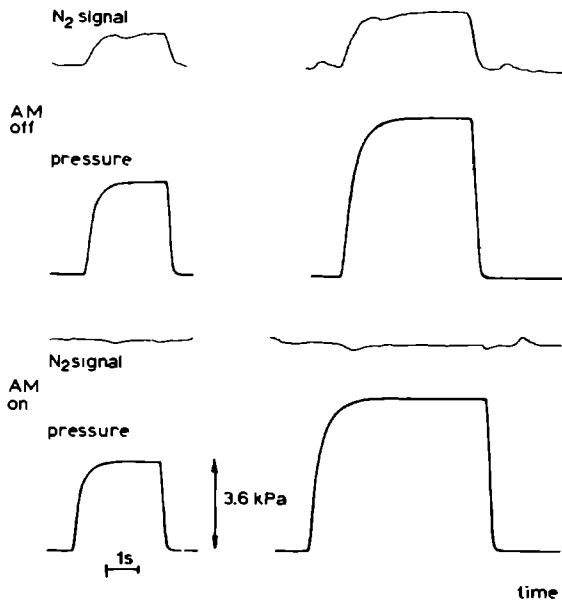


Fig.5.11: *The nitrogen signal is directly proportional to the applied total pressure at the sample point when the anaesthetics module (AM) is switched off (top). Compensation is realized when the module is on (bottom).*

#### 5.4.3.2 Influence on static accuracy.

In the course of a calibration procedure as described above, errors may occur owing to several causes. These may be considered under three headings: (1) zero-offset errors, (2) gain errors, (3) correction errors.

With regard to (1), suppose an unknown zero-offset be present on one or more channels when the chart recorder is zeroed and the mass spectrometer is calibrated. Consequently all (unknown) offsets are summated when the anaesthetics module is switched on, and a faulty conversion factor will result for all gas components in the summing circuit. This was experimentally confirmed.

In two cases an important zero-offset was due to the malfunctioning of a potentiometer in the SOE circuits (once in the N<sub>2</sub>O, and once in the CO<sub>2</sub> channel). Normally, a zero offset on any of the four SOE channels may be cancelled out with these potentiometers. The procedure used to minimize zero-offset was as follows. Firstly, zero-offset was minimized on the channels which are not included in the SOE, using the head amplifier zero knob. Secondly, the potentiometers were adjusted to minimize zero-offset on the four SOE channels. A digital voltmeter or an oscilloscope was used to measure the output signal.

With regard to (2), a faulty adjustment of the gain on one channel does not only lead to a measurement error on that particular channel, but also to errors on all channels in the summing circuit when the ASC is on. Errors in reading on the chart recorder are about 1% of full scale. Thus if six channels are used, a total error of about 3% maximally is introduced into the summing circuit. However, the total error is split up over all channels. Faulty gain adjustment also leads to an overcorrection or undercorrection for spectrum overlap. If the gain for nitrous oxide, measured on 30, is misadjusted, the zeroing of CO<sub>2</sub> on 44 also is incorrect. The latter adjustment was rendered particularly difficult because of the noise introduced by N<sub>2</sub>O on the CO<sub>2</sub> channel.

Lastly, the zeroing of the N<sub>2</sub>, O<sub>2</sub>, and CO<sub>2</sub> channels during corrections for spectrum overlap is subject to errors because of the same errors as mentioned for the gain adjustment.

#### 5.4.3.3 Influence on dynamic accuracy

A low signal-to-noise (S/N) ratio of 10:1 was seen on the CO<sub>2</sub> channel when mixtures containing N<sub>2</sub>O were sampled. The noise on the CO<sub>2</sub> signal results from the noise on 44 and on 30. When a nitrous oxide free gas mixture was sampled, e.g. air, noise almost disappeared (see for illustration fig.7.8). The use of a chart recorder with a smaller frequency response than the Gould-Brush 481 will attenuate noise (confirmed experimentally).

It will be shown in chapter 6 that response times of different gases influence each other as a result of the summing circuit in the anaesthetics module.

#### 5.4.4 Viscosity changes

Steady-state errors were evaluated as follows. The CO<sub>2</sub> output signal of the mass spectrometer sampling a calibrated gas mixture with 4.71% CO<sub>2</sub> (Scholander analysis) in air, was recorded on the chart recorder. Then a mixture of CO<sub>2</sub> in Ar was sampled: carbon dioxide was mixed with argon until the signal from the CO<sub>2</sub> channel equaled the signal of the CO<sub>2</sub> in air. A sample of the CO<sub>2</sub>/Ar mixture was analysed by the Scholander apparatus, which yielded 4.80% CO<sub>2</sub>. The difference is within the errors of the procedure.

#### 5.4.5 Resolving power

One of the attractive features of the quadrupole mass analyser, i.e. adjustable resolving power, was used to find a compromise between resolving power and sensitivity. In this study mass peaks always differed at least 2 u. The resolving power was adjusted until the peaks had rounded tops on one hand, while peaks differing 2 u were nearly completely resolved on the other hand. The calculated resolving power in the fig.3.9 is 28, measured at 5% of the 44 peak height.

## PERFORMANCE OF LONG SAMPLING TUBES: THEORY

## 6.1 INTRODUCTION

Varying partial pressures of respired gases are used as input signal for the mass spectrometer recording system. This *respiratory input signal* is transformed into a visible curve by the instrument system as a whole, ranging from the tip of the sampling tube to the output display, e.g. a chart recorder. The static and dynamic accuracy of the instrument system is determined by the features of its components (Fry, 1960; Gielen, 1971). The performance of the first component, i.e. the inlet line, is given by three parameters mutually related: transit time, response time, and sample flow. Transit time and response time are inversely proportional to sample flow. However, these three "performance parameters" should be as small as possible for the following reasons.

A *short transit time* and a *short response time* of the total system guarantee a fast and accurate measurement of dynamic events. The highest frequency that can be handled by the system is related to its 10 to 90% response time by the equation (Skilling, 1968):

$$t_r \times f_{co} = 0.35 \quad (6.1)$$

where  $t_r$  is the 10 to 90% response time of the system, and  $f_{co}$  is its upper cut-off frequency. At this frequency the output signal amplitude falls to 70.7% of the true value (McCray and Cahill, 1973). Whenever transit or response times are measured, the results depend on the performance of the complete system. Transit times of the components are additive, but response times obey the equation:

$$t_r = \sqrt{(\sum t_i^2)} \quad (6.2)$$

where  $t_i$  is the response time of each component (Skilling, 1968).

A *small sample flow* is desired for five reasons. Firstly, the inlet system is less easily contaminated by particles (water droplets, dust, soda lime). Secondly, a higher sample flow corresponds to a higher pressure in the mass spectrometer. This may lead to faulty measurements (see section 3.3) or technical troubles, e.g. a rapidly burnt out filament. Thirdly, a sample flow, which is too high compared with the patient's minute volume, distorts the respired waveforms. Fourthly, a small sample flow is needed for monitoring low flow anaesthesia. Fifthly, the switching artifacts, which are due to the valves of a multi-patient inlet system, are related to the sample flow (chapter 8). Fowler (1969) reports that sample flow should be less than 1% of the respiratory minute volume of the subject under study.

Replacement of the sample capillary by an inlet line with other properties (geometry or material) will alter the performance parameters of the inlet system. Lengthening of the response time is caused by the factors which disturb the shape of a gas front before it enters the analyzer:

1. interaction between the gas phase and the sampling tube material (adsorption, absorption),
2. a dead volume in the inlet system, e.g. a valve,
3. molecular diffusion, convection (= flow of a medium), and decompression.

Signal transmission in long inlet lines is improved by minimizing the first two factors. Interaction between gas phase and tube can be avoided by selecting capillaries of appropriate material; when valves are needed in the inlet line, they should introduce minimal dead volume. If these first two factors have been eliminated, distortion of the respiratory signal is only dictated by the physical phenomena of convection, molecular diffusion, and decompression. Then the limit of improvement of signal transmission is reached. This physical limit can be calculated from a process model predicting the shape and the dimensions of the response for certain process inputs. The information provided by the model serves to judge the approach to this ideal limit, if a selection procedure between sam-

pling tubes of various materials and geometry is to be made by experimental observation. Differences between observed and calculated responses call for an explanation for the discrepancy. The shape of the experimental responses may help to explain the difference. It should be realized that the process model only predicts the response of part of the inlet system, i.e. the inlet line, whereas the total response time follows from eq.6.2.

In this chapter, a process model for tubes of two configurations will be described. Experimental results will be presented in the next chapter.

## 6.2 PROCESS MODEL FOR TUBES WITH UNIFORM DIAMETER

Long sampling tubes for respiratory mass spectrometry are similar to capillary gas chromatography columns. A mathematical model of the processes occurring within gas chromatography columns was described by Golay (1958). This model can be applied to inlet lines of a respiratory mass spectrometer, as reported previously (Cramers et al., 1981), if the factors related to adsorption are eliminated from the calculations.

### 6.2.1 Hagen-Poiseuille's law for fluids (liquids or gases)

The steady laminar flow of a fluid of constant density, i.e. incompressible flow, through a "very long" tube of circular cross-section is governed by the Hagen-Poiseuille law. In such a flow, a parabolic velocity distribution is established with a constant mean velocity ( $\bar{v}$ ), which equals half the maximum velocity ( $v_m$ ). This is illustrated in fig.6.1. The product of the area of the tube cross section and the mean velocity yields the volume rate of fluid flow, which is given as (Moore, 1962):

$$\frac{dV}{dt} = \frac{(p_i - p_o) r^4 \pi}{8 L \eta} \quad (6.3)$$

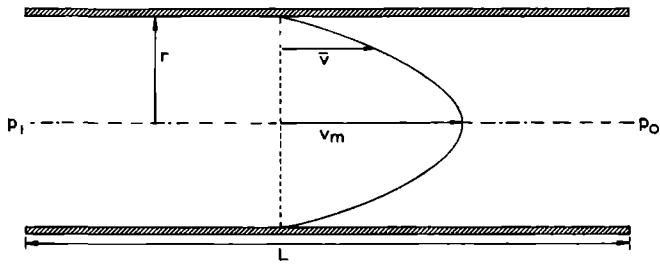


Fig.6.1: Laminar flow of a liquid in a tube with inlet pressure  $p_1$  and outlet pressure  $p_0$  establishes a parabolic velocity profile with a constant mean velocity  $\bar{v}$  that is half the maximum velocity  $v_m$ .

where  $V$  is the volume of fluid,  $t$  is time,  $p_1$  is the pressure at the inlet, and  $p_0$  at the outlet of the tube;  $r$  and  $L$  are the radius and the length of the tube, respectively, and  $\eta$  is the viscosity of the fluid. This formula is adapted for a gas stream, i.e. a compressible medium, in several steps.

Firstly, the pressure versus distance function is calculated. Eq.6.3 holds for gases if it is transformed into the differential form:

$$\frac{dV_x}{dt} = - \frac{dp_x}{dx} \times \frac{r^4 \pi}{8 \eta} \quad (6.4)$$

where  $x$  is the coordinate in the axial direction,  $V_x$  is the volume of gas at a distance  $x$  from the inlet, and  $p_x$  is the local pressure at  $x$ . The volume of gas is a function of pressure according to the law of Boyle-Mariotte given by:

$$p_x V_x = \text{constant} \quad (6.5)$$

Combining the eqs.6.4 and 6.5, integrating, and manipulating algebraically yield the pressure versus distance function given as:

$$p_x = p_i \sqrt{1 - \frac{x (P^2 - 1)}{L P^2}} \quad (6.6)$$

where  $P = p_i/p_o$ . This function is illustrated in fig.6.2, where a comparison is made with incompressible (liquid) flow.

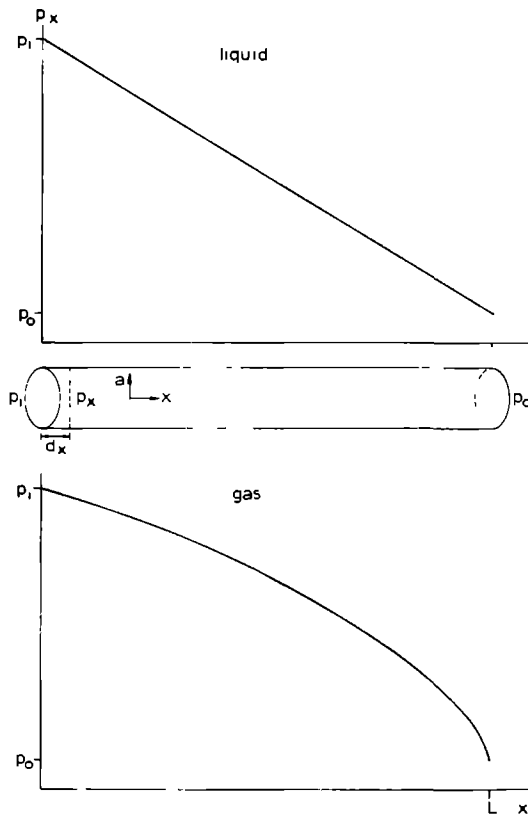


Fig.6.2: Pressure versus distance functions in a tube with length  $L$  for incompressible (liquid) and compressible (gas) flow. The ratio  $P (= p_i/p_o)$  is 10.



Secondly, the linear gas velocity is calculated. Gas velocity not only has a parabolic distribution in the radial direction of the tube, but also depends on the position in the axial direction, i.e. on local pressure. The velocity distribution in both directions is given as:

$$v_{ax} = - \frac{dp_x}{dx} \times \frac{(r^2 - a^2)}{4 \eta} \quad (6.7)$$

where a is the coordinate in the radial direction. Combining eqs.6.6 and 6.7, integrating over the distance x, and letting a = r/√2, yield the mean linear gas velocity at any position in the tube:

$$\bar{v}_x = \frac{p_i r^2}{16 \eta L} \times \left\{ \frac{(P^2 - 1)}{x (P^2 - 1)} \right\} \quad (6.8)$$

$$P^2 \sqrt{1 - \frac{L}{P^2}}$$

The relationships in eq.6.7 and eq.6.8 are illustrated in fig.6.3.

Lastly the volume rate of gas flow, or shortly gas flow, measured at any position in the tube, i.e. at the local pressure, is given as:

$$F_x = \bar{v}_x \pi r^2 \quad (6.9)$$

The gas flow measured at the inlet (x = 0 in eq.6.8) is given as:

$$F_i = \frac{\pi p_i r^4 (P^2 - 1)}{16 \eta L P^2} \quad (6.10)$$

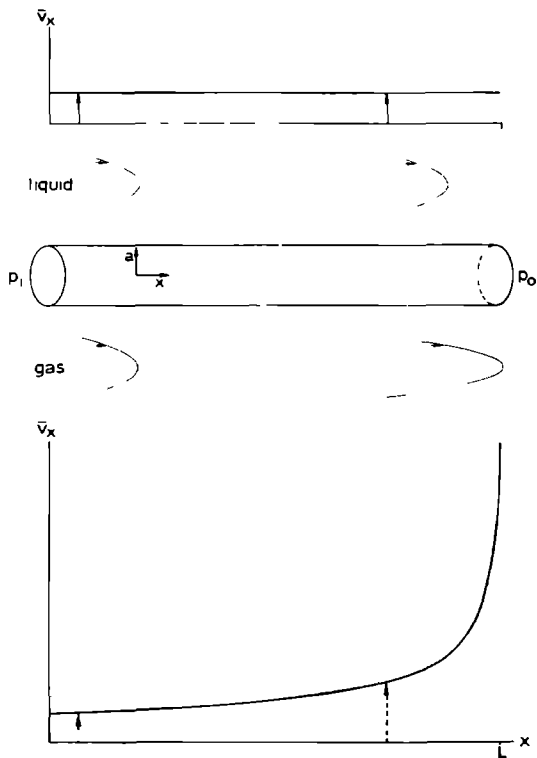


Fig.6.3: Mean velocity versus distance functions in a tube with length  $L$  for incompressible (liquid) and compressible (gas) flow. The ratio  $P (= p_i/p_o)$  is 10.

### 6.2.2 General formulae

A process model predicts the response (process output) of a system to a stimulus (process input). The system used for the model is not the real system that is to be described, but behaves like the real system under specified conditions. Certain process inputs are very useful from the combined viewpoint of experimental execution and mathematical analysis. These inputs are the "step", "pulse", and

"impulse" inputs as defined further. They are illustrated in fig.6.4 as functions of time (t).

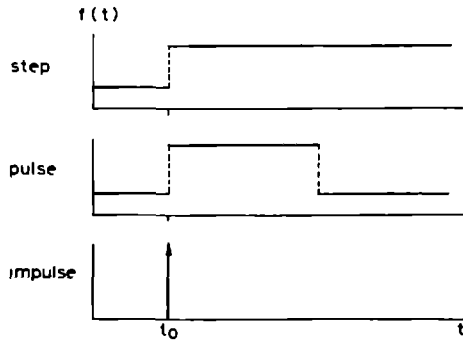


Fig.6.4: *Process inputs convenient for mathematical analysis of a process model.*

The "step" has one fixed value for  $t$  smaller than  $t_0$ , and another fixed value for  $t$  equal to or greater than  $t_0$ . A "pulse" input is a step input of finite duration returning to its initial value. An "impulse" input is the limit approached by a pulse input, when the duration of the pulse approaches zero, and the integral of the input with respect to time (= the area of the pulse) remains finite and constant. If the step jumps from zero to 1, or if the integral of the impulse equals 1, they are called "unit step" and "unit impulse" (= Dirac delta function), respectively. The delta function is the derivative of the step function (Riggs, 1970).

Gas molecules injected instantaneously into a carrier gas, which is flowing viscously through a tube, will spread in axial direction under the combined effects of:

- convection (producing a parabolic velocity profile)
- molecular diffusion (in radial and axial direction)
- decompression

The simultaneous action of convection and radial diffusion is called the "Taylor mechanism". Taylor (1953) showed that the dispersal of a soluble matter produced by convection is reduced by the effect of radial diffusion. His analysis was refined by Aris (1956) and Philip (1963), and formed the basis for the work of Golay (1958). The three effects mentioned are taken into account by the presented mathematical model, illustrated in fig.6.5.

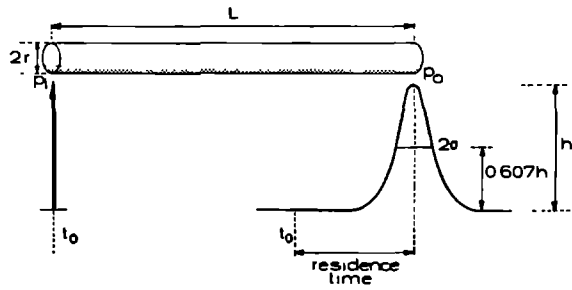


Fig.6.5: Schematic representation of the process model used in this study. A sample gas impulse, injected into a carrier gas stream flowing viscously through a tube, is distorted into a Gaussian function with standard deviation  $\sigma$ . Pressures at the inlet and outlet of the tube are  $p_i$  and  $p_o$ , respectively.

An impulse input is used for mathematical convenience. The impulse is broadening to a wider band, and accordingly the partial pressure versus time function assumes the shape of the Gaussian or normal distribution function, which has a variance given as (Golay, 1958; Giddings, 1964):

$$\sigma^2 = \left( 2 \frac{D_o}{\bar{v}_o} + \frac{\bar{v}_o r^2}{24 D_o} \right) f \frac{t_M^2}{L} \tag{6.11}$$

where  $D_o$  is the diffusion coefficient of the sample gas at tube outlet pressure,  $\bar{v}_o$  is the mean linear gas velocity at tube outlet pressure,  $t_M$  is the "residence time" (see fig.6.5), and  $f$  is

Giddings correction factor. The latter takes the decompression effect into account and is given as:

$$f = \frac{9 (P^4 - 1)(P^2 - 1)}{8 (P^3 - 1)^2} \quad (6.12)$$

The value of  $f$  varies between 1 ( $P = 1$ ) and  $9/8$  ( $P \rightarrow \infty$ ). In gas chromatography, it is common practice to use the parameter  $H$  (relative band broadening) instead of  $\sigma^2$  in determining band broadening;  $H$  is given as:

$$H = \sigma^2 \frac{L}{t_M^2} \quad (6.13)$$

The "residence time" of the gas peak maximum is given as (see fig.6.5):

$$t_M = \frac{L}{\bar{v}} \quad (6.14)$$

where  $\bar{v}$  is the average linear gas velocity, which is given as:

$$\bar{v} = f_2 \bar{v}_0 \quad (6.15)$$

where  $f_2$  is the James-Martin factor, which is given as (James and Martin, 1952):

$$f_2 = \frac{3 (P^2 - 1)}{2 (P^3 - 1)} \quad (6.16)$$

The average linear gas velocity  $\bar{v}$  is that velocity which produces a residence time equal to the residence time which could be attained by a constant mean velocity. Calculating  $\bar{v}_0$  from eq.6.8 ( $x = L$ ), and combining with eq.6.16 and eq.6.15, yield:

$$\bar{v} = \frac{3 r^2 p_i (P^2-1)^2}{32 \eta L P(P^3-1)} \quad (6.17)$$

For an ideal gas, the values of both the linear gas velocity and the diffusion coefficient at any position in the tube are inversely proportional to the local pressure. This is expressed as:

$$p_i \bar{v}_i = p_o \bar{v}_o = \bar{p} \bar{v} = \text{constant} \quad (6.18)$$

$$p_i D_i = p_o D_o = \bar{p} \bar{D} = \text{constant} \quad (6.19)$$

where  $\bar{v}_i$  is the mean linear gas velocity at tube inlet pressure,  $D_i$  and  $\bar{D}$  are the diffusion coefficients at inlet and average pressure  $\bar{p}$ , respectively. Combining eqs.6.15, 6.16, and 6.18 yields the average pressure:

$$\bar{p} = p_o \frac{2 (P^3-1)}{3 (P^2-1)} \quad (6.20)$$

From eqs.6.18 and 6.19 it follows that:

$$\frac{D_o}{\bar{v}_o} = \frac{\bar{D}}{\bar{v}} \quad (6.21)$$

Relative band broadening is found by combining eqs.6.11, 6.13, and 6.21:

$$H = \left( 2 \frac{\bar{D}}{\bar{v}} + \frac{\bar{v}_r^2}{24\bar{D}} \right) f \quad (6.22)$$

$\uparrow \quad \uparrow \quad \uparrow$   
 (1) (2) (3)

The three phenomena dictating the distortion of a gas front can be recognized in eq.6.22: molecular axial diffusion (1), "Taylor's

mechanism" (2), and decompression (3). Alternatively, the "apparent or measured band broadening" is derived from eq.6.13, and is given as:

$$\sigma = t_M \sqrt{\left( \frac{H}{L} \right)} \quad (6.23)$$

Thus the process model predicts that, after an impulse input, the process output has the shape of a Gaussian function with a standard deviation  $\sigma$ . Since an impulse function is the derivative of a step function, the process output after a step input will have the form of a "cumulative" or "integrated" normal distribution function, which is known as the normal probability integral. The relationship between normal distribution function and normal probability integral is clarified in textbooks (Defares, Sneddon and Wise, 1973), and is illustrated in fig.6.6. The 10 to 90% response time after a step input can be calculated in terms of  $\sigma$  (Wissenschaftliche Tabellen, Ciba Geigy):

$$t_r = 2.56 \times \sigma \quad (6.24)$$

### 6.2.3 Atmospheric inlet, vacuum outlet conditions

Under the conditions of respiratory mass spectrometry ( $p_i = p_B$ ,  $D_i = D_B$ ,  $P \gg 1$ ,  $f = 9/8$ ), the general formulae reduce to simpler equations.

Average linear gas velocity:

$$\bar{v} = \frac{3 r^2 p_B}{32 \eta L} \quad (6.25)$$

Average pressure:

$$\bar{p} = \frac{2}{3} p_B \quad (6.26)$$

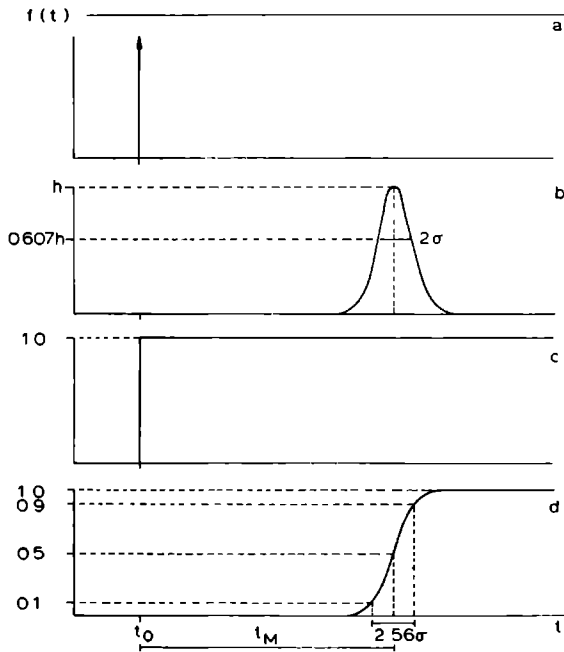


Fig.6.6: An impulse (a) or a step (c) input of the process model is transformed into a Gaussian function (b) or a normal probability integral (d), respectively.

Gas flow at the inlet:

$$F_B = \frac{\pi p_B r^4}{16 \eta L} \quad (6.27)$$

Substitution of eq.6.26 into eq.6.19 yields:

$$\bar{D} = \frac{3}{2} D_B \quad (6.28)$$



## 6.2.4 Calculation of performance parameters

A 70%/30%  $N_2O/O_2$  mixture at 298K was chosen as carrier gas mixture having a viscosity of  $16.54 \times 10^{-6}$  Pa.s, i.e. 0.89 times the viscosity of air (Nunn, 1977). The inlet pressure is 101325 Pa and P was taken 100, since the outlet pressure has a value approaching the pressure in the sample chamber ( $\approx 1$  kPa). For nitrous oxide and oxygen, the binary diffusion coefficient was calculated according to Fuller et al. (1966). For impulses of other gases, a ternary gas mixture exists and accordingly a ternary diffusion coefficient had to be calculated. The binary diffusion coefficient of the sample gas was calculated in  $O_2$  and in  $N_2O$ . Then a fraction-weighted (ternary) diffusion coefficient was calculated as follows:

$$D_x = 0.7D_{x,N_2O} + 0.3D_{x,O_2} \quad (6.29)$$

where  $D_x$  is the ternary diffusion coefficient of the sample gas x, and  $D_{x,N_2O}$  and  $D_{x,O_2}$  are its binary diffusion coefficients. A list of the various diffusion coefficients used in the present study is given in table 6.1. The performance parameters were calculated by means of a calculation program JOSUT2 written in Fortran (see fig.6.7): examples are given in tables 6.1, 6.2, and 6.3.

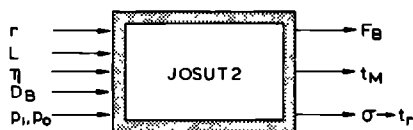


Fig.6.7: *Input and main output variables of the program JOSUT2.*

## 6.2.5 Discussion

Table 6.1 shows that the response time of a sample gas depends on its diffusivity (for a tube with a given geometry).

Table 6.1: Performance parameters of a 30 m line (0.58 mm i.d.)  
*Values of diffusion coefficients ( $D_B$ ), residence time ( $t_M$ ), sample flow ( $F_B$ ), and response times ( $t_r$ ) calculated for various sample gases.*

Sample gas	$D_B$ ( $\text{m}^2 \cdot \text{s}^{-1}$ )	$t_M$ (s)	$F_B$ ( $\text{ml} \cdot \text{min}^{-1}$ )	$t_r$ (ms)
N <sub>2</sub> O	$14.83 \times 10^{-6}$	18.64	17.02	155
O <sub>2</sub>	$14.83 \times 10^{-6}$	18.64	17.02	155
N <sub>2</sub>	$16.91 \times 10^{-6}$	18.64	17.02	147
CO <sub>2</sub>	$13.18 \times 10^{-6}$	18.64	17.02	163
Ar	$15.86 \times 10^{-6}$	18.64	17.02	151
HAL	$6.15 \times 10^{-6}$	18.64	17.02	231
ENF	$6.02 \times 10^{-6}$	18.64	17.02	233
ISO	$6.02 \times 10^{-6}$	18.64	17.02	233

Table 6.2: Performance parameters of a 2 m line  
*Values of the residence time ( $t_M$ ), sample flow ( $F_B$ ) and response time ( $t_r$ ), for a tube with a length of 2 m and various radii, calculated for CO<sub>2</sub> as sample gas.*

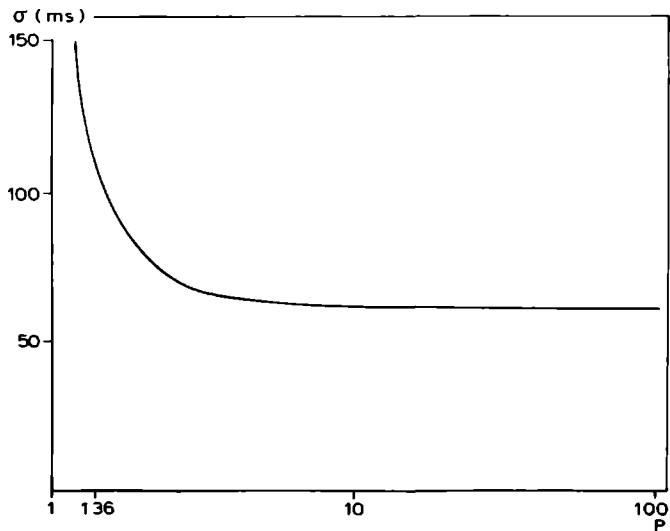
r (mm)	$t_M$ (s)	$F_B$ ( $\text{ml} \cdot \text{min}^{-1}$ )	$t_r$ (ms)
0.5	0.028	2255	10
0.25	0.112	140	10
0.2	0.174	58	10
0.15	0.310	18	11

Table 6.3: Performance parameters of a 20 m and a 40 m line  
*Values of the residence times ( $t_M$ ), sample flows ( $F_B$ ) and response times ( $t_r$ ), for tubes with lengths of 20 m and 40 m, and various radii, calculated for  $CO_2$  as sample gas.*

r (mm)	20 m			40 m		
	$t_M$ (s)	$F_B$ (ml.min <sup>-1</sup> )	$t_r$ (ms)	$t_M$ (s)	$F_B$ (ml.min <sup>-1</sup> )	$t_r$ (ms)
1.0	0.697	3608	104	2.786	1804	208
0.5	2.786	226	104	11.15	113	209
0.4	4.35	92	104	17.42	46	210
0.3	7.74	29	106	30.96	15	221
0.25	11.15	14	109	44.58	7	244
0.2	17.42	6	121	69.66	3	324

Table 6.2 shows that the contribution of a 2 m capillary is not of considerable importance to the total response time of a mass spectrometer capillary system, which is usually about 100 ms for commercially available respiratory mass spectrometers (Sodal, 1979). On the contrary, a 20 m or 40 m inlet line will increase the effective response time of the system, formed by the basic response of the instrument and the response time of the line (see table 6.3). Table 6.3 shows that, for a given length of tube, the increase depends on the radius. The expected effective response time can be calculated by means of eq.6.2, if the basic response of the mass spectrometer is known.

The relationships between some of the variables of the model will now be discussed for a 30 m inlet line. Fig.6.8 shows the relationship between signal distortion, determined by  $\sigma$ , and the ratio of inlet- and outlet pressure. In respiratory mass spectrometers P approximates 100, but a P of 1.36 is used by Ozanne et al. (1981) in order to store the respiratory signal in the long inlet line. Fig.6.8 shows that signal distortion minimally must be doubled by the latter sampling mode. This has been confirmed by the same



**Fig.6.8:** *Signal distortion ( $\sigma$ ) plotted against the ratio of inlet and outlet pressure ( $P$ ) of the tube. The semilogarithmic graph was calculated for a 30 m tube (0.5 mm radius) with  $CO_2$  as sample gas.*

authors, who reported that the "frequency response of stored data was halved" compared to direct data.

The relationship between  $\sigma$  and the diffusivity ( $D$ ) of sample gases used in clinical practice is shown in fig.6.9, which illustrates that the value of  $\sigma$  not only depends on  $D$  (first term in eq.6.11), but also on the relation of  $D$  to the radius of a given length of tube (second term in eq.6.11), and thus to the average linear gas velocity. So  $\sigma$  is not a monotonous function of  $D$ , as illustrated in fig.6.9 for the tube with the smallest radius: with increasing diffusivities,  $\sigma$  first falls to a minimum, then raises again. Accordingly, signal distortion of two sample gases, one with high, the other with low diffusivity, can be equal for a given geometry of the tube. However, their  $\sigma$  may be higher than for a sample gas with intermediate diffusivity. In clinical respiratory mass spectrometry, only the descending part of the curve is relevant where sample gases with the highest diffusivity have the lowest  $\sigma$ . This is due to the relations between the values of  $D$  and  $r$  which are

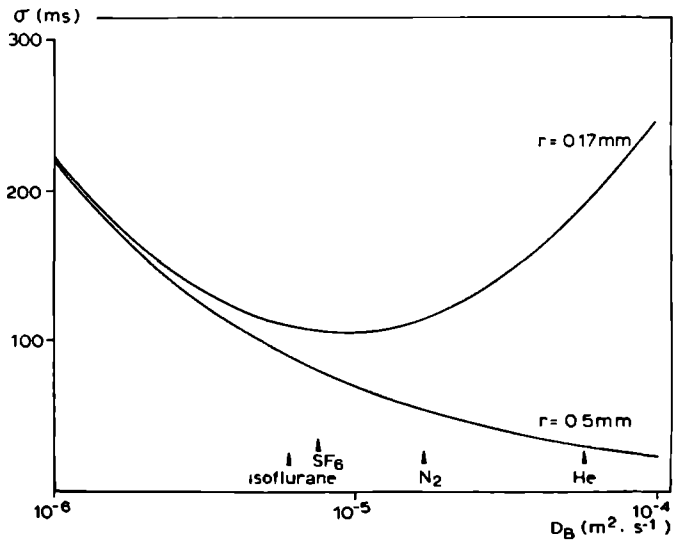


Fig.6.9: Signal distortion ( $\sigma$ ) as a function of the diffusion coefficient for two different radii in a 30 m tube. The diffusivities of gases and vapours used in clinical practice are indicated.

used in clinical practice. Tubes of relatively large diameters are chosen as inlet lines to ensure a short transit time. These relations will lead to a practical rule of thumb given now.

If a high average linear gas velocity exists in the inlet line, eq.6.22 reduces to:

$$H_s = \frac{\bar{v}_r^2}{24\bar{D}} f \quad (6.30)$$

where  $H_s$  is the "simplified" version of  $H$ . A "simplified" version of  $\sigma$  is found by combining eqs.6.14, 6.23, 6.25, and 6.30. If atmospheric inlet-vacuum outlet conditions exist, if the carrier gas is a 70%/30%  $N_2O/O_2$  mixture, and if atmospheric pressure equals 101325 Pa, then the "simplified" apparent band broadening is given as:

$$\sigma_s = 7.376 \times 10^{-6} \frac{L}{\sqrt{D_B}} \quad (6.31)$$

Eq.6.31 shows that the response time of an inlet line will depend only on its length and the diffusion coefficient of the sample gas considered. If a sample gas with an intermediate diffusivity such as nitrogen ( $D_B = 16.91 \times 10^{-6} \text{ m}^2 \cdot \text{s}^{-1}$ ) is chosen as sample gas, the combination of eqs.6.24 and 6.31 yields:

$$t_r \approx 0.0046 L \approx 0.005 L \quad (6.32)$$

Thus it can be concluded as a rule of thumb that the response time of an inlet line will increase 5 ms per metre (for gases with intermediate diffusivities). The response time estimated with this rule of thumb will differ less than 10% from the real value if the second term in eq.6.22 is five times greater than the first, or if:

$$\frac{\bar{v}_r^2}{24\bar{D}} > \frac{10\bar{D}}{\bar{v}} \quad (6.33)$$

Substitution of eq.6.25 into eq.6.33, manipulating algebraically, and substitution of the same values for viscosity, diffusion coefficient, and atmospheric pressure as mentioned above, yield:

$$\frac{L}{r^3} < 1.5 \times 10^{12} \quad (6.34)$$

If the condition of the last inequality, which guarantees a high average linear gas velocity, is fulfilled, the rule of thumb holds.

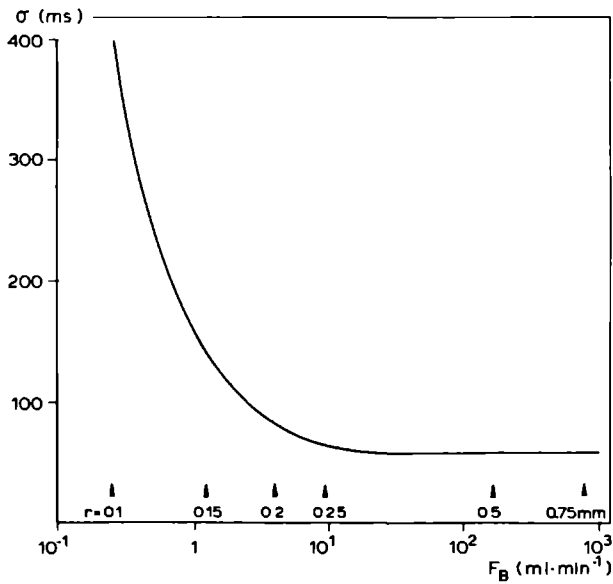


Fig.6.10: *Semilogarithmic plot of signal distortion ( $\sigma$ ) against sample flow ( $F_B$ ) for a 30 m tube. The radii needed for attaining the flow are indicated.*

Fig.6.10 shows the relationship between  $\sigma$  and sample flow for a 30 m inlet line: higher flows guarantee smaller signal distortion. It can be seen that  $\sigma$  is minimally improved by a tube drawing off a flow higher than 10 ml·min<sup>-1</sup>. However, fig.6.11 shows that the residence time then is 25 s. Thus there is an immediate conflict between a small residence time and a low sample flow for a given length of inlet line.

If the three performance parameters should be kept as small as possible, a compromise must be made by choosing the highest sample flow that is acceptable and does not cause technical troubles. At that point a practical problem arises. When the highest acceptable flow, say 50 ml·min<sup>-1</sup>, has been chosen, an inlet line with a suitable diameter must be found among commercially available tubings. Since there is only a limited range of internal diameters, the resulting flow is either too high or too small. This is illustrated

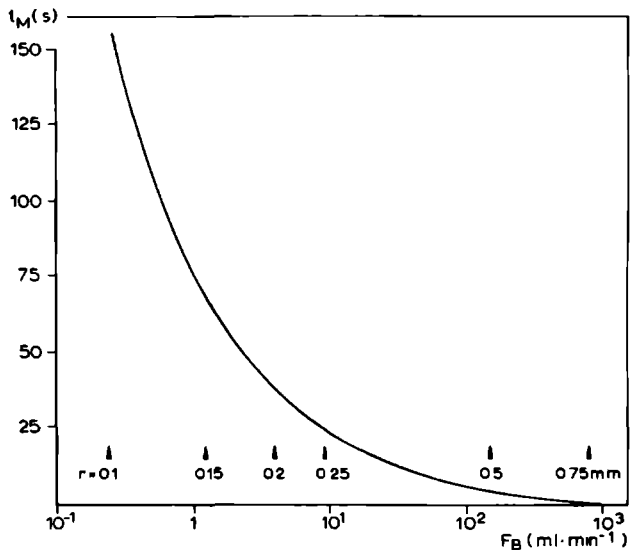


Fig.6.11: *Semilogarithmic plot of residence time ( $t_M$ ) against sample flow ( $F_B$ ) for a 30 m tube. The radii needed for attaining the flow are indicated.*

in table 6.3. Sample flows of  $7 \text{ ml}\cdot\text{min}^{-1}$  or less, for instance, are too small for normal operation of a commercially available respiratory mass spectrometer using normally a sample flow of  $20 \text{ ml}\cdot\text{min}^{-1}$ . A solution to this problem is offered by the combination of two lengths of tubing having different diameters. These "combined" tubes are treated in the next section.



## 6.3 PROCESS MODEL FOR COMBINED TUBES

The distance between patient and mass spectrometer may be bridged by a "combined" inlet line which consists of two parts in series with different diameters. Provided the diameters are given, the presented model allows calculation of:

- the lengths of the two parts for any desired sample flow, or alternatively the sample flow for given part lengths,
- the resulting total residence time and band broadening.

### 6.3.1 Calculation of geometry or flow

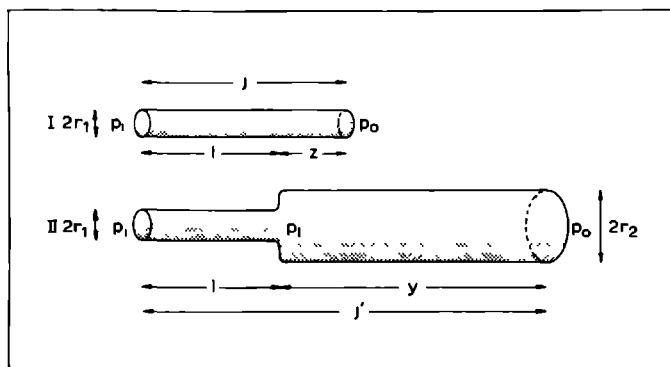


Fig.6.12: Geometry of combined tubes.

Suppose the sample flow is given. A combined tube may be regarded as a tube with uniform diameter, of which a part ( $z$ ) has been replaced by another length of tubing ( $y$ ) with different diameter (see fig.6.12). The flow through the combination equals the flow through the uniform tube. Thus the flow through  $z$  equals the flow through  $y$ . It follows that:

$$\frac{z}{y} = \frac{r_1^4}{r_2^4} = j'' \quad (6.35)$$

where  $r_1$  and  $r_2$  are the radii of the lengths  $z$  and  $y$ , respectively, and  $j''$  is a constant. The length  $j$  of the tube with uniform diameter (tube I) can be calculated from the desired sample flow by means of eq.6.10. The length of the combined tube (tube II) is the distance to be bridged ( $j'$ ). After rearranging eq.6.35, the following system of equations is obtained:

$$l + z = j \quad (6.36)$$

$$l + y = j' \quad (6.37)$$

$$z = yj'' \quad (6.38)$$

where  $j$ ,  $j'$  and  $j''$  are known. The three unknowns  $l$ ,  $y$ , and  $z$  can be calculated from this system of equations. Suppose for instance a distance of 30 m is to be bridged by a combined inlet line, sucking off  $25 \text{ ml} \cdot \text{min}^{-1}$  of a 70%/30%  $\text{N}_2\text{O}/\text{O}_2$  mixture at atmospheric pressure. Tubings with an internal diameter of 0.2 mm and 1 mm are available. The combined tube must be a combination of 0.24 m (0.2 mm i.d.) and 29.76 m (1 mm i.d.).

If the lengths of the two parts are given (instead of the sample flow) a similar system of equations is obtained, allowing to calculate the unknowns (sample flow,  $z$ ).

### 6.3.2 General formulae

The formulae derived for a tube with uniform diameter are applied to each part of the combined tube, taking into account the appropriate pressures ( $p_i$ ,  $p_1$ ,  $p_o$ ) and pressure ratios. This leads to the performance parameters of the combination. The following pressure ratios are used:

$$p_i/p_o = P \quad (\text{tube I}) \quad (6.39)$$

$$p_1/p_o = P' \quad (\text{tube II}) \quad (6.40)$$

Combining eqs.6.39 and 6.40 yields:

$$p_i/p_1 = P/P' \quad (\text{tube II}) \quad (6.41)$$

The results of interest from the algebraic manipulation will be given in an appendix at the end of this chapter.

### 6.3.3 Calculation of performance parameters

A program JOSCOM, based on the general formulae for combined tubes, was written in Fortran. Fig.6.13 shows that JOSCOM had two versions, depending on the input variables.

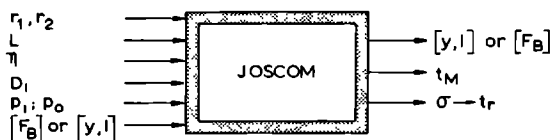


Fig.6.13: *The input and main output variables of the program JOSCOM. The sample flow or the lengths of the parts are alternatively used.*

One version of the program (sample flow is given) is now illustrated. Suppose the distance between patient and mass spectrometer is 20 m. The available tubings have an internal diameter of 0.38 mm and 1 mm, whereas the highest acceptable sample flow is  $67.5 \text{ ml} \cdot \text{min}^{-1}$ . The carrier gas mixture is a 70%/30%  $\text{N}_2/\text{O}_2$  gas mixture at 298K with a viscosity of  $16.54 \times 10^{-6} \text{ Pa} \cdot \text{s}$  and the sample gas is  $\text{CO}_2$  with a ternary diffusion coefficient of  $13.18 \times 10^{-6} \text{ m}^2 \cdot \text{s}^{-1}$ . The ratio  $P$  is 100.

The two possible solutions are shown in table 6.4. The pressure versus distance function and the velocity profile were calculated for the tube offering the smallest apparent band broadening, according to the eqs.6.44 and 6.45 on one hand, and the eqs.6.49 and 6.50 on the other. The profiles are shown in fig.6.14 and fig.6.15.

Table 6.4: Two solutions for a combined tube of 20 m  
*The performance parameters and other variables of a 20 m tube using two parts with an internal diameter of 0.2 mm and 1 mm.*

	Solution I		Solution II	
	First part	Second part	First part	Second part
radius (mm)	0.19	0.5	0.5	0.19
length (m)	0.997	19.003	19.003	0.997
pressure ratio	1.875	53.34	1.182	84.59
$\bar{v}$ (m.s <sup>-1</sup> )	12.55	4.027	1.548	17.59
$t_M$ (s)	0.08	4.719	12.27	0.06
$\sigma$ (s)	0.003	0.039	0.096	0.002
$F_B$ (ml.min <sup>-1</sup> )	67.5		67.5	
total $t_M$ (s)	4.798		12.33	
total $\sigma$ (s)	0.039		0.096	

#### 6.3.4 Discussion

These calculations illustrate that a combined tube allows to attain any desired sample flow. The length of tubing with the smallest diameter is to be used at the inlet side of the combined tube in order to ensure the smallest  $\sigma$ . This sequence will be used throughout the further study. The question is raised if the other performance parameters of the combined tube are identical to those of a uniform tube, which would bridge the same distance and draw off the same sample flow. Therefore the results for a 20 m combined tube, listed in table 6.4, are compared with those of a uniform tube.

A program JOSUT was written which first calculates the necessary radius of the uniform tube (via eq.6.10), then calculates its transit time and response time (see fig.6.16). Table 6.5 shows that the combined tube has a smaller residence time and a smaller response time.

The pressure and velocity versus distance functions are illustrated in the figures 6.14 and 6.15, showing that the gas in the

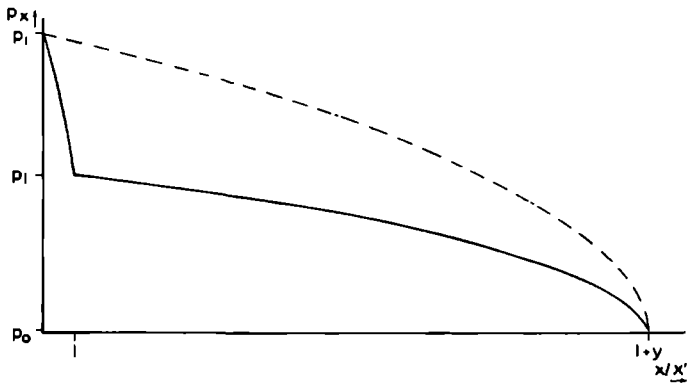


Fig.6.14: *Pressure versus distance functions of a 20 m (1+y) combined tube and a 20 m uniform tube (same sample flow). P = 100.*

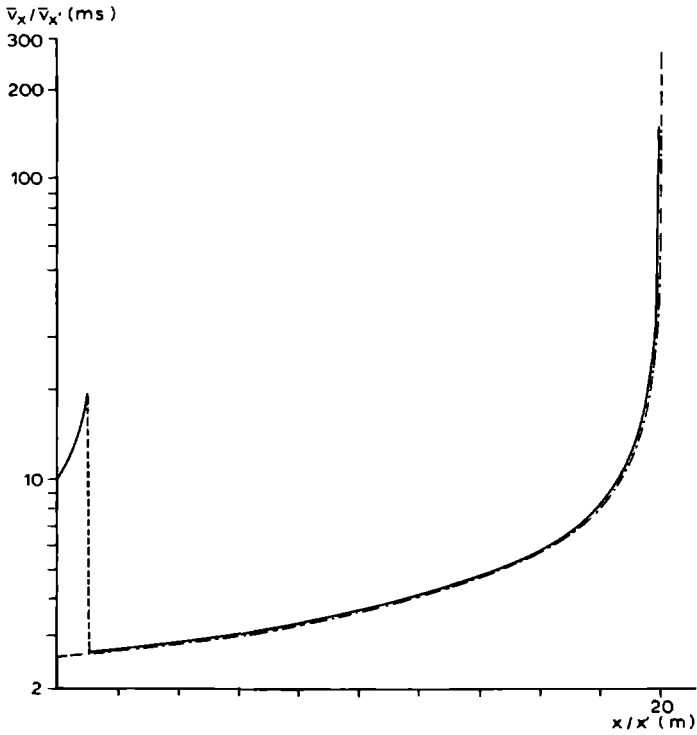


Fig.6.15: *Semilogarithmic plot of the mean velocity versus distance functions of a 20 m combined tube and a 20 m uniform tube having the same sample flow. P = 100.*

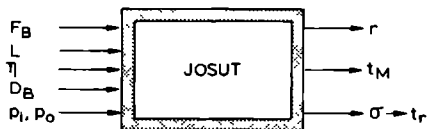


Fig.6.16: The input and main output variables of the program JOSUT.

Table 6.5: Comparison of a combined tube with a uniform one Values of the performance parameters for a 20 m combined and a 20 m uniform tube with identical sample flow;  $CO_2$  is the sample gas in a 70%/30%  $N_2O/O_2$  carrier gas mixture.

	Combined tube	Uniform tube
$r_1$ (mm)	0.19	
$r_2$ (mm)	0.5	
$r$ (mm)		0.3698
$F_B$ (ml.min <sup>-1</sup> )	67.5	67.5
$t_M$ (s)	4.798	5.093
$\sigma$ (s)	0.039	0.041
$t_r$ (s)	0.100	0.105

first part of the combined tube reaches a much higher linear velocity than in the corresponding length of the uniform tube. At the junction of both parts, the linear gas velocity drops drastically, and follows from there very closely the velocity versus distance function of the uniform tube. The ratio of the velocities at both sides of the junction equals  $r_2^2/r_1^2$  (law of mass conservation). At the outlet the velocity of the uniform tube is higher. The average linear gas velocities in the two parts of the combined tube (12.55 m.s<sup>-1</sup> and 4.027 m.s<sup>-1</sup>) are both higher than the average linear gas velocity in the uniform tube (3.927 m.s<sup>-1</sup>). Accordingly, the total residence time will be shorter for the combined tube; the resulting total response time is also shorter.

In the foregoing example, lengths of tubing with commercially available diameters were used for the two parts of the combined tube. However, the question may be raised if the performance parameters could be further optimized by the use of tubings with internal diameters which are not currently available. This question will be answered in chapter 9.

In conclusion, the mathematical model presented allows to predict the performance parameters of ideal (no gas-tube interaction) inlet lines. The performance of real tubes made of various materials will be investigated in the next chapter.

## APPENDIX

In this appendix the length  $l$  will be written  $\ell$  to avoid confusion with the number one (1).

The pressure versus distance function.

Similarly to eq.6.6, the pressure versus distance function in tube I is given by:

$$p_x = p_i \sqrt{1 - \frac{x (P^2 - 1)}{(\ell + z) P^2}} \quad (6.42)$$

Substitution of  $x$  by  $\ell$  in eq.6.42 yields the local pressure at a distance  $\ell$ , which is given as:

$$p_\ell = p_i \sqrt{1 - \frac{\ell (P^2 - 1)}{(\ell + z) P^2}} \quad (6.43)$$

Analogously to eq.6.6, the pressure versus distance function in tube II is given by:

$$p_x = p_i \sqrt{1 - \frac{x (P^2 - P'^2)}{\ell P^2}} \quad (0 < x < \ell) \quad (6.44)$$

$$p_{x'} = p_\ell \sqrt{1 - \frac{x' (P'^2 - 1)}{y P'^2}} \quad (0 < x' < y) \quad (6.45)$$

where  $x'$  is a new coordinate in the axial direction, with its origin at the junction of the two parts of tube II. Substitution of eq.6.43 into eq.6.40 and combining with eq.6.39 yields:

$$P' = P \sqrt{1 - \frac{\ell (P^2 - 1)}{(\ell + z) P^2}} \quad (6.46)$$



Similarly to eq.6.20 the average pressure in tube II is given as:

$$\bar{p}_1 = \frac{2}{3} p_i \frac{(P^3 - P'^3)}{P(P^2 - P'^2)} \quad (6.47)$$

$$\bar{p}_2 = \frac{2}{3} p_i \frac{(P'^3 - 1)}{P(P'^2 - 1)} \quad (6.48)$$

where  $\bar{p}_1$  and  $\bar{p}_2$  are the average pressures in the first and second part of tube II, respectively.

Mean velocity versus distance function.

Similarly to eq.6.8, the mean velocity versus distance function in tube II is given by:

$$\bar{v}_x = \frac{p_i r_1^2}{16\eta l} \times \left\{ \frac{(P^2 - P'^2)}{x(P^2 - P'^2)} \right\} \quad \text{for } 0 < x < l \quad (6.49)$$

$$P^2 \sqrt{\left[ 1 - \frac{x(P^2 - P'^2)}{l P^2} \right]}$$

$$\bar{v}_{x'} = \frac{p_i r_2^2}{16\eta y} \times \left\{ \frac{(P'^2 - 1)}{x'(P'^2 - 1)} \right\} \quad \text{for } 0 < x' < y \quad (6.50)$$

$$P'^2 \sqrt{\left[ 1 - \frac{x'(P'^2 - 1)}{y P'^2} \right]}$$

The average velocity in tube II is given as:

$$\bar{v}_1 = \frac{3 p_i r_1^2 (P^2 - P'^2)^2}{32 \eta l P(P^3 - P'^3)} \quad (6.51)$$

$$\bar{v}_2 = \frac{3 p_1 r_2^2 (P'^2 - 1)^2}{32 \eta y P(P'^3 - 1)} \quad (6.52)$$

where  $\bar{v}_1$  and  $\bar{v}_2$  are the average velocities in the first and second part of tube II, respectively.

### Band broadening.

The diffusion coefficients at average pressure in tube II are found after combination of eqs.6.19 and 6.47, yielding:

$$\bar{D}_1 = \frac{3}{2} D_1 \frac{P(P^2 - P'^2)}{(P^3 - P'^3)} \quad (6.53)$$

and after combination of eqs.6.19 and 6.48, yielding:

$$\bar{D}_2 = \frac{3}{2} D_1 \frac{P(P'^2 - 1)}{(P'^3 - 1)} \quad (6.54)$$

where  $\bar{D}_1$  and  $\bar{D}_2$  are the diffusion coefficients at average pressure in the first and second part of tube II, respectively. Relative band broadenings are given as:

$$H_1 = \left( 2 \frac{\bar{D}_1}{\bar{v}_1} + \frac{\bar{v}_1 r_1^2}{24 \bar{D}_1} \right) f' \quad (6.55)$$

$$H_2 = \left( 2 \frac{\bar{D}_2}{\bar{v}_2} + \frac{\bar{v}_2 r_2^2}{24 \bar{D}_2} \right) f'' \quad (6.56)$$

where  $H_1$ , and  $H_2$  are the relative band broadening in the first and second part of tube II, respectively; Giddings correction factors in the first and second part of tube II are given as :

$$f' = \frac{9 (P^4 - P'^4)(P^2 - P'^2)}{8 (P^3 - P'^3)^2} \quad (6.57)$$

$$f'' = \frac{9 (P'^4 - 1)(P'^2 - 1)}{8 (P'^3 - 1)^2} \quad (6.58)$$

**Residence time and variance.**

The total residence time is given as:

$$t_T = t_1 + t_2 = \frac{l}{\bar{v}_1} + \frac{y}{\bar{v}_2} \quad (6.59)$$

where  $t_1$  and  $t_2$  are the residence time in the first and second part of tube II, respectively. The total variance is given as:

$$\sigma_T^2 = \sigma_1^2 + \sigma_2^2 = \frac{lH_1}{\bar{v}_1^2} + \frac{yH_2}{\bar{v}_2^2} \quad (6.60)$$

where  $\sigma_1^2$  and  $\sigma_2^2$  are the variance in the first and second part of the tube, respectively.

## CHAPTER 7

### PERFORMANCE OF LONG SAMPLING TUBES: EXPERIMENTS

This chapter is set out in two parts; the first describes the experimental study in the laboratory, and the second part illustrates the clinical use of long sampling tubes.

#### 7.1 EXPERIMENTAL STUDY IN THE LABORATORY

Tubes of various materials were tested since the interaction between gas phase and tube material was known to influence response time. Once a tube with acceptable performance parameters had been selected, a sampling system for several patients could be constructed.

The five stages of the experimental study were:

(1) A pilot study was made with polyethylene tubes of different geometry to test not only their properties, but also the experimental set-up. Polyethylene was chosen to start with, since some results from another study were available although the experimental conditions were different (Gillbe, Heneghan and Branthwaite, 1981).

(2) The Centronic standard capillary was tested.

(3) Tubes of teflon, PVC, steel, glass, and nylon were evaluated. In the course of this stage, it became clear that the nylon under study had favourable qualities. The fourth objective of this thesis given in chapter 1 was, therefore, reformulated to limit the number of tests with this material, and to search directly for an inlet line meeting practical needs. Thus the objective was to select an inlet line showing the following properties:

- Length = 30 m. This length allows the remote operation of a mass spectrometer in most situations.
- Sample flow = maximally  $50 \text{ ml} \cdot \text{min}^{-1}$  (air). This limit was chosen for two reasons. Firstly, it was considered small enough to

avoid problems mentioned for high flows. Secondly, the process model predicts, for the chosen length and flow, a transit time and response times acceptable in clinical practice.

- Transit time and response times approximating those predicted by the model.
- Easy to handle.

(4) The selected nylon inlet line was tested in combination with a solenoid valve, then redesigned for clinical use and tested again.

(5) A multi-patient inlet system using four of the selected lines and valves was constructed.

The inlet lines were fitted to the normal inlet port since plumbing in the inlet system of the mass spectrometer was avoided.

### 7.1.1 Materials and methods

Step changes in partial gas pressure of sample gases were generated in a 70%/30%  $N_2O/O_2$  carrier gas mixture, since this is the most widely used anaesthetic gas mixture. A step change was chosen from the three model inputs illustrated in fig.6.4, since it was more easily produced than the others. The apparatus used for generating the step changes was described in chapter 5. Step changes of 10 kPa (or approximately 10% of atmospheric pressure) guaranteed on one hand a strong change in the electrical output signal of the mass spectrometer, but did not dilute excessively the carrier gas mixture on the other hand.

A set of rotameters delivered  $N_2O$ ,  $O_2$ ,  $N_2$ ,  $CO_2$ , and Ar. Halothane, enflurane, and isoflurane were vaporized in a Cyprane Fluotec Mk III, a Cyprane Enfluratec, and a Draeger Vapor, respectively. Gas mixtures were led to the two chambers of the step change apparatus via two independent systems. The mass spectrometer was calibrated via the inlet line to be tested. An air conditioned room was selected for the experiments to avoid temperature and humidity changes. The set-up is illustrated in fig.7.1.

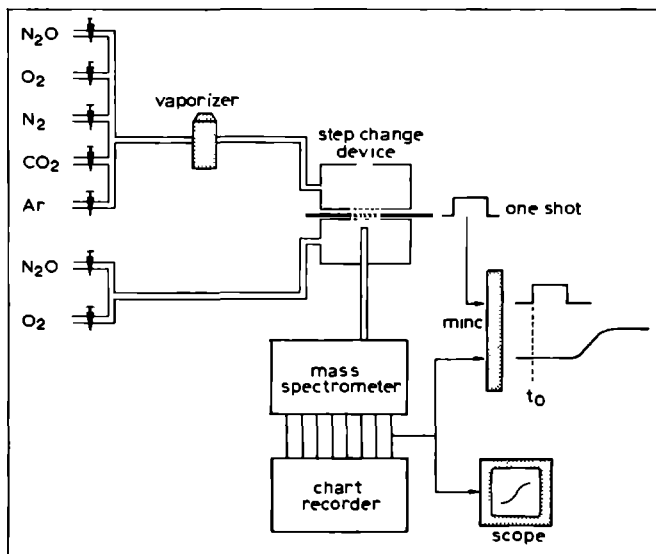


Fig.7.1: *Experimental set-up.* A step change in partial gas pressure is generated at time  $t_0$ . The trigger signal and the signal of the sample gas under study are fed to the AD-converter of the MINC.

The following step changes were produced:

	on transients	off transients
$N_2O$	65 → 75%	75 → 65%
$O_2$	25 → 35%	35 → 25%
$N_2$	0 → 10%	10 → 0%
$CO_2$	0 → 10%	10 → 0%
Ar	0 → 10%	10 → 0%
volatiles	0 → 3%	3 → 0%

The sample gases  $N_2O$ ,  $O_2$ ,  $CO_2$ ,  $N_2$ , Ar, halothane, enflurane, and isoflurane were measured on the  $m/q$  values 30, 32, 44, 28, 40, 117, 51, and 51, respectively. Each transient was carried out three to ten times, with or without the anaesthetics module. The mass spec-

trometer output signal of the gas under study and the trigger signal from the step change apparatus were fed on-line to the AD-converter of the MINC computer. However, during the pilot study for polyethylene tubes, both signals were recorded on the Hewlett Packard instrumentation recorder. Visual control of all signals was possible on the eight channel Gould Brush chart recorder. During on-line data acquisition, the mass spectrometer output signal of the gas under study was also visible on a Hewlett Packard oscilloscope.

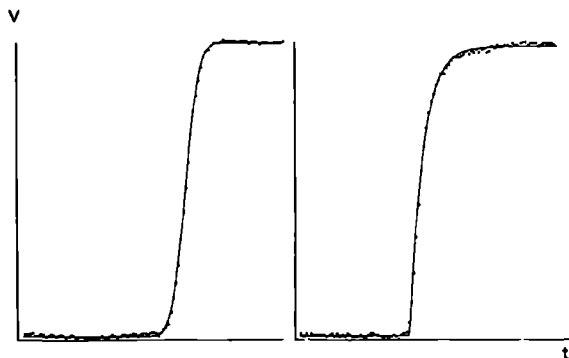


*Fig.7.2: Two examples of a response to a step function. The difference between the curve fitting according to a normal probability integral model (left) or an exponential model (right) is illustrated.*

The data acquisition was followed by data analysis using the program MASFIE which performed curve fitting on the digitized transient signal. This least squares fitting program used alternatively an exponential or a normal probability integral fitting model (see fig.7.2). The best fitting curve was indicated by the smallest  $\chi^2$ . MASFIE calculated response times and transit times.

Gas flows were measured with the bubble flow meter described in chapter 5. For practical purposes, flows were measured when sampling room air. Accordingly, all observed and calculated values for flows, which are given in the text or tables, have been measured or calcu-

lated with air to facilitate direct comparison. The sample flow of an inlet line is one of the input variables of JOSCOM. Since the sample flows were measured with air, the value of the sample flow fed to JOSCOM was divided by 0.89, i.e. the relationship between the viscosity of air and of a 70%/30% N<sub>2</sub>O/O<sub>2</sub> gas mixture (Nunn, 1977).

The inlet lines used during the experimental study were made of commercially available tubing:

- polyethylene 0.38 mm i.d. : Portex 800/110/120
- polyethylene 0.58 mm i.d. : Portex 800/110/200
- polyethylene 1 mm i.d. : Portex 800/110/300
- teflon 0.58 mm i.d. : Talas (Ommen, Holland)
- PVC 0.58 mm i.d. : Talas
- steel 0.5 mm i.d. : Chrompack (Middelburg, Holland)
- nylon 0.25 mm i.d. : Portex 800/205/100
- nylon 1.07 mm i.d.
- fused silica 0.2 mm i.d. : Chrompack

The solenoid valves were manufactured by Kuhnke.

### 7.1.2 Results

The results of the experimental study are now presented and compared with those predicted by the process model. All values given for the residence times apply to the on transients of nitrogen, and were measured on the normal probability integral fits (except for the Centronic capillary). The presented results of response times and residence times are the means of three to ten measurements; the number of measurements and the standard errors of means are given. The results for the sample flows are the means of two measurements. The best fitting curve found by MASFIE is indicated in the tables by an E (exponential fit) or an N (normal probability integral fit). Differences between the means were investigated with an unpaired Student's t-test;  $P < 0.01$  was considered significant. The results for each type of inlet line will be followed by a specific discussion, whereas a more general discussion is given at the end.



### 7.1.2.1 Centronic inlet capillary

The results for this capillary, i.e. an unheated capillary with a length of 1.25 m, are given first, since it is useful to have an estimation of the "basic response" of the mass spectrometer before the results of the long inlet lines are presented. The diameter of the capillary was not exactly known, but is in the range from 0.25 to 0.30 mm. A value of 0.293 mm, which was calculated from the measured flow and length of the capillary, was used in the calculation of the performance parameters. Table 7.1 lists the results for the measured and calculated performance parameters.

The measured residence time (0.216 s) is 0.089 s longer than predicted by the model (0.127 s). It should be remembered that the model only calculates the residence time for the capillary itself, and not for other parts of the gas handling system or a possible delay produced in the step change apparatus.

Table 7.1 shows great differences between the response times predicted by the model and the measured values. It may be concluded that the contribution of the capillary to the response time of the mass spectrometer-capillary system is not of considerable importance. Another explanation would suppose a strong interaction between all gases and the capillary wall. However this will not be supported by the results for nitrogen and argon in any of the long inlet lines. Since the response times for  $N_2O$ ,  $O_2$ , and  $CO_2$  do not differ considerably from the response times of nitrogen and argon, it is concluded that the presented values are due to the instrument's basic response, which is theoretically defined as the response after a step change created in front of the molecular leak. This view is supported by the exponential form of the transient signals of all gases, explained by a wash-out process. It will be seen in the experiments with the long inlet lines that the exponential curve will change into a curve with the shape of the normal probability integral.

The 10% to 90% response times shown in table 7.1 are in good agreement with those reported in the literature. It is concluded that the step function, generated by the step response device, has a time constant short enough in comparison to the events to be measured, and that the experimental set-up produces reliable values.

Table 7.1: Performance parameters of the Centronic capillary  
*Experimental and predicted values for the residence time ( $t_M$ ), sample flow ( $F_B$ ), and response times ( $t_r$ ) for various sample gases with or without the anaesthetics module (+ or - in column M). Column N shows the number of experiments, and column F shows the best fitting model: exponential (E) or normal probability integral (N). Significant differences ( $P < 0.01$ ) are indicated in columns I (between anaesthetics module on or off) and in column II (between on and off transients) with '\*'.*

Measured  $t_M = 0.216$  s (SEM = 0.001) (calculated  $t_M = 0.127$  s)

Measured  $F_B = 24$  ml.min<sup>-1</sup>

	On transients				Off transients				Model	
Gas M	N	F	$t_r$ (ms)	SEM I	N	F	$t_r$ (ms)	SEM I	$t_r$ (ms)	II
N <sub>2</sub> O +	5	E	59	1	5	E	64	1	6	*
N <sub>2</sub> O -	5	E	62	1	5	E	68	1	6	*
O <sub>2</sub> +	5	E	70	2	5	E	68	1	6	
O <sub>2</sub> -	5	E	69	2	5	E	68	1	6	
N <sub>2</sub> +	5	E	64	1	5	E	61	1	6	
N <sub>2</sub> -	5	E	60	1	5	E	60	1	6	
CO <sub>2</sub> +	5	E	75	1	5	E	73	2	7	
CO <sub>2</sub> -	5	E	69	2	5	E	71	1	7	
Ar +	5	E	65	1	5	E	68	1	6	
Ar -	5	E	65	1	5	E	65	1	6	
HAL +	3	E	362	4	3	E	359	3	10	
HAL -	3	E	364	5	3	E	355	1	10	
ENF +	3	E	286	1	3	E	300	1	10	
ISO +	3	E	280	4	3	E	270	2	10	

The response times shown for the volatile anaesthetics, in particular halothane, are long. This was a real problem, especially because the response time for halothane was deteriorating over a period of a few months. Neither replacing used for brandnew capillaries, nor changing the method of generating the step function at the inlet (swift withdrawal of the capillary from a gas mixture containing halothane) did offer any improvement. Even the use of an inlet capillary made of fused silica, known in gas chromatography as a very inert material, did not improve the response time for halothane. It was concluded that the basic response of the instrument for halothane was much longer than expected, or that the performance of the mass spectrometer had worsened in the course of time since its manufacturing. Spence and Davis (1981), for instance, reported a 0% to 90% response time of 235 ms for halothane measured with the Centronic 200 MGA.

The differences found between the response times of the same gas either with the anaesthetics module or without are statistically not significant, and of no practical importance. The same holds for differences between on and off transients of the same gas, except for N<sub>2</sub>O that shows a small difference.

Since the Centronic capillary is expensive, a capillary was home made using nylon with an internal diameter of 0.25 mm. The length was the same as the original capillary, i.e. 1.25 m, but the sample flow was 13 ml.min<sup>-1</sup>, which could be expected from the model predicting 12.5 ml.min<sup>-1</sup>. The resulting response times for all sample gases were very near those of the original capillary, although the residence time was slightly longer (0.265 s). The difference between the measured and the theoretical residence time was about the same as for the original capillary (0.091 s). The halothane response times, 0.436 s and 0.447 s for the on and off transient respectively, were significantly longer than for the original capillary.

#### 7.1.2.2 Polyethylene tubes

Three lengths (9.85 m, 20 m, and 30 m) of polyethylene tubing with a uniform diameter of 0.58 mm, and two combined tubes with a total length of 29.5 m (4.1 m + 25.4 m) and 30 m (1 m + 29 m) were tested.

The parts of the combined tubes had an internal diameter of 0.38 mm and 1 mm. The results are shown in tables 7.2, 7.3, 7.4, 7.5, and 7.6. The results for the different types of tubes are discussed in three steps: first the tubes with uniform diameter, then the combined tubes are treated, and lastly some general remarks for the two types are made.

### *Tubes with uniform diameter*

The observed values of the response times for the various sample gases may be classified into three groups: the nitrogen-argon group, halothane, and the group containing the rest of the sample gases ( $N_2O$ ,  $O_2$ ,  $CO_2$ ). As an example of the first group the observed and calculated (model) values for the off transients of argon measured without the anaesthetics module are illustrated in fig.7.3, showing a nearly linear relationship between  $t_r$  and tube length. This was expected from eq.6.32. The gap between the observed and theoretical values is due to the basic response of the mass spectrometer.

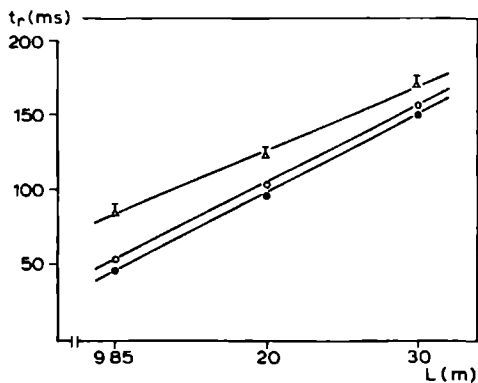


Fig.7.3: *Regression lines through the calculated (model) (•) and observed (Δ) values for the off transients of argon (anaesthetics module off) plotted against the length of polyethylene tubes with 0.58 mm i.d.. The third regression line is fitted through the values (○) obtained by means of eq.6.2 allowing to correct the observed values for the contribution of the basic response of the mass spectrometer from table 7.1. Vertical bars represent 3×SEM.*

The observed total response times of the combinations long line and mass spectrometer can be corrected by means of eq.6.2, if the observed value for argon obtained with the 1.25 m capillary (65 ms: see table 7.1) is used as the basic response time of the mass spectrometer. Fig.7.3 shows that the corrected values are very close to the theoretical values. It is concluded for this first group that the theoretical limits for the response times are approached, and that neither nitrogen nor argon interacts with polyethylene tubing. The last conclusion is supported by the observation that the transients for argon and nitrogen have the shape of the normal probability integral for all three lengths of tubing, as predicted by the process model.

Halothane has very long response times, increasing exponentially with length. A very strong interaction between halothane and polyethylene is likely.

The response times for the third group ( $N_2O$ ,  $O_2$ ,  $CO_2$ ) are situated between those of the first two groups. Response times are increasing exponentially with length, and the gap between observed and model values is increasing accordingly (fig.7.4). An intermediate interaction between gas phase and tube is suggested.

### *Combined tubes*

The same three groups defined above can be recognized in tables 7.5 and 7.6, although the disparity between the response times of the groups is smaller, owing to the shorter response times for  $N_2O$ ,  $O_2$ ,  $CO_2$ , and halothane in comparison with those obtained with the 30 m tube with uniform diameter. Thus the 29.5 m combined tube performs better than the 30 m tube with uniform diameter having a comparable sample flow. Comparing the results of both combined tubes show that a higher sample flow shortens markedly the response time for halothane. The performance parameters of the second combined tube are acceptable in clinical practice, except for the response time of halothane.

### *All tubes*

The effect of the anaesthetics module on the response time of an individual gas is puzzling. No statistically significant differences

are found in the argon/nitrogen group. Carbon dioxide transients could not be measured without anaesthetics module because of a too noisy signal, which was probably due to the combination of the small CO<sub>2</sub>-signal in the high N<sub>2</sub>O-signal and the use of a tape recorder.

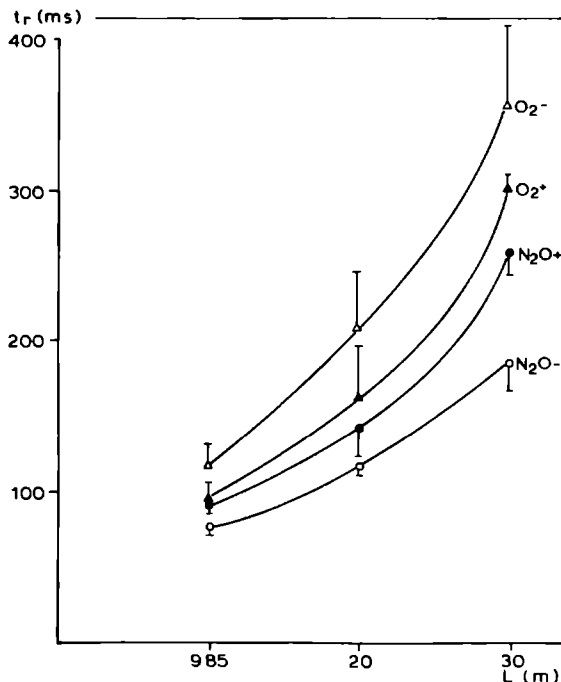


Fig.7.4: Values of observed response times for N<sub>2</sub>O and O<sub>2</sub> (on transients), measured with the anaesthetics module (+) or without (-), plotted against the length of polyethylene tubing with 0.58 mm i.d.. Vertical bars represent 3×SEM.

An example of the N<sub>2</sub>O/O<sub>2</sub> group is shown in fig.7.4, where the values of the on transients for N<sub>2</sub>O and O<sub>2</sub> are illustrated for tubes with uniform diameter. Without the anaesthetics module, response times for oxygen are longer than those for nitrous oxide. If the anaesthetics module is switched on, the response times for both

gases are "averaged" since the on transient of either  $N_2O$  or  $O_2$  is imperatively accompanied by an off transient of  $O_2$  or  $N_2O$ , respectively. Accordingly, the differences found between the transients of  $O_2$  and  $N_2O$  measured with the anaesthetics module are much smaller and statistically not significant, except for the 30 m line (see tables 7.2, 7.3, and 7.4). Thus the anaesthetics module influences, as expected, the dynamic accuracy of the mass spectrometer.

An analogous situation is seen for the off transients of the uniform tubes: response times for  $O_2$  are longer than for  $N_2O$ , and are averaged with the anaesthetic mode on (no significant differences exist between the transients for  $N_2O$  and  $O_2$  with the anaesthetic mode on).

The same observation ( $t_{r,O_2} > t_{r,N_2O}$ ) was made for the on and off transients of the combined tubes without the anaesthetics module. A similar "averaging" effect of the anaesthetics module was observed, although the smaller differences remained significant.

The disparity between the on and off transient for one sample gas was statistically significant in 25 cases. The on transients for Ar,  $O_2$ ,  $N_2$ , and  $CO_2$  were invariably longer in these cases than the off transients; they were shorter for  $N_2O$  and halothane (with exception in one case for halothane). These differences are not well documented in the literature, since mostly only off transients are reported.

*Conclusion.* From the results of the pilot study with polyethylene tubes, the following is concluded: (1) the limits of the process model can be experimentally approached if sample gases do not interact with the tube material; (2) a combined tube shows shorter response times and residence time than a uniform tube with comparable sample flow; (3) on-line data acquisition is to be preferred; (4) polyethylene is not suitable for clinical practice, because of its very strong interaction with halothane. Therefore other materials were investigated.

Table 7.2: Polyethylene tube: 9.85 m length, 0.58 mm i.d. Experimental and predicted values for the residence time ( $t_M$ ), sample flow ( $F_B$ ), and response times ( $t_r$ ) for various sample gases with or without the anaesthetics module (+ or - in column M). Column N shows the number of experiments, and column F shows the best fitting model: exponential (E) or normal probability integral (N). Significant differences ( $P < 0.01$ ) are indicated in columns I with '\*' (between anaesthetics module on or off), and in column II with '\*' (between on and off transients). The differences between the on transients of  $N_2O +$  and  $O_2 +$ , and between the off transients of  $N_2O +$  and  $O_2 +$  (column III) were not significant.

Measured  $t_M = 2.104$  s (SEM = 0.001) (calculated  $t_M = 2.009$  s)

Measured  $F_B = 50$  ml.min<sup>-1</sup> (calculated  $F_B = 46$  ml.min<sup>-1</sup>)

	On transients				Off transients				Model		
Gas M	N	F	$t_r$ (ms)	SEM I	N	F	$t_r$ (ms)	SEM I	$t_r$ (ms)	II	III
$N_2O +$	7	N	90	2 *	7	N	93	5	49		
$N_2O -$	7	N	76	2	7	N	83	2	49		
$O_2 +$	7	N	94	4 *	7	N	86	3 *	49		
$O_2 -$	7	E	117	5	7	E	112	6	49		
$N_2 +$	7	N	85	2	8	N	80	2	46		
$N_2 -$	7	N	81	1	7	N	83	2	46		
$CO_2 +$	7	N	101	1	7	N	101	2	52		
Ar +	9	N	89	1	7	N	84	2	47		
Ar -	8	N	92	1	7	N	85	2	47	*	
HAL +	7	E	599	9 *	7	E	750	18	75	*	
HAL -	8	E	659	7	7	E	691	13	75		



Table 7.3: Polyethylene tube: 20 m length, 0.58 mm i.d.

Experimental and predicted values for the residence time ( $t_M$ ), sample flow ( $F_B$ ), and response times ( $t_r$ ) for various sample gases with or without the anaesthetics module (+ or - in column M). Column N shows the number of experiments, and column F shows the best fitting model: exponential (E) or normal probability integral (N). Significant differences ( $P < 0.01$ ) are indicated in columns I with '\*' (between anaesthetics module on or off), and in column II with '\*' (between on and off transients). The differences between the on transients of  $N_2O +$  and  $O_2 +$ , and between the off transients of  $N_2O +$  and  $O_2 +$  (column III) were not significant.

Measured  $t_M = 8.011$  s (SEM = 0.001) (calculated  $t_M = 8.283$  s)

Measured  $F_B = 25$  ml.min<sup>-1</sup> (calculated  $F_B = 23$  ml.min<sup>-1</sup>)

Gas M	On transients				Off transients				Model		
	N	F	$t_r$ (ms)	SEM I	N	F	$t_r$ (ms)	SEM I	$t_r$ (ms)	II	III
$N_2O +$	7	N	139	6 *	6	N	166	6 *	100	*	
$N_2O -$	7	N	117	2	6	N	129	3	100	*	
$O_2 +$	6	E	160	9	6	N	145	5 *	100		
$O_2 -$	6	E	207	13	5	E	183	6	100		
$N_2 +$	7	N	130	2	7	N	123	2	95		
$N_2 -$	7	N	132	4	7	N	121	2	95		
$CO_2 +$	7	E	208	3	7	E	210	6	106		
Ar +	7	N	142	2	7	N	121	1	97	*	
Ar -	7	N	152	3	7	N	123	1	97	*	
HAL +	7	E	2598	32 *	7	E	2945	33 *	153	*	
HAL -	5	E	2873	26	7	E	2699	18	153	*	

Table 7.4: Polyethylene tube: 30 m length, 0.58 mm i.d.

Experimental and predicted values for the residence time ( $t_M$ ), sample flow ( $F_B$ ), and response times ( $t_r$ ) for various sample gases with or without the anaesthetics module (+ or - in column M). Column N shows the number of experiments, and column F shows the best fitting model: exponential (E) or normal probability integral (N). Significant differences ( $P < 0.01$ ) are indicated in columns I with '\*' (between anaesthetics module on or off), in column II with '\*' (between on and off transients), and in column III with '\$' (between the on transients of  $N_2O +$  and  $O_2 +$ ). The differences between the off transients of  $N_2O +$  and  $O_2 +$  (column III) were not significant.

Measured  $t_M = 17.750$  s (SEM = 0.004) (calculated  $t_M = 18.64$  s)

Measured  $F_B = 16$  ml.min<sup>-1</sup> (calculated  $F_B = 15$  ml.min<sup>-1</sup>)

Gas M	On transients				Off transients				Model		
	N	F	$t_r$ (ms)	SEM I	N	F	$t_r$ (ms)	SEM I	$t_r$ (ms)	II	III
$N_2O +$	4	E	258	5 *	5	E	285	11 *	155		\$
$N_2O -$	5	N	185	6	4	N	222	7	155	*	
$O_2 +$	5	E	294	2 *	4	E	245	10 *	155	*	
$O_2 -$	4	E	354	17	5	E	308	12	155		
$N_2 +$	4	N	187	6	5	N	163	2	147	*	
$N_2 -$	5	N	182	4	5	N	165	2	147	*	
$CO_2 +$	3	E	505	18	5	E	414	11	163	*	
Ar +	5	N	206	4	3	N	173	4	151	*	
Ar -	5	N	220	3	3	N	171	2	151	*	
HAL +	3	E	7512	78 *	4	E	8931	468	231		
HAL -	5	E	8277	116	5	E	9088	161	231	*	

Table 7.5: 29.5 m polyethylene combined tube: 4.1 + 25.4 m. Experimental and predicted values for the residence time ( $t_M$ ), sample flow ( $F_B$ ), and response times ( $t_r$ ) for various sample gases with or without the anaesthetics module (+ or - in column M). Column N shows the number of experiments, and column F shows the best fitting model: exponential (E) or normal probability integral (N). Significant differences ( $P < 0.01$ ) are indicated in columns I with '\*' (between anaesthetics module on or off), in column II with '\*' (between on and off transients), and in column III with '\$' (between the on transients of  $N_2O +$  and  $O_2 +$ ) and with '@' (between the off transients of  $N_2O +$  and  $O_2 +$ ).

Measured  $t_M = 16.063$  s (SEM = 0.003) (calculated  $t_M = 14.30$  s)

Measured  $F_B = 16$  ml.min<sup>-1</sup> (calculated  $F_B = 18$  ml.min<sup>-1</sup>)

Gas M	On transients				Off transients				Model		
	N	F	$t_r$ (ms)	SEM I	N	F	$t_r$ (ms)	SEM I	$t_r$ (ms)	II	III
$N_2O +$	6	N	201	3 *	8	N	226	6 *	140	*	\$ @
$N_2O -$	7	N	159	4	7	N	189	9	140	*	
$O_2 +$	8	E	232	6 *	8	N	184	2 *	140	*	*
$O_2 -$	7	E	285	6	7	E	253	4	140	*	
$N_2 +$	7	N	176	6	7	N	152	6	135		
$N_2 -$	7	N	163	6	7	N	155	3	135		
$CO_2 +$	7	E	309	9	7	N	243	7	146	*	
Ar +	7	N	180	6	7	N	168	5	137		
Ar -	7	N	184	6	7	N	162	4	137		
HAL +	5	E	3595	111	5	E	4546	124	200	*	
HAL -	5	E	3926	54	5	E	4090	47	200		

Table 7.6: 30 m polyethylene combined tube: 1 + 29 m.

Experimental and predicted values for the residence time ( $t_M$ ), sample flow ( $F_B$ ), and response times ( $t_r$ ) for various sample gases with or without the anaesthetics module (+ or - in column M). Column N shows the number of experiments, and column F shows the best fitting model: exponential (E) or normal probability integral (N). Significant differences ( $P < 0.01$ ) are indicated in columns I with '\*' (between anaesthetics module on or off), in column II with '\*' (between on and off transients), and in column III with '@' (between the off transients of  $N_2O +$  and  $O_2 +$ ). The differences between the on transients of  $N_2O +$  and  $O_2 +$  were not significant.

Measured  $t_M = 10.833$  s (SEM = 0.002) (calculated  $t_M = 9.64$  s)

Measured  $F_B = 48$  ml.min<sup>-1</sup> (calculated  $F_B = 52$  ml.min<sup>-1</sup>)

Gas M	On transients				Off transients				Model		
	N	F	$t_r$ (ms)	SEM I	N	F	$t_r$ (ms)	SEM I	$t_r$ (ms)	II	III
$N_2O +$	6	N	182	8	7	N	198	4	144		@
$N_2O -$	5	N	151	4	7	N	184	6	144	*	
$O_2 +$	7	N	193	2 *	7	N	176	2	144	*	
$O_2 -$	7	E	246	2	4	N	179	3	144	*	
$N_2 +$	7	N	157	5	7	N	158	4	136		
$N_2 -$	7	N	167	5	6	N	153	3	136		
$CO_2 +$	7	N	230	4	7	E	238	11	153		
Ar +	7	N	170	5	10	N	158	4	140		
Ar -	7	N	182	5	10	N	154	4	140	*	
HAL +	7	E	2171	56	5	E	2205	142	222		
HAL -	5	E	2335	103	5	E	2224	105	222		

### 7.1.2.3 Various materials

A brief review is now given of the materials which were tested but discarded for further study or clinical use: teflon, PVC, steel, and glass.

#### *Teflon*

Table 7.7: Teflon tube: 30 m length, 0.58 mm i.d.  
*Experimental and predicted values for the residence time ( $t_M$ ), sample flow ( $F_B$ ), and response times ( $t_r$ ) (on transients) for various sample gases with the anaesthetics module (+ in column M).*

---

Measured  $t_M = 18.7$  s (SEM = 0.0) (calculated  $t_M = 18.6$  s)

Measured  $F_B = 14$  ml.min<sup>-1</sup> (calculated  $F_B = 15$  ml.min<sup>-1</sup>)

Gas M	$t_r$ (ms)	model
N <sub>2</sub> O +	1500	155
O <sub>2</sub> +	1500	155
N <sub>2</sub> +	500	147
CO <sub>2</sub> +	2600	163
Ar +	600	151
HAL +	2000	231

A teflon tube of 30 m with an internal diameter of 0.58 mm was tested. The transients could not be fitted by either of the fitting models because of the bi-exponential shape of the transients of all

gases. Therefore response times had to be measured with the aid of a chart recorder running at a speed of  $100 \text{ mm.s}^{-1}$ . The response times shown in table 7.7 are much longer for all gases, except halothane, than those obtained with a comparable polyethylene tube. It was concluded that the material under study could not be used in clinical practice, and that the laws governing gas-tube interaction were more complicated than expected initially.

### *PVC*

Even longer response times were obtained with a 30 m PVC tube. The material was excluded from further investigation, although it has some favorable properties.

### *Steel*

As reported previously, stainless steel had an unacceptably long response time for halothane (Ponte, Lerou and van der Vegt, 1981). After cleaning with trichloroethylene a marked shortening of the response time was found, suggesting that a greasy material was used during the fabrication of the stainless steel tubes. However, not only the results remained unsatisfactory, but the material seemed also unsuited for use in the operating theatre because of its stiffness. Other authors have reported the use of metal tubes (stainless steel and copper) for the measurement of respiratory and inert gases in human centrifuges and intensive care units (Demange, Jacquemin and Tibal, 1966; Crawford Mc Aslan, 1976).

### *Glass*

Since satisfactory results were obtained with 18 metres of 0.8 mm bore glass tubing (Ponte, Lerou and van der Vegt, 1981), it was decided to test a longer and smaller bore inlet line. A glass tube with a length of 32 m (coiled into a helix with a diameter of 100 mm) and an internal diameter of 0.566 mm, was prepared and deactivated at the Eindhoven University of Technology. Since computer facilities were not available at the moment of the tests, the

Table 7.8: Glass tube: 32 m length, 0.566 mm i.d.

*Experimental and predicted values for the residence time ( $t_M$ ), sample flow ( $F_B$ ), and response times ( $t_r$ ) for various sample gases with the anaesthetics module (+ in column M) (NVM = no valid measurement).*

Measured  $t_M = 26.7$  s (SEM = 0.0) (calculated  $t_M = 22.27$  s)

Measured  $F_B = 13$  ml.min<sup>-1</sup> (calculated  $F_B = 13$  ml.min<sup>-1</sup>)

	On transients	Off transients	
Gas M	$t_r$ (ms)	$t_r$ (ms)	model
N <sub>2</sub> O +	170	NVM	168
O <sub>2</sub> +	NVM	155	168
N <sub>2</sub> +	180	165	160
CO <sub>2</sub> +	220	215	176
Ar +	180	165	164
HAL +	420	450	247

response times had to be measured on a chart recorder running at a speed of 100 mm.s<sup>-1</sup>. It should be realized that reading errors up to 10 ms can occur with this method. The results given in table 7.8 are the means of two measurements. The results prove that the theoretical limits can be reached if an appropriate material is used.

Before further testing, it was decided to search for a material offering a better compromise between performance and ease of handling.

#### 7.1.2.4 Nylon

The test of nylon tubes was performed in three steps:

- (1) step 1: three different combined inlet lines of about 30 m:
  - (a) first line: 0.25 m + 30 m (selected for clinical use)
  - (b) second line: 0.4 m + 30 m
  - (c) third line: 0.1 m + 30 m
- (2) step 2: inlet line-valve combinations
- (3) step 3: the selected line was redesigned for clinical use and tested in the final sampling system for the monitoring of four patients.

##### *Step 1: three combined inlet lines of about 30 m*

*First inlet line.* This line, made of a combination of 0.25 m nylon tube (0.25 mm i.d.) and 30 m nylon tube (1.07 mm i.d.), was initially tested at the end of the pilot study and the test had to be recorded. Since the sample flow ( $47 \text{ ml}\cdot\text{min}^{-1}$ ) approximated that of the second combined polyethylene tube ( $48 \text{ ml}\cdot\text{min}^{-1}$ ), the results for both inlet lines were comparable. The results for the nylon tube, listed in table 7.9, showed much shorter response times for halothane than those obtained with the polyethylene tube. Moreover, the transients of all other sample gases had the shape of the normal probability integral. It was concluded that the gas-tube interaction was less in the nylon under study than in the previously tested polyethylene.

Six months later a new tube with the same configuration and a measured sample flow of  $49 \text{ ml}\cdot\text{min}^{-1}$ , was tested on-line to compare the two methods of data acquisition on one hand, and to check the reproducibility of the results on the other. The results are shown in table 7.10. No statistically significant differences were found between the response times obtained with the two methods, except for the on transients of  $\text{CO}_2$  measured with the anaesthetics module, and for all transients of halothane. However, it was already mentioned that the halothane response time had worsened in the course of time. A chronological review of this unfortunate finding will be given at the end of the experimental study. To answer the question whether a



lower sample flow would also produce satisfactory results, a second inlet line was tested.

*Second inlet line: 30 m + 0.4 m.* The performance parameters of this line, listed in table 7.11, combine a low sample flow ( $33 \text{ ml. min}^{-1}$ ), an acceptable delay time, and response times approaching the theoretical limits, with the exception of halothane. The latter observation might be solely due to the instruments basic response.

This line is to be preferred when an extra low sample flow is needed. It can be expected that even at a flow of  $20 \text{ ml. min}^{-1}$ , i.e. the sample flow of a standard inlet capillary, this nylon combination still approximates the theoretically predicted limits. However, a higher flow was thought to be advantageous when the inlet line is fitted to a switching valve, which introduces a dead volume.

*Third inlet line.* To answer the question if it was advantageous to concentrate the resistance of the inlet line more at its tip, a combination was built of 0.1 m fused silica (0.2 mm i.d.) and 30 m nylon (1.07 mm i.d.). The fused silica had the extra advantage of being an inert material. The sample flow ( $53 \text{ ml. min}^{-1}$ ) was close to the sample flow of the first nylon inlet line. Tables 7.12 and 7.10 show that the performance parameters of the first and third line are generally comparable, except for halothane. However, the nylon fused silica combination was tested a few months before the nylon nylon combination. A beneficial effect of the tube configuration and the fused silica could not be excluded. It was concluded that the tested line had no major advantages over the nylon nylon combination. Moreover, fused silica is fragile and expensive.

The same remarks given for the polyethylene tubes apply to all three nylon inlet lines (differences between the on and off transients, between the results with or without anaesthetics module; "averaging" effect).

The first nylon inlet line was selected for use in the operating theatres because it offered a good "compromise" between performance and ease of handling. It did not kink readily and could be installed, handled, and replaced more easily than glass tube.

Table 7.9: First nylon inlet line (recorded)

Combination of 0.25 + 30 m with 0.25 and 1.07 mm i.d.

Experimental and predicted values for the residence time ( $t_M$ ), sample flow ( $F_B$ ), and response times ( $t_r$ ) for various sample gases with or without the anaesthetics module (+ or - in column M). Column N shows the number of experiments, and column F shows the best fitting model: exponential (E) or normal probability integral (N). Significant differences ( $P < 0.01$ ) are indicated in columns I (between anaesthetics module on or off), and in column II (between on and off transients) with '\*'.

Measured  $t_M = 11.376$  s (SEM = 0.003) (calculated  $t_M = 10.69$  s)

Measured  $F_B = 47$  ml.min<sup>-1</sup> (calculated  $F_B = 46$  ml.min<sup>-1</sup>)

	On transients				Off transients				Model	
Gas M	N	F	$t_r$ (ms)	SEM I	N	F	$t_r$ (ms)	SEM I	$t_r$ (ms)	II
N <sub>2</sub> O +	5	N	182	8	5	N	175	3	150	
N <sub>2</sub> O -	4	N	151	1	5	N	160	8	150	
O <sub>2</sub> +	5	N	174	1 *	5	N	165	1 *	150	*
O <sub>2</sub> -	5	N	196	2	4	N	177	3	150	*
N <sub>2</sub> +	5	N	163	9	5	N	158	2	141	
N <sub>2</sub> -	5	N	158	5	5	N	159	3	141	
CO <sub>2</sub> +	6	N	210	4	5	N	192	4	159	
CO <sub>2</sub> -	5	N	186	7	5	N	189	10	159	
Ar +	6	N	172	9	5	N	164	5	146	
Ar -	6	N	178	3	5	N	162	3	146	*
HAL +	5	E	395	14	6	E	478	9	229	*
HAL -	4	E	403	21	6	E	450	11	229	

Table 7.10: First nylon inlet line (on line)

Combination of 0.25 + 30 m with 0.25 and 1.07 mm i.d.

Experimental and predicted values for the residence time ( $t_M$ ), sample flow ( $F_B$ ), and response times ( $t_r$ ) for various sample gases with or without the anaesthetics module (+ or - in column M). Column N shows the number of experiments, and column F shows the best fitting model: exponential (E) or normal probability integral (N). Significant differences ( $P < 0.01$ ) are indicated in columns I (between anaesthetics module on or off) with '\*', in column II (between on and off transients) with '@', and in column III (between the recorded test and the test on line) with '@' (on transients) and with '\$' (off transients).

Measured  $t_M = 11.350$  s (SEM = 0.000) (calculated  $t_M = 10.69$  s)Measured  $F_B = 49$  ml.min<sup>-1</sup> (calculated  $F_B = 46$  ml.min<sup>-1</sup>)

Gas M	On transients				Off transients				Model		
	N	F	$t_r$ (ms)	SEM I	N	F	$t_r$ (ms)	SEM I	$t_r$ (ms)	II	III
N <sub>2</sub> O +	3	N	178	3 *	3	N	186	6	150		
N <sub>2</sub> O -	3	N	154	3	3	N	169	3	150		
O <sub>2</sub> +	3	N	176	3	3	N	164	1 *	150		
O <sub>2</sub> -	3	N	182	9	3	N	169	0	150		
N <sub>2</sub> +	3	N	160	4	3	N	166	1	141		
N <sub>2</sub> -	3	N	160	5	3	N	162	0	141		
CO <sub>2</sub> +	5	N	192	1 *	3	N	192	1	159		@
CO <sub>2</sub> -	3	N	177	3	3	N	179	2	159		
Ar +	3	N	175	0	3	N	164	0	146	*	
Ar -	3	N	179	1	2	N	161	0	146	*	
HAL +	3	E	677	3	3	E	771	3	229	*	@ \$
HAL -	3	E	679	3	4	E	756	5	229	*	@ \$

Table 7.11: Second nylon inlet line

Combination of 0.4 + 30 m with 0.25 + 1.07 mm i.d.

Experimental and predicted values for the residence time ( $t_M$ ), sample flow ( $F_B$ ), and response times ( $t_r$ ) for various sample gases with or without the anaesthetics module (+ or - in column M). Column N shows the number of experiments, and column F shows the best fitting model: exponential (E) or normal probability integral (N). Significant differences ( $P < 0.01$ ) are indicated in columns I (between anaesthetics module on or off), and in column II (between on and off transients) with '\*'.

Measured  $t_M = 13.370$  s (SEM = 0.006) (calculated  $t_M = 12.85$  s)

Measured  $F_B = 33$  ml.min<sup>-1</sup> (calculated  $F_B = 32.0$  ml.min<sup>-1</sup>)

	On transients				Off transients				Model	
Gas M	N	F	$t_r$ (ms)	SEM I	N	F	$t_r$ (ms)	SEM I	$t_r$ (ms)	II
N <sub>2</sub> O +	3	N	172	2 *	3	N	179	1	153	
N <sub>2</sub> O -	3	N	157	1	3	N	169	4	153	
O <sub>2</sub> +	3	N	177	0 *	3	N	165	1	153	*
O <sub>2</sub> -	3	N	191	2	3	N	171	1	153	*
N <sub>2</sub> +	3	N	167	3	3	N	162	1	145	
N <sub>2</sub> -	3	N	165	2	3	N	161	1	145	
CO <sub>2</sub> +	3	N	192	2 *	3	N	195	1	161	
CO <sub>2</sub> -	3	N	173	1	3	N	180	2	161	
Ar +	3	N	176	0	3	N	164	0	149	
Ar -	3	N	179	0	3	N	162	0	149	
HAL +	3	E	710	4	3	E	776	7	230	*
HAL -	3	E	719	10	3	E	770	1	230	*

Table 7.12: Third nylon inlet line.

Combination of 0.1 m fused silica and 30 m nylon.

Experimental and predicted values for the residence time ( $t_M$ ), sample flow ( $F_B$ ), and response times ( $t_r$ ) for various sample gases with or without anaesthetics module (+ or - in column M). Column N shows the number of experiments, and column F shows the best fitting model: exponential (E) or normal probability integral (N). Significant differences ( $P < 0.01$ ) are indicated in columns I (between anaesthetics module on or off) with '\*', in column II (between on and off transients) with '@', and in column III (between this combination and the combination 0.25 + 30 m) with '\$' (on transients) and with '§' (off transients).

Measured  $t_M = 10.784$  s (SEM = 0.002) (calculated  $t_M = 10.58$  s)

Measured  $F_B = 53$  ml.min<sup>-1</sup> (calculated  $F_B = 47$  ml.min<sup>-1</sup>)

Gas M	On transients				Off transients				Model		
	N	F	$t_r$ (ms)	SEM I	N	F	$t_r$ (ms)	SEM I	$t_r$ (ms)	II	III
N <sub>2</sub> O +	5	N	172	3 *	5	N	182	1 *	150		
N <sub>2</sub> O -	5	N	144	1	5	N	166	2	150	*	@
O <sub>2</sub> +	5	N	174	3 *	5	N	163	2	150		
O <sub>2</sub> -	5	N	194	2	5	N	170	2	150	*	
N <sub>2</sub> +	5	N	157	1	4	N	159	1	141		\$
N <sub>2</sub> -	5	N	160	2	5	N	157	1	141		
CO <sub>2</sub> +	10	N	196	1 *	5	N	196	1 *	159		
CO <sub>2</sub> -	5	N	214	3	5	N	184	3	159	*	@
Ar +	5	N	174	1 *	5	N	163	1	145	*	
Ar -	5	N	183	1	5	N	160	1	145	*	
HAL +	6	E	472	3	5	E	500	5	229	*	@ \$
HAL -	4	E	466	6	5	E	492	4	229	*	@

## Step 2: inlet line-valve combinations

The selected inlet line and a shorter line composed of the same material (20 m + 0.26 m) were tested in combination with a valve. If possible, the mass spectrometer should be installed as near a paediatric operating room as possible to profit from the shorter delay and response times.

Table 7.13: Nylon 30 m combined tube with valve

*Experimental and predicted values for the residence time ( $t_M$ ), sample flow ( $F_B$ ), and response times ( $t_r$ ) for various sample gases with the anaesthetics module (+ in column M). Column N shows the number of experiments, and column F shows the best fitting model: exponential (E) or normal probability integral (N). Values of the same line obtained without valve are shown in column I (on transients), and in column II (off transients).*

Measured  $t_M = 11.388$  s (SEM = 0.002) (calculated  $t_M = 10.69$  s)

Measured  $F_B = 49$  ml.min<sup>-1</sup> (calculated  $F_B = 46$  ml.min<sup>-1</sup>)

Gas M	On transients				I	Off transients				Model	
	N	F	$t_r$ (ms)	SEM		N	F	$t_r$ (ms)	SEM		II
N <sub>2</sub> O +	5	N	208	3	178	4	N	211	1	186	150
O <sub>2</sub> +	5	N	197	1	176	5	N	186	1	164	150
N <sub>2</sub> +	5	N	185	1	160	5	N	185	1	166	141
CO <sub>2</sub> +	5	N	210	2	192	6	N	214	1	192	159
Ar +	5	N	192	0	175	5	N	189	0	164	146
HAL +	5	E	607	8	677	4	E	669	18	771	229

Tables 7.13 and 7.14 show the results for both lines. Only transients with the anaesthetics module were measured as the mass spectrometer was to be used in this mode during clinical practice. The higher cut off frequency of this 20 m line ( $f_{CO} = 2.11$  Hz for  $CO_2$ ) compared to that of the 30 m line ( $f_{CO} = 1.67$  Hz for  $CO_2$ ) is advantageous in the monitoring of children.

Table 7.14: Nylon 20 m combined tube with valve  
*Experimental and predicted values for the residence time ( $t_M$ ), sample flow ( $F_B$ ), and response times ( $t_r$ ) for various sample gases with the anaesthetics module (+ in column M). Column N shows the number of experiments, and column F shows the best fitting model: exponential (E) or normal probability integral (N). Column I and column II show values for the 30 m line with valve.*

Measured  $t_M = 6.706$  s (SEM = 0.002) (calculated  $t_M = 5.65$  s)

Measured  $F_B = 49$  ml.min<sup>-1</sup> (calculated  $F_B = 49$  ml.min<sup>-1</sup>)

Gas M	On transients				Off transients				Model		
	N	F	$t_r$ (ms)	SEM	I	N	F	$t_r$ (ms)	SEM	II	$t_r$ (ms)
N <sub>2</sub> O +	3	E	174	3	208	3	N	162	2	211	100
O <sub>2</sub> +	3	N	163	1	197	3	N	150	0	186	100
N <sub>2</sub> +	3	N	146	1	185	3	N	147	0	185	94
CO <sub>2</sub> +	3	N	166	1	210	3	N	169	1	214	105
Ar +	3	N	156	0	192	3	N	150	0	189	97
HAL +	3	E	520	2	607	3	E	564	4	669	153
ENF +	3	E	375	1		3	E	430	1		155
ISO +	3	E	388	14		3	E	437	9		155

### *Step 3: multiple user inlet system*

The selected inlet line was redesigned for clinical use on two points, since not only less careful handling but also obstruction of the inlet lines by small particles was expected.

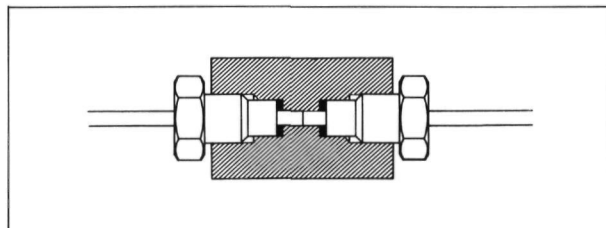


*Fig.7.5: Union without dead volume for joining the different parts of the inlet line and sampling system (enlarged). The bolt compresses the O-ring and allows to exchange components. (Made and drawn by G. Toenders.)*

Firstly, the small bore tube fixed in front of the rest of the inlet line during the experimental study was housed totally into the wider bore tubing to prevent kinking of the fine tubing at the tip. Secondly, a practical solution had to be found for changing obstructed lines. Therefore the long wider bore tube was divided into two parts of 2.1 m and 27.9 m, called "patient probe" and "transport probe", respectively. A coupling device without dead volume was developed to join both parts (see fig.7.5). The construction of this union allowed to replace a blocked patient probe in two minutes by a spare one. Since it was expected that obstruction would occur mostly at the upstream end of the inlet line, the presence of a few spare patient probes could solve most of the problems of obstructed lines (if any). The downstream end of the transport probe was connected to the valve via a 0.1 m length of the same nylon tubing as was used for the inlet line and an identical union as shown in fig.7.5. This construction allowed exchanging of the transport probe if needed. The tip of the patient probe was glued into an ISO



Table 7.15: Final version of the selected line

*Experimental and predicted values for the residence time ( $t_M$ ), sample flow ( $F_B$ ), and response times ( $t_r$ ) for various sample gases with the anaesthetics module (+ in column M) after redesign for clinical use. Column N shows the number of experiments, and column F shows the best fitting model: exponential (E) or normal probability integral (N). Column I and II show values of the line obtained before redesigning.*

Measured  $t_M = 11.263$  s (SEM = 0.003) (calculated  $t_M = 10.69$  s)

Measured  $F_B = 50$  ml.min<sup>-1</sup> (calculated  $F_B = 46$  ml.min<sup>-1</sup>)

Gas M	On transients				Off transients				Model		
	N	F	$t_r$ (ms)	SEM	I	N	F	$t_r$ (ms)	SEM	II	$t_r$ (ms)
N <sub>2</sub> +	3	N	188	2	185	3	N	185	1	185	141
CO <sub>2</sub> +	3	N	218	3	210	3	N	215	1	214	159
HAL +	3	E	631	2	607	3	E	688	4	669	229
ENF +	3	E	483	3		3	E	569	8		232
ISO +	3	E	480	3		3	E	515	15		232

15 mm connector so that sample gas was sucked off centrally in the breathing system.

To be sure that the redesigning had no major influence on the performance parameters, the final version of the inlet line was tested for a few sample gases. The results are listed in table 7.15 and are comparable to those obtained before the redesign.

Four of the redesigned 30 m inlet lines and four miniature solenoid valves were assembled to form a system for sequential sampling, shown in fig.7.6. The valves were circularly mounted to minimize

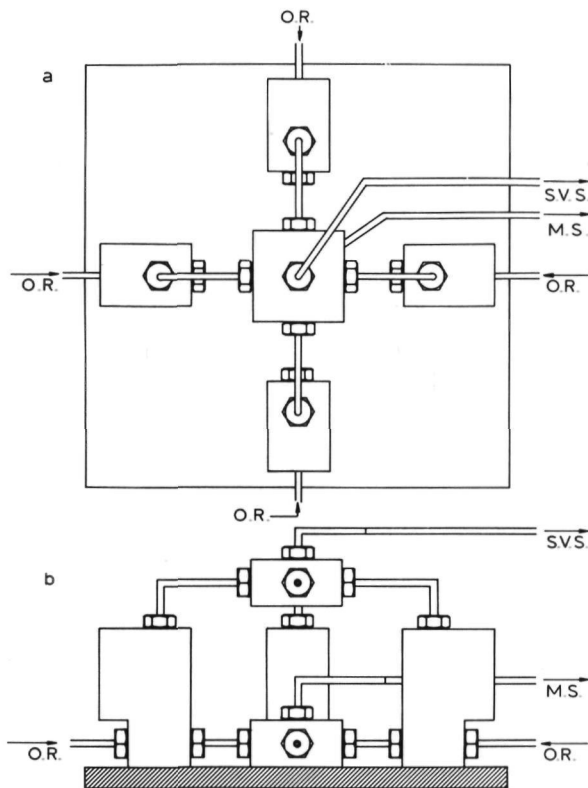


Fig.7.6: *Top (a) and side (b) view of the sampling system for four patients. Four circularly mounted valves direct the sample flows from the four operating rooms (O.R.) to the mass spectrometer (M.S.), or the separate vacuum source (S.V.S.)(made and drawn by G. Toenders).*

dead volume. A separate vacuum source was needed to maintain the sample flow through each inlet line not being connected to the mass spectrometer. This arrangement guaranteed that current respiratory signals were fed to the instrument. All unions between the different parts of the assembly were of the described type and each union proved to be (helium) leak free. A length of 0.15 m nylon tubing

fitted with a Luer connector completed the link between the valves and the normal inlet port of the mass spectrometer. A valve control unit, described in the next chapter, allowed to direct the gas of one of the four lines to the mass spectrometer by switching the appropriate valves.

### 7.1.3 General discussion

Lack of information about the structure and composition of the various polymers used for manufacturing the tested tubes prevented to find correlations between solubility coefficients in the polymers and the observed response times. The results of this study should therefore not be applied to tubes of materials carrying the same generic name, since various modifications of polymers (crosslinking, plasticizing, crystallising, and fillers) affect the gas-polymer interactions (Stannett, 1968). Perhaps other polymer modifications showing less interaction with the anaesthetic gases will be found in the near future.

The decrease in response times in the polyethylene combined tube in comparison with a 30 m uniform tube (same flows) is stronger than the model predicts. This may be explained as follows. There is a relation between the partial pressure of the sample gas and the contact area between both phases on one hand, and the adsorbed and absorbed amount of gas on the other. (Fig.6.14 shows the pressure versus distance functions for both types of tube.) The product of the average pressure and the area of the inner surface of the tube (or the sum of the products for both tube parts) is smaller for the combined tube.

The unfortunate observation that halothane response times were increasing in the course of the study is illustrated in table 7.16. Apparently contamination of the gas handling system could not be avoided.

Comparison of the presented results and those reported by others is difficult as the experimental conditions were different. Moreover, response times are given in the various reports as 10 to 90%, 0 to 90%, or 0 to 95% response times. Table 7.17 shows the performance parameters of various inlet lines in clinical use. Ozanne

Table 7.16: Chronological values of halothane response times  
*The halothane response time for tubes with comparable sample flows as a function of time.*

day	on transient (ms)	off transient (ms)	sample flow (ml.min <sup>-1</sup> )	tube no.
0	395	478	47	1
7	452	526	52.6	2
120	472	500	52.6	2
165	710	776	32.6	3
166	677	771	49	1

Table 7.17: Comparison of various inlet lines  
*Values of the performance parameters of inlet lines, reported by Ozanne et al. (1981)(1), Spence (1981)(2), Gillbe et al. (1981)(3), and this study (4 and 5). Transients are off transients. Symbols: ny = nylon, pe = polyethylene, u = tube with uniform diameter, c = combined tube.*

Tube	Sample flow (ml.min <sup>-1</sup> )	t <sub>M</sub> (s)	t <sub>R</sub> N <sub>2</sub> (ms)	t <sub>R</sub> CO <sub>2</sub> (ms)	t <sub>R</sub> HAL (ms)	t <sub>R</sub> %
1) 30 m nylon u	180	6.4	200	250	280	10-90%
2) 45 m nylon u	20	26	560	625	1050	0-90%
3) 32.25 m pe c	42	13.9	?	860	?	0-95%
4) 30.25 m ny c	49	11.4	166	192	771	10-90%
5) 30.40 m ny c	33	13.4	162	195	776	10-90%

et al. (1981) reported that their results for the response time shown in table 7.17 must be doubled when the outlet pressure of the inlet lines is increased to 75 kPa in order to store the respiratory signal.

Goodwin (1979) measured 10 to 90 percent response times for capillaries of 1 mm and 2 mm bore with lengths of up to 90 m, but mentioned neither tube material nor sampling flow and did not test anaesthetic agents. He found that response times were proportional to capillary length but were independent of radius. His result, that the increment of response time per unit tube length is  $4 \text{ ms.m}^{-1}$ , is in agreement with eq.6.32, where  $4.6 \text{ ms.m}^{-1}$  was calculated. In his experiments the tested inlet line was fitted directly to the molecular leak.

## 7.2 EXPERIMENTAL STUDY IN THE OPERATING THEATRE

The Centronic mass spectrometer and the eight-channel chart recorder were installed in the operating theatres of the Department of Obstetrics and Gynaecology (head Prof. Dr T.K. Eskes) of the Sint Radboud University Hospital, Nijmegen. The equipment was located in one of the two operating theatres, but the long inlet lines allowed the analysis of the respiratory gases of the two patients. The main objectives of this part of the study were:

- to compare the performance of a long inlet line with that of an inlet line of conventional length in a clinical situation,
- to illustrate the clinical use of long sampling tubes.

### 7.2.1 Long versus short inlet line

The short inlet line was a combination of the same materials as used for the selected long inlet line: 0.4 m of 0.25 mm bore nylon tubing was housed in a 2 m length of tubing, inner diameter 1.07 mm. This configuration was chosen for two reasons. First, the sample flows of short and long line had to be comparable ( $44 \text{ ml.min}^{-1}$  and  $50 \text{ ml.min}^{-1}$  were measured). Secondly, the short line had to be connected to one of the valves of the multi-patient sampling system. The design of the multi-patient system and the difference in transit times of the two lines (0.3 s cf. 11.3 s) allowed to analyse the same breath sampled through each of the two lines. Therefore, two

breaths sampled through the short line were first recorded, then the valves were switched and the same two breaths, sampled through the long line, were analysed. Thus it was possible to compare directly the respired waveforms of gas that had been sampled through both inlet lines simultaneously. Fig.7.7 shows that the isoflurane single breath curves sampled through the long line are only slightly blunted.

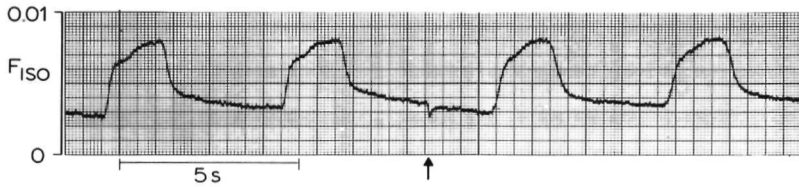


Fig.7.7: Comparison of the same two breaths of isoflurane sampled through the short (2 m) line (left), and through the long (30 m) inlet line (right). The arrow indicates switching lines.

## 7.2.2 Clinical use of long sampling tubes

Following components were routinely analyzed in the respiratory air of anaesthetized patients: nitrogen, oxygen, carbon dioxide, nitrous oxide, argon, and one volatile anaesthetic (halothane, enflurane, or isoflurane).

### 7.2.2.1 Monitoring of fractional gas concentrations

Five examples of checking and controlling the composition of anaesthetic gas mixtures are now given. Fig.7.8 shows the waveforms of respired CO<sub>2</sub> at the mouth during controlled ventilation on one hand, and spontaneous breathing on the other hand. The capnograms at a breathing frequency of 20 breaths.min<sup>-1</sup>, and the "cardiogenic" oscillations produced during slow spontaneous ventilation at the end of anaesthesia are well preserved.

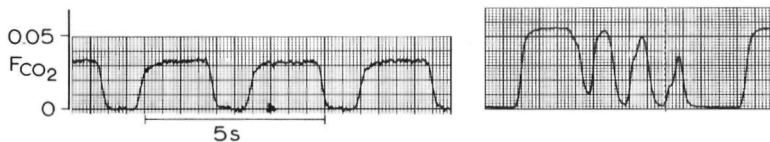


Fig.7.8: *Capnograms obtained via the 30 m inlet line during controlled ventilation ( $20 \text{ breaths} \cdot \text{min}^{-1}$ ) with a  $\text{N}_2\text{O}/\text{O}_2$  mixture (left), and during spontaneous air breathing via the endotracheal tube at the end of anaesthesia (right). Note the difference in noise, and the cardiogenic oscillations.*

The administration of isoflurane for a very short procedure is illustrated in fig.7.9. The narrow "peak" at the start is caused by opening the vaporizer. The recording shows that it takes some time before the inspiratory level of the volatile anaesthetic is constant, owing to the anaesthetic uptake by breathing circuit components.

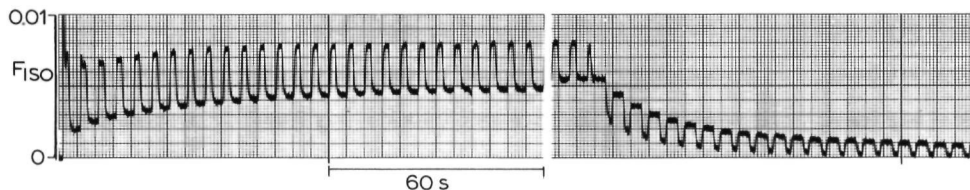


Fig.7.9: *Wash-in and wash-out of isoflurane during a laparoscopy*

The waveforms in fig.7.10 show the (unintentional) admixture of room air disturbing normal nitrous oxide wash-in at the start of general anaesthesia.

Fig.7.11 provides an illustration of sequential monitoring of patients in two operating theatres: only oxygen and halothane waveforms are shown.

Fig.7.12 illustrates that the mass spectrometer instantaneously detects a leakage of air into the circle system when closed-circuit anaesthesia is started after denitrogenation of the patient.

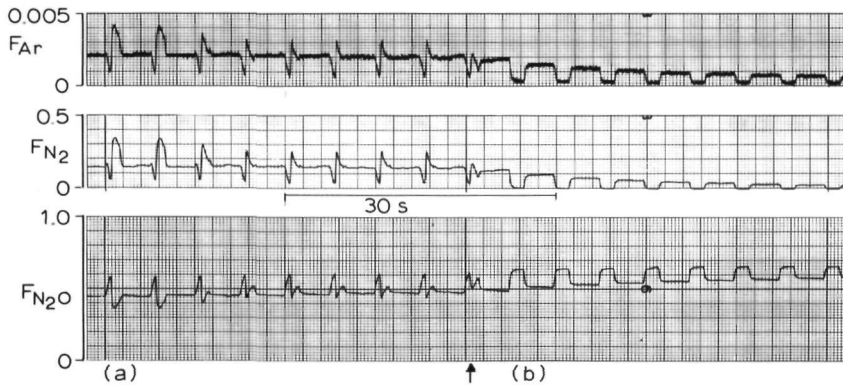


Fig.7.10: *Unintentional air admixture just after the start of general anaesthesia, while the patient was supposed to breathe a 2/1 N<sub>2</sub>O/O<sub>2</sub> mixture (a). Normal wash-in of N<sub>2</sub>O, and wash-out of N<sub>2</sub> and Ar are resumed at the arrow after closing the air inlet valve of the ventilator (b).*

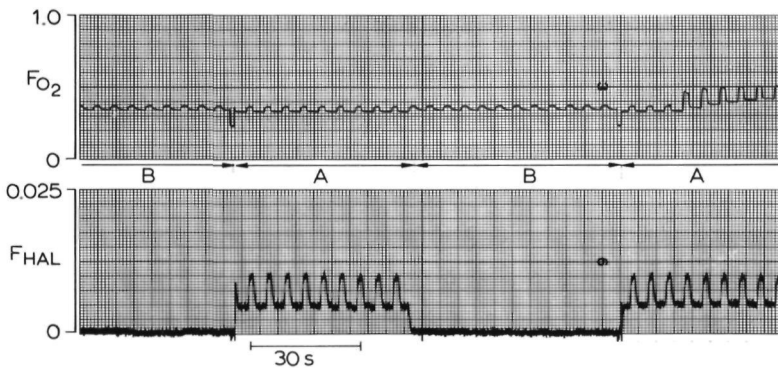


Fig.7.11: *Sequential sampling from operating rooms A and B. In room A halothane is administered, and the F<sub>I,O<sub>2</sub></sub> is just being raised. In room B no halothane is used.*



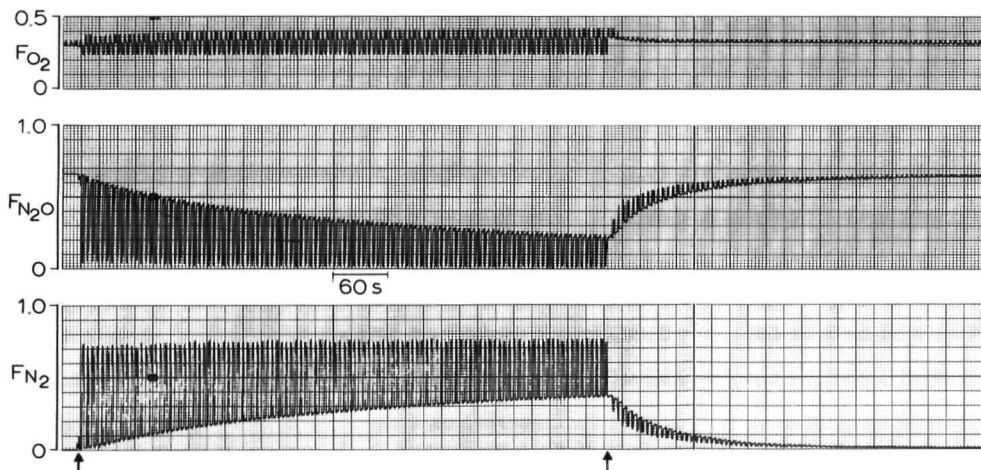


Fig.7.12: *Example of a leaking circle system. At the first arrow a closed-circuit anaesthesia is started (fresh gas flow is  $0.25 \text{ l.min}^{-1} \text{ O}_2$ ). An oxygen analyser with a slow response did not detect the leak. At the second arrow fresh gas flow is raised ( $2$  and  $1 \text{ l.min}^{-1} \text{ N}_2\text{O}$  and  $\text{O}_2$ , respectively).*

#### 7.2.2.2 Estimation of pulmonary blood flow

It was realized that the simple manoeuvre of  $\text{N}_2\text{O}$  wash-in, carried out at the start of general anaesthesia, might provide information about the circulatory condition of the patient. The present investigation explored the possibility to estimate pulmonary capillary blood flow from the  $\text{N}_2\text{O}$  wash-in curve. The objective was not to investigate thoroughly the proposed method, but to perform a pilot study that might be a base for further investigations.

Kety (1951) derived an expression that describes the alveolar gas fraction ( $F_A$ ) of a foreign gas, e.g.  $\text{N}_2\text{O}$ , as a function of time after a step change in the inspiratory gas fraction ( $F_I$ ). It is possible to deduce the pulmonary blood flow from this expression, if the course of the ratio  $F_A/F_I$  as a function of time is known, and if the ratio  $V_D/V_T$  is estimated via the Bohr equation ( $V_D$  = dead space,  $V_T$  = tidal volume).

Five female patients (ASA I), scheduled for laparoscopy, age from 22 to 37 years, were induced with fentanyl 0.1 mg, gallamine ( $0.3 \text{ mg.kg}^{-1}$ ), and pentothal ( $5 \text{ mg.kg}^{-1}$ ). Suxamethonium ( $1 \text{ mg.kg}^{-1}$ ) facilitated intubation. Patients were connected to an Engstrom ventilator, already running with a fresh gas mixture of 2/1 nitrous oxide/oxygen to guarantee a stepwise change in the inspiratory  $\text{N}_2\text{O}$  fraction. Breathing frequency was 12 per minute. Expired gas escaped to the atmosphere via a 2-litre breathing bag at the outlet of the ventilator. One 30 m inlet line continuously sampled at the mouth of the patient during the first five minutes of anaesthesia. During this period (no surgical stimulus was applied), a  $\text{N}_2\text{O}$  wash-in curve was recorded on the XY-recorder, and the capnogram recorded on the Gould Brush recorder. Immediately after this period, gas was sampled via another 30 m line from the breathing bag to measure the mean expiratory  $\text{CO}_2$  fraction. Respiratory minute volume was timed on the ventilator spirometer.

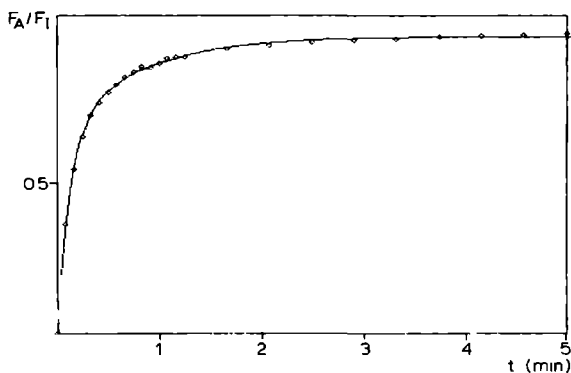


Fig.7.13: Curve fitted by the program JOSEXP through the points obtained by plotting the ratio of the alveolar ( $F_A$ ) to the inspiratory ( $F_I$ )  $\text{N}_2\text{O}$  fractions against time.

A biexponential curve was fitted through the values of  $F_A/F_I$  by a program JOSEXP (see fig.7.13), generating the necessary factors to calculate the capillary pulmonary blood flow from Kety's equation.

Table 7.18 lists the results. An error analysis is beyond the scope of this thesis, but the presented results are such that the estimation of the pulmonary blood flow with the aid of a step change in inspiratory  $N_2O$  fraction should be further investigated in the future.

Table 7.18: Estimation of pulmonary blood flow  
*Values of the ratio anatomical dead space ( $V_D$ ) to tidal volume ( $V_T$ ) and capillary pulmonary blood flow ( $\dot{Q}_{cp}$ ) in five female patients.*

Patient	weight (kg)	age (years)	$V_D/V_T$	$\dot{Q}_{cp}$ (l.min <sup>-1</sup> )
1	74	37	0.263	7.85
2	56	22	0.324	7.58
3	81	33	0.268	8.81
4	60	34	0.235	4.89
5	69	36	0.289	5.69

## CHAPTER 8

### SIMULTANEOUS MONITORING OF FOUR PATIENTS

Sequential analysis of the respiratory gases from several patients by a centrally located mass spectrometer causes a dead period before new results are available. While the sample gas from one line is analysed, and the results are displayed in the operating theatre, the gas from all other patients is drawn off by a separate vacuum source and is not analysed. Consequently, the anaesthetist receives no information about his patient during considerable time periods. Sucking off sample gas between the periods of analysis guarantees that current information is presented to the mass spectrometer when the sampling system switches from one line to the other (see fig.1.1).

An alternative to this "slow" sequential monitoring was given in a preliminary report (Ponte, Lerou and van der Vegt, 1981). A system, sampling sequentially the respiratory gases of four patients at a frequency higher than their breathing frequency, was proposed to realize simultaneous monitoring of four patients with one mass spectrometer. This chapter describes the further developments of this system, its theoretical background, the testing of its parts, its applications, and its limitations.

#### 8.1 SAMPLING THEORY

Digitizing analog signals is a necessary step in the process of signal analysis by digital computers. During this step, an analog (continuous) input signal is being sampled at a fixed sampling rate by an analog to digital converter (ADC). The analog signal is transformed into a sequence of discrete samples so that the waveform is represented by a series of numbers, as illustrated in fig.8.1. If the sampling rate is high enough the analog signal can be reconstructed from the digital data. If the sampling rate is too low,

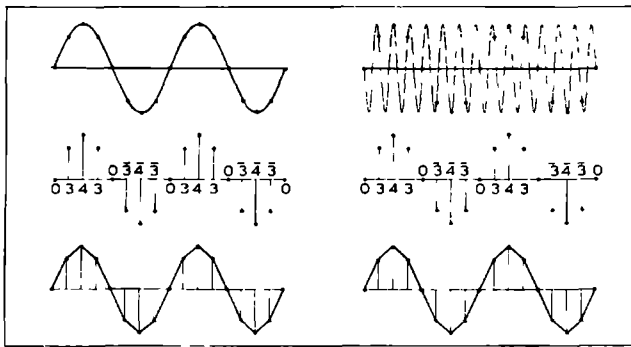


**Fig.8.1:** *Two analog electric signals are converted into two sequences of discrete samples so that the signals are represented by a series of numbers. Left: the sampling rate is high enough to recover the original signal. Right: the too low sampling rate yields a signal without resemblance to the original signal (aliasing error). A linear interpolation between the sample points illustrates that the interpolation method also determines the minimum sampling rate to recover a signal within allowable error limits (After J.P. Blackburn (Scurr and Feldman, 1974), by courtesy of W. Heinemann Medical Books Ltd).*

errors are made when recovering the original signal (foldover or aliasing error). The selection of sampling<sup>2</sup> rates is governed by theoretical considerations.

A starting point for selecting sampling rates is Shannon's Sampling Theorem, which states: "If a time function contains only frequency components below  $F$  cycles per second,  $2F$  samples per second suffice to represent it perfectly and permit perfect recovery". The limitations of this theory were investigated by Gardenhire

---

<sup>2</sup> The reader will recognize that "to sample" has another meaning in the language of signal analysis than used thus far. "Sampling" in respiratory mass spectrometry means the continuous process of drawing off the sample gas through the inlet system, whereas "sampling" in signal analysis refers to the discontinuous process of taking a sample at fixed intervals.

(1964) who showed that it only holds for ideal data with a frequency spectrum cutting off perfectly above frequency  $F$ , and for an optimum reconstruction method interpolating between successive samples, i.e. a Wiener filter. He calculated the minimum sampling rate for non-ideal data as a function of the manner in which the frequency spectrum of the analog signals falls off, the reconstruction method, and the allowable error in recovering the signals.

So far sampling of electric signals at fixed intervals has been treated. Respiratory signals could be sampled similarly under their gaseous form by cyclic interruption of the gas stream from one line. Thus the gas from different inlet lines could be sequentially fed to the mass spectrometer at a much higher frequency than used for normal slow sequential monitoring. An example of a system for four patients will clarify the difference between both types of monitoring. Suppose that sampling periods of 20 seconds are used for one operating theatre with the "slow" method. During this period a few breaths are analysed, the information for the anaesthetist is updated, then no more information is available to him during 60 seconds (see fig.8.2). The proposed system, on the other hand, uses a sampling period of a fraction of a second on each inlet line. In the ideal situation this period would be infinitesimally short so that the complete respired waveforms of the four patients could be recovered and made simultaneously available to the anaesthetists in the four operating rooms (see schematically in fig.8.3). Therefore the raw output signal of the mass spectrometer has to be rearranged to assemble the information of one patient. Since the performance of a pneumatic system switching at high frequencies from line to line has its limitations, the ideal situation can only be approached.

It is concluded from the foregoing that both the frequency spectrum of the respiratory input signal and the maximum attainable switching frequency of the pneumatic system must be evaluated to test the proposed method.

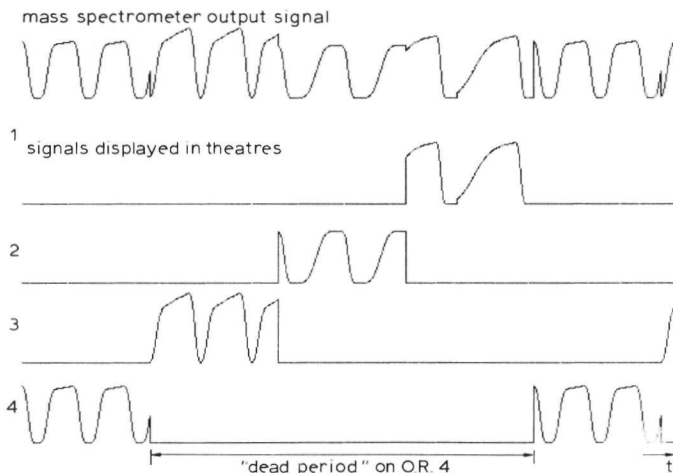


**Fig.8.2:** *Scheme of sequential analysis of the airway gases of four patients. Complete respiratory waveforms are displayed. No information is available in one operating theatre during the dead period.*

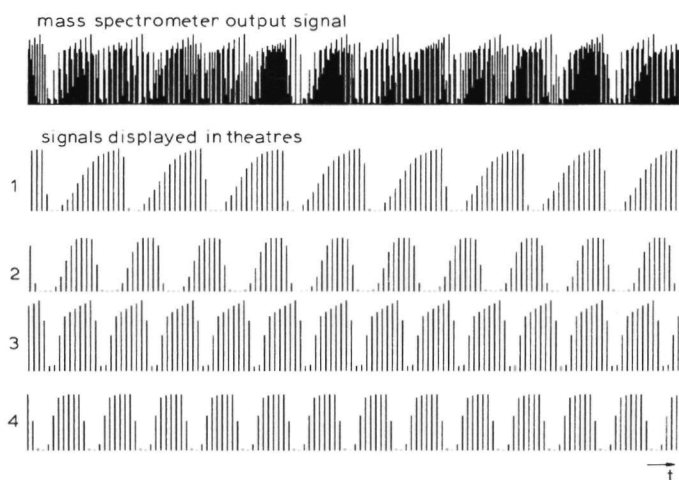


**Fig.8.3:** *Scheme of the proposed method (same respiratory signals as in fig.8.2). The mass spectrometer output signal has to be rearranged and reconstructed for each patient. A continuous monitoring of the four patients is realized.*

## 8.2 SYSTEM DESIGN

### 8.2.1 The pneumatic sampling system

The system described in the previous chapter was used. Valves manufactured by Skinner caused mechanical troubles at high switching frequencies, and were replaced by Kuhnke valves (24 V solenoid valves). The performance of the separate vacuum source is important, not only because the performance parameters of the inlet lines depend on it, but also because the artifacts on the output signal generated by switching lines were influenced by the vacuum performance. Both points will be illustrated further.

### 8.2.2 The valve control unit

An electronic unit controlled the switching of the valves in three modes. Firstly, the valves could be switched manually by a push button on the unit to sample during any desired period on the same inlet line. Secondly, the valves could be switched at a frequency governed by a square wave generator. In this mode the total sampling time was automatically shared between the four lines. In the third mode, illustrated in fig.8.4, the timing of the valves was controlled by the internal clock of the mass spectrometer via the control unit. In each of the three modes it was possible to overlap the opening of the valves by zero to 50 ms (Y in fig.8.4).

### 8.2.3 Sample and hold circuits

The raw output signal of each channel of the mass spectrometer could be fed to four sample and hold circuits, one for each patient. Each circuit was gated "on" during the last 50 ms of the sampling period on one line and held the signal until the circuit was updated. Thus parallel outputs were provided, one for each patient and each gas of interest. This hardware solution for rearranging the signals and the resulting step interpolation between successive samples were considered satisfactory to illustrate the principles and the possibilities of the proposed method.



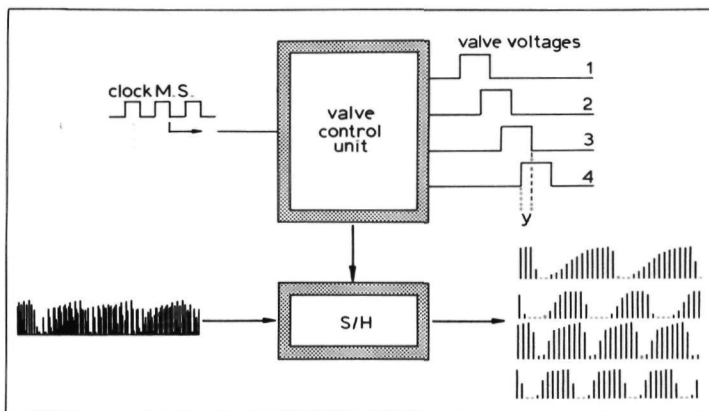


Fig.8.4: *The valve control unit. This unit transforms the signal from the internal clock of the mass spectrometer (M.S.) into the voltages for switching the valves (Y = adjustable overlap time), and controls the opening of the sample and hold circuits (S/H) which rearrange the raw output signals.*

### 8.3 SYSTEM EVALUATION

#### 8.3.1 Respiratory input signal

The frequency spectrum of the respiratory input signal was evaluated as follows. Gas was sampled from a ventilated patient (breathing frequency  $12 \text{ breaths} \cdot \text{min}^{-1}$ ) through the standard inlet capillary on one hand, and the 30 m inlet line on the other. The  $\text{CO}_2$ -signals were recorded on the instrumentation tape recorder. A fast Fourier transform of the  $\text{CO}_2$ -signals of twelve consecutive breaths (showing a linearly rising plateau) allowed to calculate the power content of their frequency spectra, which are shown in fig.8.5. Controlled ventilation was chosen since a valid Fourier analysis requires that the length of the respiratory cycles and the shape and magnitude of the respired waveforms are constant (Attinger and Mc Donald, 1966).

Fig.8.5 shows that both spectra have their main peak at the breathing frequency (0.21 Hz), and that the signal obtained with the long line has a poorer spectrum where frequencies higher than

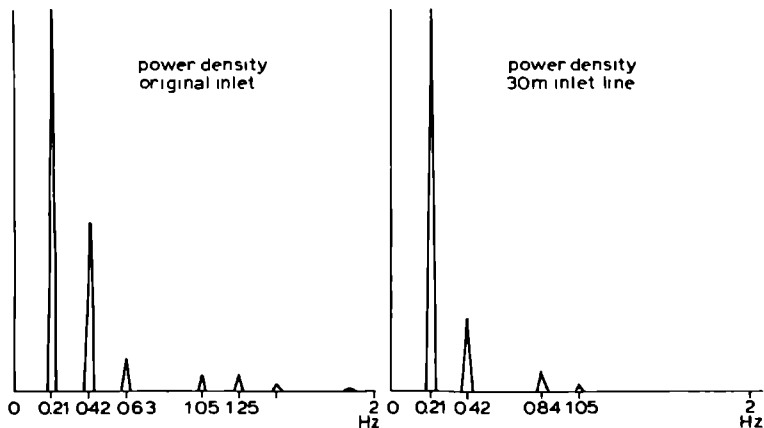


Fig.8.5: *Power spectrum of the frequencies present in the respiratory CO<sub>2</sub>-signal of a ventilated patient, obtained via the standard inlet capillary (left) and the selected 30 m line (right).*

1.05 Hz are virtually eliminated. According to Gardenhire (1964), a sampling rate of 2.1 Hz or 6.2 Hz must be used to recover the complete signal with a Wiener optimum filter or a linear interpolation method respectively (5% RMS error). This means that the sampling period on each line is maximally 0.119 s or 0.04 s, respectively (for a pneumatic system with four users).

### 8.3.2 Separate vacuum source

The separate vacuum source, responsible for the gas transport through the inlet lines during the period that the sample gas is not fed to the mass spectrometer, was evaluated by measuring the sample flow through one inlet line. Three vacuum sources were tested: the central vacuum supply, a separate rotatory pump, and the mass spectrometer transport pump via the blood gas inlet port (illustrated in figs.5.1 and 5.4). The sample flows, drawn off by the various vacuum sources and via the different inlets, were measured twice and the means are listed below:

- respiratory inlet, blood gas inlet off: 50 ml.min<sup>-1</sup>

- respiratory inlet, blood gas inlet on: 50 ml.min<sup>-1</sup>
- blood gas inlet: 49 ml.min<sup>-1</sup>
- separate rotatory pump: 49 ml.min<sup>-1</sup>
- central vacuum: 40 ml.min<sup>-1</sup>

The following conclusions were made: (1) gas sampling via the blood gas inlet as a second vacuum source did not influence the sample flow via the respiratory inlet port; (2) nearly identical performance parameters could be expected from the long inlet lines when connected to the blood gas inlet as when connected to the respiratory inlet (this had the practical advantage that no other rotatory pump had to be installed); (3) the central vacuum supply was not suited as separate vacuum source.

### 8.3.3 Switching artifact

Switching from one line to another produced an artifact on the mass spectrometer output signal owing to transient pressure changes. It was tried to minimize these artifacts because they prolonged the time needed to make a valid measurement. It was supposed that the switching artifacts would be minimal if the time to switch lines was zero, if the conductances  $G_1$  of all inlet lines were identical, if the conductances of the tubings to the mass spectrometer transport pump ( $G_2$ ) and separate vacuum source ( $G_3$ ) were identical, and if the pump performance of the separate vacuum source and transport pump would match (see fig.8.6). In other words, if the artifacts were due to pressure changes, they had to disappear if the local pressures on corresponding points of the four inlet lines and the two tubings to the vacuum sources were identical. Moreover, it was expected that the anaesthetics module would have an important influence on the artifacts.

First the conductances of the inlet lines were matched by cutting off very short lengths of the small diameter tubing until approximately equal flows were measured. The four inlet lines had a sample flow of 47, 48, 47, and 49 ml.min<sup>-1</sup> respectively (means of two measurements). Higher sample flows augmented the switching artifacts, probably because of the higher local pressure at the valves.

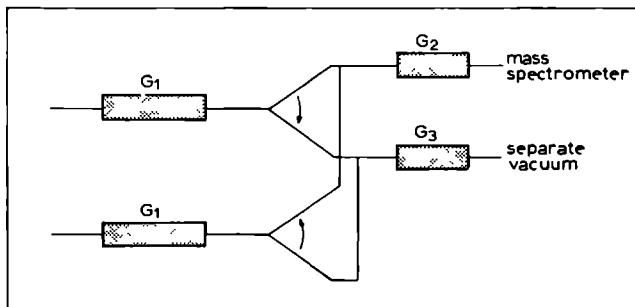


Fig.8.6: *Work hypothesis to minimize artifacts on the output signal. The switching of two valves is symbolized by the arrows. Artifacts should be minimal if the conductances of the two inlet lines ( $G_1$ ) match, if the conductances of the connecting tubes ( $G_2$  and  $G_3$ ) match, if the switching time is zero, and if the vacuum sources match.*

Secondly, the sample system as described in the previous chapter was symmetrically constructed to ensure equal conductances of all corresponding parts. Thirdly, the electronics of the valve control unit was set to switch the valves without overlap ( $Y = 0$ ).

Fourthly, the artifacts on the  $N_2$ ,  $O_2$ , and Ar channel were estimated with the valves switching at a low frequency during room air sampling (see fig.8.7). The switching artifacts were grossly influenced by the separate vacuum source: the greatest artifacts were seen with the central vacuum. They were also proportional to the output signal, but were attenuated by the use of the anaesthetics module, which let the artifacts virtually disappear when the blood gas inlet was used as separate vacuum. These artifacts were considered acceptable. The artifacts disappeared completely when the connecting tube between switching valve and the gas handling system was minimally obstructed by scarcely turning the inlet selector valve towards its closed position. This was probably due to the slightly smaller sample flow via the blood gas inlet which was 2 % lower than via the respiratory inlet. The artifacts reappeared when obstructing the connecting tube to the blood gas inlet by means of a needle

valve. All these observations supported the work hypothesis. After the described adjustments an overlap time was no longer needed to minimize the artifacts, in contrast to a previous report when adjustments were not made (Ponte, Lerou and van der Vegt, 1981).

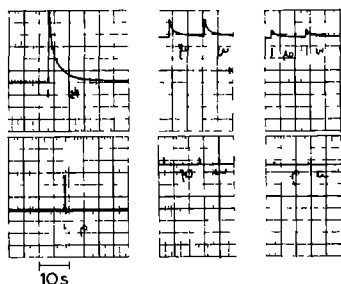


Fig.8.7: *Recordings of the switching artifacts on the  $N_2$  channel when room air was sampled. On the upper row the anaesthetics module is off, on the lower row it is on. Three separate vacuum sources were tested: the central vacuum supply (left), a separate rotatory pump (middle), and the mass spectrometer transport pump via the blood gas mode inlet (right).*

### 8.3.4 Sampling rate

The maximum attainable sampling rate per inlet line (or switching frequency of the valve) is determined by the number of lines, the features (e.g. dead volume) of the valves and connecting tube, and the response time of the mass spectrometer recording system. The latter depends on the sampled gas. The features of the valves were estimated by generating a "pulse" of the gases of interest at the valves.

The valve control unit was set at a low switching frequency. Inlet line No.1 was sucking off a 2/1  $N_2O/O_2$  gas mixture containing 10% sample gas or 3% of a volatile anaesthetic, while inlet line No.2, 3 and 4 were drawing off a 2/1  $N_2O/O_2$  mixture. At the start of each experiment, the gas from line No.1 was fed to the mass spectrometer; the gas from the other lines was sucked off by the sepa-

rate vacuum source. The valves were then switched with an interval of five seconds following the sequence No.1-2-3-4. Switching from line No.1 to No.2, or from line No.4 to No.1 generated an off or an on transient, respectively. The mass spectrometer output signal of the gas under study and the voltages activating the valves were recorded on the chart recorder running at a speed of  $100 \text{ mm.s}^{-1}$ . The overlap time of the control unit (Y in fig.8.4) was set to zero, and the anaesthetics module was on.

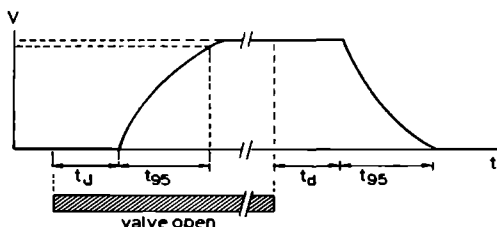


Fig.8.8: *Diagram of intervals and responses times after valve opening and closing. "Valve open" = solenoid is activated.*

An example of a recording is shown schematically in fig.8.8. An interval of approximately 100 ms was seen between the activation of the valve and the instant where the gas signal began to alter. This interval was due to the transit time of the gas to travel down the connecting tube between valve and sample chamber, since the interval lengthened considerably by inserting a length of tubing between valve and inlet port. The times needed by the gas signal to rise to 95 % of its final value or to decay to 5 % of its starting value ( $t_{95}$ ) were virtually identical and are listed in table 8.1. The results show that the tested system could not ensure the sampling rate that was calculated above in order to recover the complete input signal of all gases. The sampling periods needed to make valid measurements were too long, in particular for the volatiles. The requirement to recover the entire signal was abandoned for the time being.

Table 8.1: Features of the Kuhnke valves

*Values for the interval ( $t_d$ ), the zero to 95% response time ( $t_{95}$ ), and  $t_{tot}$  ( $t_d+t_{95}$ ) after opening of a valve.*

gas/vapour	$t_d$ (ms)	$t_{95}$ (ms)	$t_{tot}$ (ms)
N <sub>2</sub> O	90	130	220
O <sub>2</sub>	95	110	205
N <sub>2</sub>	90	115	205
CO <sub>2</sub>	90	130	220
Ar	100	110	210
halothane	100	830	930
enflurane	90	750	840
isoflurane	90	700	790

An overlap time could be reintroduced to increase the sampling rate because of the delay that was seen before the gas signal began to alter. The final switching scheme provided an opening time of 250 ms for each valve with an overlap time of 50 ms, resulting in a sampling rate of 1.25 Hz per line. These numbers were chosen to guarantee valid measurements even when the sample flow is slightly reduced by an increased inlet line resistance. Moreover, a sampling rate which is slightly higher and therefore at the margin of the possibilities of the system is prone to invalid measurements without a considerable increase in information.

## 8.4 DISCUSSION

### *What information does the system provide ?*

To answer this question, a respiratory signal obtained with a 30 m inlet line is schematically illustrated in fig.8.9. A capnogram is taken as an example and a 1/2 ratio of the inspiration to the expiration time is supposed. The time needed by the descending limb RS of the signal to reach the baseline, i.e. the inspiratory frac-

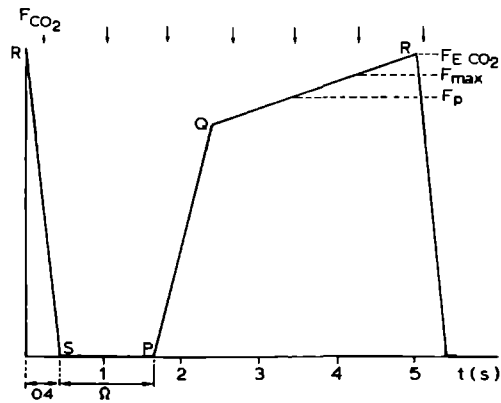


Fig.8.9: Scheme of a capnogram obtained via a 30 m inlet line. The arrows indicate the sampling points. The inspiratory CO<sub>2</sub> level (period  $\Omega$ ) is detected at every breath up to 16.67 breaths.min<sup>-1</sup>.  $F_{max}$  is the highest value detected, and  $F_p$  is its preceding value. The maximum error made by the system in the measurement of the end-expiratory fraction is discussed in the text.

tional gas concentration or  $F_I$ , depends on the frequency reponse of the inlet system and totaled 0.4 s with the selected 30 m inlet line. The duration of the period SP is given as:

$$\Omega = \frac{60}{3N} - 0.4 \quad (8.1)$$

where  $N$  is the number of breaths per minute. The  $F_I$  of each breath is detected if the sampling rate is greater than  $\Omega^{-1}$ , or if:

$$f_s \geq \frac{N}{20-0.4N} \quad (8.2)$$

where  $f_s$  is the sampling rate. Conversely, eq.8.2 allows to calculate the maximum number of breaths per minute where the  $F_I$  is



detected at each breath, if  $f_s$  is constant. When  $f_s = 1.25$  Hz, this maximum is  $16.67 \text{ breaths.min}^{-1}$ . If the breathing frequency is greater than  $16.67 \text{ breaths.min}^{-1}$ , the sampling system detects the  $F_I$  only once in two or more breaths, depending on the phase angle between the two periodic signals, i.e. the respiratory and the sampling signal.

A few points are detected on the expiratory phase PQR of the capnogram if  $N < 16.67 \text{ breaths.min}^{-1}$ . Among these, the highest value measured ( $F_{\text{max}}$ ) is the best estimate of the end-tidal  $F_{\text{CO}_2}$  of that breath ( $F_{E',\text{CO}_2}$ ). The error between the highest value detected and the true  $F_{E',\text{CO}_2}$  depends on the shape of the capnogram. No error exists if there is a horizontal plateau. If the plateau is linearly rising, the value of the error varies from breath to breath as the distance between the sample with the highest value and the end-tidal point R varies. However, the maximal error can be calculated from the information delivered by the system as illustrated in fig.8.9. In a first approximation it is supposed that the maximal error occurs when the last sample on the plateau is at the maximal interval, i.e. 0.8 s, from the end-tidal point. Since the sample intervals are identical, the maximal error is equal to the difference between the values of the maximum sample and its preceding sample, or:

$$\text{maximal error} = F_{\text{max}} - F_p \quad (8.3)$$

The maximal error is slightly smaller than calculated with eq.8.3 as the sample with the highest value is always at a shorter interval from the end-tidal point than the supposed 0.8 s. For the best estimate of the  $F_{E',\text{CO}_2}$  that may be displayed, the following corrected value may be used:

$$F_c = F_{\text{max}} + \frac{F_{\text{max}} - F_p}{2} \quad (8.4)$$

For instance, suppose that the true  $F_{E',CO_2}$  is 5% and that the maximal error is 0.3%. The displayed values for  $F_{max}$  will vary between 4.7 and 5%, whereas the value for  $F_c$  will vary between 4.85% and 5.15%.

Other information which can be calculated from the sample values is the slope of the plateau (if it is linearly rising). If the capnogram has or takes suddenly an abnormal form the maximal error no longer equals the difference between  $F_{max}$  and  $F_p$ . The value of this difference may be used as indicator of the shape of the expiratory part of the capnogram. If the capnogram takes suddenly an abnormal form, e.g. by kinking of the endotracheal tube, the value changes suddenly.

### *What information does the system not provide?*

At the sampling rate of 1.25 Hz no valid information is obtained about the volatile anaesthetics since the opening time of the valves is too short (see table 8.1). The inspiratory and end-expiratory levels of the other gases are detected at unpredictable intervals if the breathing frequency is higher than 16.67 breaths.min<sup>-1</sup>. Thus the tested system makes continuous sampling necessary for: (1) the valid analysis of volatile anaesthetics, (2) the complete waveforms of the respired gases, and (3) breathing frequencies higher than 16.67 breaths.min<sup>-1</sup>. A basic solution to overcome that need will be given below. A practical solution for the time being might be to combine both sampling modes, to interrupt manually or automatically the fast sampling system and to switch over to continuous analysis for a short period. The last solution is acceptable for several reasons.

Firstly, the  $F_I$  and the  $F_{E'}$  of the volatiles do not alter as fast as the other gases in most situations, particularly in low flow systems, and volatile anaesthetics are not always administered. Secondly, continuous display of the complete waveforms of all gases and vapours during the entire operation is seldom asked for. The anaesthetist who wants to see an entire waveform of a gas or vapour receives that information at regular intervals or he can ask for it at crucial moments. At the same time he can evaluate the true error

between  $F_C$  and  $F_E'$ . Thirdly, the interruption of the fast sampling for only a short period will suffice for analysis of the complete respired waveforms of patients with a high breathing frequency: at 25 breaths.min<sup>-1</sup>, two complete breaths are analysed in 4.8 seconds. Any desired scheme for the automatic switching from one sampling mode to the other might be controlled by a microprocessor or micro-computer adjusting the scheme to the actual needs of the users.

### *How can the system be improved?*

The tested system cannot attain sampling rates high enough to reconstruct complete respiratory waveforms. A speculation about a basic solution is to propose the construction of a "multi-molecular leak mass spectrometer": four appropriate micro valves, one for each patient, might act as molecular leaks. Switching rates of the leaks would only be determined by the basic response of the mass spectrometer. A blue-print has been made.

## 8.5 CLINICAL APPLICATIONS

This section illustrates the principle of the simultaneous monitoring of four patients with one mass spectrometer. Only two patients were monitored since there were only two operating rooms available. The other two inlet lines of the system sampled room air. The artifacts seen on the recordings are due to the sample and hold circuits of the prototype. Illustrations are given on the following points:

- functioning of the system at a breathing frequency of 12 and 16 breaths.min<sup>-1</sup> (fig.8.10),
- simultaneous monitoring (fig.8.11),
- adjustment of  $F_{I,O_2}$  (fig.8.12).

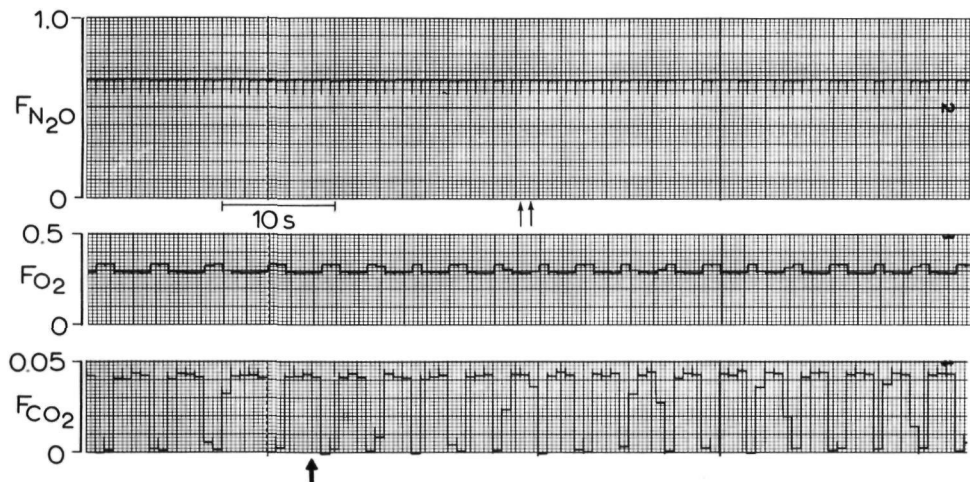


Fig.8.10: Recordings of  $N_2O$ ,  $O_2$ , and  $CO_2$  from a single patient. At the arrow breathing frequency is changed from 12 to 16 breaths. $min^{-1}$ . Artifacts on the signals (thin arrows) are due to the sample and hold circuits of the prototype.

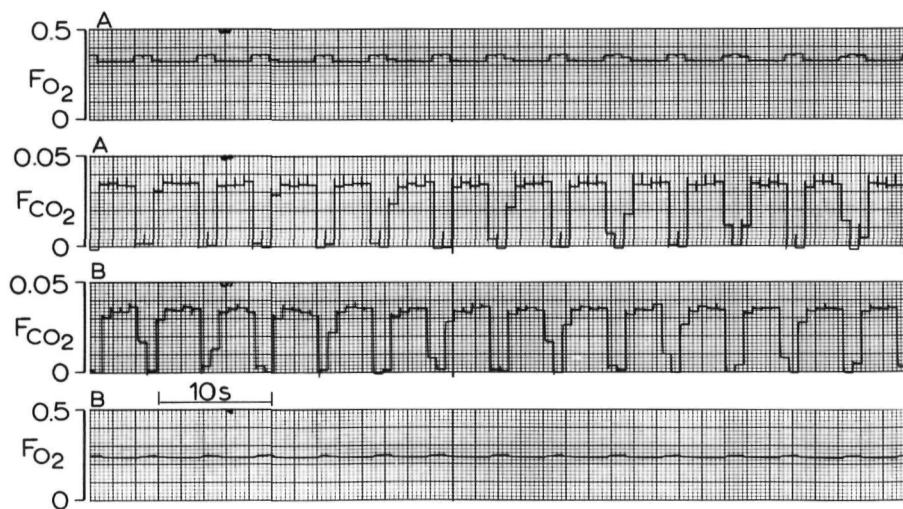


Fig.8.11: Simultaneous monitoring of patients in rooms A and B.

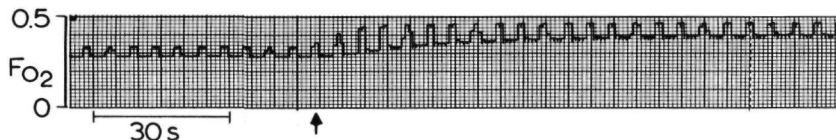


Fig.8.12: *Adjustment of  $F_{I,O_2}$  in one operating room.*

## 8.6 CONCLUSIONS

The tested system provides the inspiratory concentration, and the end-expiratory concentration (with a known uncertainty) of the respiratory gases (except the volatile anaesthetics) of *each breath* of *four* patients provided their breathing frequency is lower than  $16 \text{ breaths} \cdot \text{min}^{-1}$ . Moreover, information on the slope of the expiratory part of the respired waveforms is obtained. Thus the tested system provides a monitoring without dead periods.

## FUTURE DEVELOPMENT: MULTI-PART INLET LINE

This chapter describes a logical extension of the theory presented in chapter 6.

## 9.1 OPTIMUM RADII FOR A TUBE WITH TWO PARTS

The question was raised if the performance parameters of inlet lines composed of two parts might be further optimized by using other combinations of radii than commercially available. Therefore a program GRID was written in Fortran allowing to calculate the total residence time ( $t_M$ ), and total apparent band broadening ( $\sigma$ ) as a function of a range of radii ( $r_1$  and  $r_2$ ) for any desired sample flow and total length (fig.9.1).

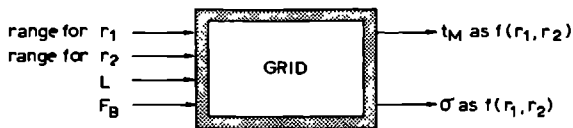


Fig.9.1: *Input and main output variables of GRID.*

The range of radii for  $r_1$  on one hand and  $r_2$  on the other was fed to GRID, which plotted the resulting residence times and apparent band broadenings three-dimensionally as a function of  $r_1$  and  $r_2$ . An example of such a plot for the residence times is shown in fig.9.2. The length and sample flow were the same as in the examples in chapter 6, i.e. 20 m and  $67.5 \text{ ml} \cdot \text{min}^{-1}$ .

Fig.9.2 illustrates that the residence time reaches a minimum for a certain combination of radii. A graphical solution to the problem

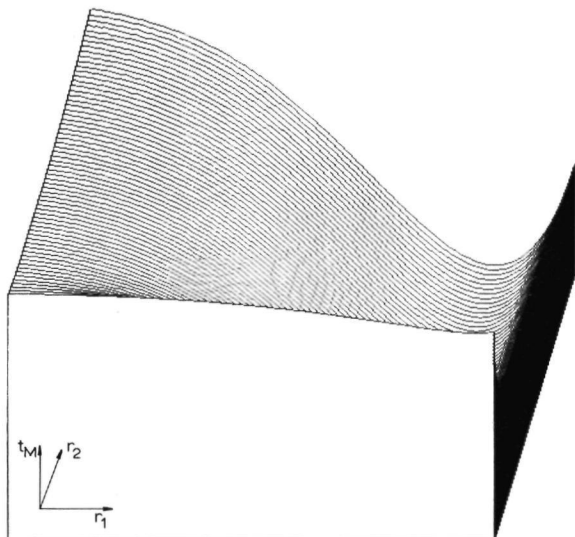
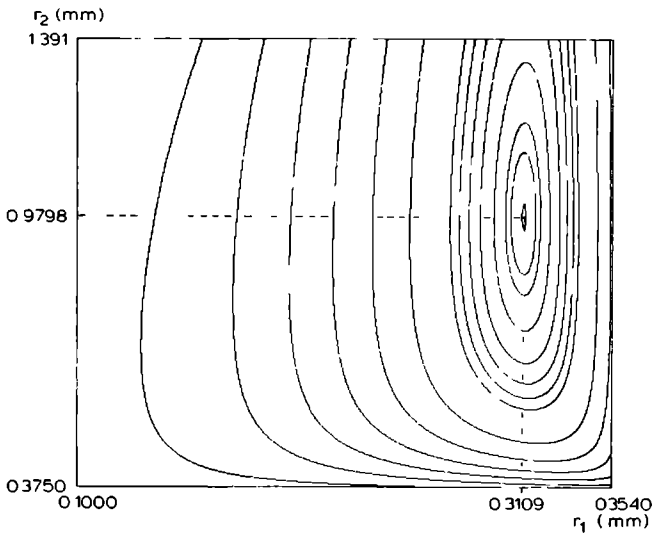


Fig.9.2: *Three-dimensional plot of  $t_M$  as a function of  $r_1$  and  $r_2$ .*

of the optimum combination of radii (minimum residence time) was found by projecting the three-dimensional figure on the  $r_1 r_2$  plane: height lines, representing identical residence times (iso-residence time lines), were plotted as a function of  $r_1$  and  $r_2$ . Then the values of the radii where the residence time reaches a minimum could be measured from the figure since the exact range of radii fed to GRID was known. An example of the procedure is shown in fig.9.3.

By feeding the graphical solutions for  $r_1$  and  $r_2$ , the desired flow, and the distance to be bridged into JOSCOM, the lengths of the two parts of the tube were calculated (see fig.9.4).

The results of the described procedure for a combined tube with a length of 20 m and a sample flow of  $67.5 \text{ ml} \cdot \text{min}^{-1}$  are given in table 9.1, where a uniform tube and two different combined tubes are compared. One of the combinations was investigated in chapter 6 and consists of commercially available tubing. Table 9.1 shows that the tube found by means of GRID has a shorter residence time. The calculated residence time and  $\text{CO}_2$ -response time in the latter tube are about 30% smaller than in the uniform tube.



**Fig.9.3:** *Iso-residence time lines as a function of  $r_1$  and  $r_2$ . The coordinates of the minimum  $t_M$  can be graphically interpolated.*

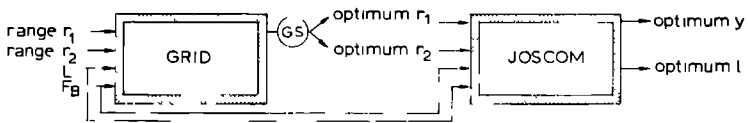


**Fig.9.4:** *The sequence of GRID, graphical solution (GS), and JOSCOM generates the optimum radii and optimum lengths (y and l) for a two-part tube.*

The velocity profile of the combined tube found with the aid of GRID is illustrated in fig.9.5, showing that very similar profiles are attained in both parts of the tube.



Table 9.1: Comparison of three inlet line configurations  
*Tube A (uniform i.d.), tube B and C (combined tubes) have identical lengths and sample flows. Tube B consists of tubing with commercially available radii. Tube C was found with the aid of GRID. Symbols:  $\bar{v}$  = average linear gas velocity,  $F_B$  = sample flow,  $t_M$  = residence time,  $\sigma$  = apparent band broadening for  $CO_2$ ,  $t_r$  =  $CO_2$  response time.*

	Tube A	Tube B		Tube C	
		part 1	part2	part 1	part 2
radius (mm)	0.3698	0.19	0.5	0.3109	0.9798
length (m)	20.0	0.997	19.003	9.883	10.117
$\bar{v}$ (m.s <sup>-1</sup> )	3.927	12.55	4.027	5.506	5.448
total length	20.0	20.0		20.0	
$F_B$ (ml.min <sup>-1</sup> )	67.5	67.5		67.5	
$t_M$ (s)	5.093	4.798		3.652	
$\sigma$ (s)	0.041	0.039		0.030	
$t_r$ (s)	0.105	0.100		0.076	

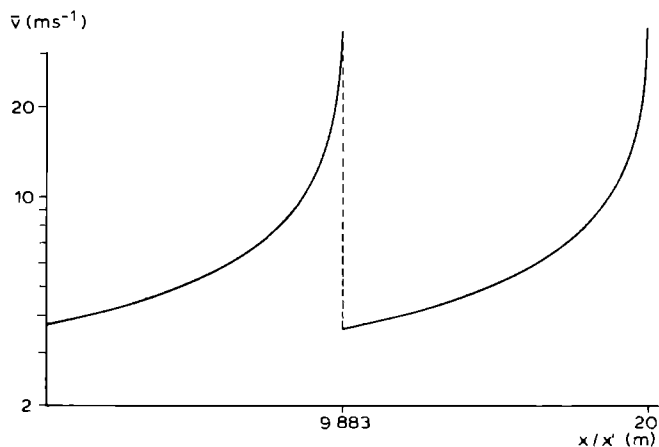


Fig.9.5: Mean velocity profile in the combined tube (length 20 m,  $r_1 = 0.3109$  mm and  $r_2 = 0.9798$ mm) found with the aid of GRID.

## 9.2 OPTIMUM RADII FOR A TUBE WITH MORE THAN TWO PARTS

An extension of the foregoing findings was to split up each of the two parts of the combined tube again. The same procedure, using GRID and JOSCOM, generated a *four-part* tube. Its performance parameters are shown in table 9.2: the residence time and apparent band broadening are further reduced in comparison with the two-part tube.

Table 9.2: Comparison of a one-, two-, and four-part tube  
*Values for some variables of an uniform tube (A), a two-part tube (C1, C2), and a four-part tube (D1, D2, D3, D4), each tube having a total length of 20 m and a sample flow of 67.5 ml.min<sup>-1</sup>. Symbols: l = part length, r = radii,  $\bar{v}$  = average linear gas velocity in each part,  $Z_i$  = ratio of the inlet and outlet pressure of each part of the tube,  $t_M$  = total residence time,  $t_r$  = CO<sub>2</sub> response time = 2.56  $\times$   $\sigma$ .*

	l (m)	r (mm)	$\bar{v}$ (m.s <sup>-1</sup> )	$Z_i$	$t_M$ (s)	$t_r$ (s)
A	20	0.370	3.927	100	5.093	0.105
C1	9.883	0.311	5.506	9.821		
C2	10.117	0.980	5.448	10.182	3.652	0.076
D1	4.920	0.268	6.943	3.090		
D2	4.963	0.471	6.960	3.178		
D3	5.054	0.843	6.897	3.176		
D4	5.063	1.500	6.906	3.207	2.908	0.059

The results for a tube made of *eight* parts are not illustrated as the search procedure became very lengthy. However, the values of the other variables in table 9.2 may lead to the following conclusion.

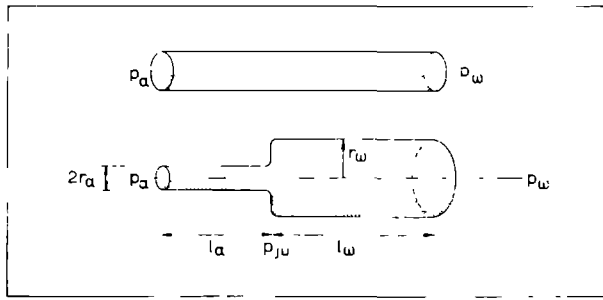


Fig.9.6: A tube length with inlet pressure  $p_\alpha$  and outlet pressure  $p_w$  is split into two parts with lengths  $l_\alpha$  and  $l_w$ , and radii  $r_\alpha$  and  $r_w$ . The pressure at the junction is  $p_{ju}$ .

If, in the search procedure for a minimum  $t_M$ , a length of tube is divided into two parts, it turns out that:

- the lengths of each part are nearly equal,
- the average linear gas velocities in both parts of the length of tube are nearly equal,
- the ratio of the pressures at the inlet and outlet of each tube part nearly equals the square root of the ratio of the inlet and outlet pressure of the divided tube length.

If these conditions are taken to be exact, the procedure of minimizing  $t_M$  is simplified. It follows that:

$$\bar{v}_\alpha = \bar{v}_w \tag{9.1}$$

where  $\bar{v}_\alpha$  and  $\bar{v}_w$  are the average linear velocities in both parts of the tube (see fig.9.6), and

$$\frac{p_\alpha}{p_{ju}} = \sqrt{Z} = \frac{p_{ju}}{p_w} \tag{9.2}$$

where  $p_{\alpha}$ ,  $p_{ju}$ ,  $p_{\omega}$  are the inlet pressure, the pressure at the junction, and the outlet pressure of the tube, respectively, and  $Z = p_{\alpha}/p_{\omega}$ .

The law of mass conservation requires that:

$$\bar{p}_{\alpha} \bar{v}_{\alpha} r_{\alpha}^2 = \bar{p}_{\omega} \bar{v}_{\omega} r_{\omega}^2 \quad (9.3)$$

where  $\bar{p}_{\alpha}$  and  $\bar{p}_{\omega}$  are the average pressures, and  $r_{\alpha}$  and  $r_{\omega}$  the radii of the two parts of the tube. Calculation of the average pressures analogously to the eqs.6.47 and 6.48, and combining with eq.9.1 and eq.9.3, yields:

$$\frac{r_{\alpha}}{r_{\omega}} = \sqrt[4]{Z} \quad (9.4)$$

The relationship in eq.9.4 can be recognized in the relations between the radii which were found in the previous examples by means of the lengthy procedure using GRID and JOSCOM (see table 9.2). Therefore the influence on the residence time and apparent band broadening of a tube was further investigated in a procedure where:

- the tube was divided in n parts of equal length,
- the ratio of in- and outlet pressures of each part was put equal to the n-th root of the ratio of the in- and outlet pressure of the whole tube.

It is expected that this procedure will give results very similar to the procedure GRID, graphical solution, and JOSCOM.

A program JOSLIM (based on the program JOSUT: see fig.6.16) and fulfilling the latter two conditions, calculated not only the radii of the n parts of the tube for any desired n, sample flow, and total length, but also the resulting total residence time and total apparent band broadening (see fig.9.7). This is illustrated in table 9.3, which shows that dividing a tube into four or eight parts of equal length reduces the residence time by 43% or 49%, respectively, compared to a tube with uniform diameter; the same figures apply for the reduction in apparent band broadening.

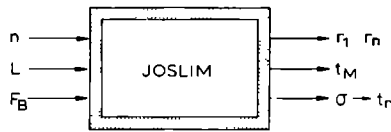


Fig.9.7: The input and main output variables of JOSLIM.

Table 9.3: Results of the program JOSLIM

Values of the total residence time ( $t_M$ ) and  $CO_2$ -response time ( $t_r$ ) for tubes divided into  $n$  parts of equal length. Each tube has a total length of 20 m, and draws off a sample flow of  $67.5 \text{ ml}\cdot\text{min}^{-1}$ . Only the range of radii is given for  $n > 4$ .

$n$	$t_M$ (s)	$t_r$ (s)	radii ( $\mu\text{m}$ )
1	5.093	0.105	370
2	3.652	0.076	312, 986
3	3.126	0.064	284, 613, 1320
4	2.888	0.059	268, 477, 849, 1510
5	2.764	0.056	258 to 1630
8	2.618	0.053	242 to 1810
16	2.543	0.051	227 to 1970
32	2.523	0.050	220 to 2050
64	2.519	0.050	216 to 2080
128	2.517	0.050	214 to 2100
256	2.517	0.050	213 to 2110

The results given by JOSLIM are very close to those found with the procedure using GRID and JOSCOM for  $n = 2, 4$  (for comparison see tables 9.3 and 9.2). Differences might be due to reading errors made during the graphical solutions. A nearly optimal solution is found by creating a tube divided into 256 equal parts. The radius and the pressure profile of such a tube are illustrated in fig.9.8.

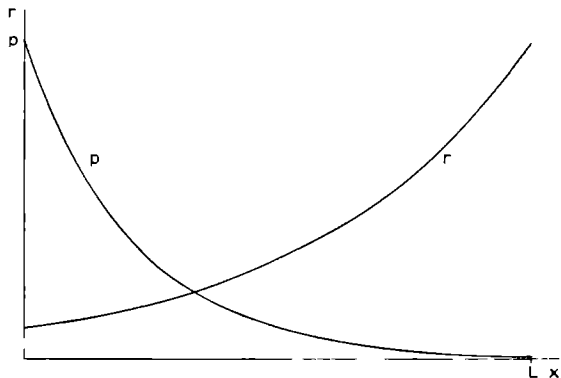


Fig.9.8: *Radius and pressure of a tube composed of 256 parts of equal length plotted against distance.*

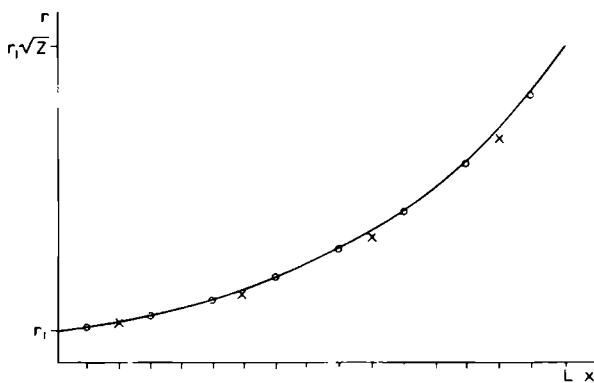


Fig.9.9: *The radii for a four- ( $\times$ ) and eight-part ( $\circ$ ) tube (calculated with JOSLIM) plotted against distance. Their radius profiles already approach the ideal profile, calculated with eq.9.5, shown in the curve.*

The radius and pressure are exponentially rising and declining, respectively. It can be shown that the radius versus distance function is given by:

$$r = r_i Z^{x/2L} \quad (9.5)$$

where  $r_i$  is the radius at the inlet,  $x$  is the coordinate of distance,  $L$  is the total length of the tube, and  $Z$  is the ratio of inlet and outlet pressure. The radius at the inlet can be calculated exactly by means of eq.6.10 for  $n \rightarrow \infty$ , taking into account that the length of the first part equals  $L/n$ , and that the ratio of inlet and outlet pressure of the first part equals  $^{n}\sqrt{Z}$ . Fig.9.9 shows that the radius versus distance function predicted by eq.9.5 is approached by the solutions found by JOSLIM when  $n \geq 4$ .

It is concluded on theoretical grounds that the optimal form for an inlet line of a respiratory mass spectrometer may be a "trumpet" form with an exponentially rising radius as a function of distance. This "sounds" promising for the future.

## SUMMARY

Respiratory mass spectrometry is a nearly ideal, though expensive method for the breath-by-breath analysis of respired gas mixtures. A solution to the problem of cost is offered by the use of long sampling tubes (say 30 m) allowing to share one mass spectrometer among several operating theatres. Thus sample gases from patients are sequentially analysed. Two implications of the sequential analysis of gas sampled through long sampling lines (signal distortion in the tubes generally made of polymers, and the "dead period" between sampling periods on one line) were simply accepted until now, although distortion was sometimes compensated by an unnecessarily high sample flow. Possible improvements in these two unwanted effects of remote mass spectrometer operation were searched for in this thesis.

Since an innovative application of the mass spectrometer was envisaged, the instrument could not be treated as a "black box". Therefore its physicochemical background, its operation, and the problems arising from its use during anaesthesia were studied and reviewed in part I of the thesis.

The performance of the quadrupole mass spectrometer Centronic 200 MGA, which incorporates an "anaesthetics module" containing a spectrum overlap eraser and an automatic sensitivity control (ASC) system, was evaluated (chapter 5). Static and dynamic accuracy proved to be satisfactory for clinical use, although the noise level on the CO<sub>2</sub> signal was much higher in a N<sub>2</sub>O/O<sub>2</sub> mixture than in air. The proper functioning of the ASC system was experimentally confirmed.

The search for a tube causing minimal distortion necessitated to work out first a mathematical model predicting the relationships between the three "performance parameters" (sample flow, transit time, and response time) of an ideal tube (no gas-tube interaction) on one hand, and its geometry on the other hand. In practice these three parameters should be as small as possible, but transit time and response time are inversely proportional to sample flow. The model was developed for two inlet configurations: "uniform tubes", i.e. tubes with uniform diameters, and "combined tubes", i.e. tubes



consisting of two parts with different diameters. Discussion of the relationships between performance parameters was facilitated by calculation programs written in Fortran. The model revealed that combined tubes would possibly offer smaller distortion and shorter transit times than uniform tubes for a given sample flow, and that as a rule of thumb the response time of a uniform tube increases with 5 ms per metre. The predictions from the model (for ideal tubes) served to judge the results of the selection procedure made by experimental observation between tubes of various materials and geometries. The objective was to select an inlet line which approached the predicted signal distortion for a given geometry, and in addition could be handled easily in clinical practice.

Inlet lines were tested by observing their responses (transit times; 10% to 90% response times) to step changes in partial gas pressure (10 kPa) for  $N_2O$ ,  $O_2$ ,  $N_2$ ,  $CO_2$ , Ar, halothane, and sometimes for enflurane and isoflurane (on and off transients). On line data acquisition (MINC computer with ADC) was mostly used, and a curve fitting program calculated transit and response times. Sample flows were measured with a bubble flow meter.

Testing the Centronic standard capillary (1.2 m length) showed that the experimental set-up produced reliable values: 10% to 90% response times for  $N_2O$ ,  $O_2$ ,  $N_2$ ,  $CO_2$ , and Ar were shorter than 75 ms. Response times for volatile anaesthetics (395 ms for the off transient of halothane) were much longer than expected and reported by others. The results for this capillary were further used as the "basic response" of the mass spectrometer.

Three lengths of uniform tube (9.85 m, 20 m, and 30 m) and two combined tubes (4.1 + 25.4 m, and 1 + 29 m), made of polyethylene, were tested. The predicted response times could only be experimentally approached for argon and nitrogen: 171 ms for argon in a 30 m tube, calculated value = 151 ms, the gap being explained by the instrument's basic response. The combined tube showed shorter transit and response times than the uniform tube with comparable length and sample flow. It was concluded that the tested polyethylene (Portex) is not suited for clinical use because of its strong interaction with halothane.

Teflon (Talas), PVC (Talas), and steel (Chrompack) tubes were discarded from clinical use because of unacceptable signal distortion. A 32 m deactivated glass tube (0.566 mm i.d.) with a sample flow of  $13 \text{ ml}\cdot\text{min}^{-1}$  approached the values predicted by the model for an ideal tube. However, glass was not suited for practical use, and since nylon showed favourable properties, it was decided to search directly for an nylon inlet line meeting practical needs. These needs were: 30 m length, a maximal sample flow of  $50 \text{ ml}\cdot\text{min}^{-1}$ , easy to handle, and "minimal" distortion. A nylon combined tube (0.4 m with 0.25 mm i.d., and 30 m with 1.07 mm i.d.) offered a low sample flow ( $33 \text{ ml}\cdot\text{min}^{-1}$ ), an acceptable transit time (13.37 s), and signal distortion approaching theoretical limits: response times for all gases were smaller than 195 ms, except for halothane. The latter observation was mainly due to the long basic response of the mass spectrometer, in addition, deteriorating in the course of time. A combined nylon inlet with a slightly higher sample flow ( $49 \text{ ml}\cdot\text{min}^{-1}$ ) was selected for clinical use to compensate for the effects of the dead volume introduced by the valves of a multi-user system. Four selected lines, redesigned so that lines could be replaced within two minutes, and four miniature solenoid valves were assembled to form a system for sequential sampling. The clinical use of this system was illustrated on several points.

A system was developed sampling sequentially the respiratory gases of four patients at a frequency much higher than their breathing frequency to exclude dead periods in patient monitoring. Respired waveforms were "reconstructed" by means of sample and hold circuits. The frequency spectrum of the respiratory input signal, evaluated by fast Fourier analysis, showed that the maximum attainable switching frequency of the system on one inlet line (1.25 Hz) was insufficient to recover "complete" respiratory waveforms of four patients (6.2 Hz would be necessary for a breathing frequency of  $12 \text{ breaths}\cdot\text{min}^{-1}$ , if a linear interpolation method is used). However, the system provides the inspiratory and the end-expiratory fractional concentrations (with a known uncertainty) of the respired gases (except the volatile anaesthetics) of *each* breath of *four* patients, provided their breathing frequency is lower than  $16 \text{ breaths}\cdot\text{min}^{-1}$ . Thus simultaneous monitoring of four patients is realized.

A speculation about future development in sampling probe design is presented in chapter 9: the response time and transit time of an inlet line consisting of more than eight parts (calculations were performed up to 256 parts) are halved in comparison to a uniform tube with equal sample flow, provided appropriate diameters are used for all parts.

# HET GEBRUIK VAN LANGE SAMPLEBUIZEN IN DE RESPIRATOIRE MASSASPECTROMETRIE

met speciale aandacht voor de simultane bewaking  
van vier patienten onder algemene anesthesie

## SAMENVATTING

Massaspectrometrie is een bijna ideale, maar dure methode om het verloop van partiële gasspanningen tijdens de ademhalingscyclus te meten. Een zeer sterke verbetering in de verhouding kosten/baten is mogelijk door gebruik te maken van lange (bv. 30 m) samplecapillairen. Deze laten toe één massaspectrometer voor meerdere operatiekamers in te zetten, waarbij de gasmonsters van verschillende patiënten na elkaar worden geanalyseerd. Twee directe gevolgen van dit sequentiële analyseren van gas dat getransporteerd wordt door lange buizen, werden tot nu toe zonder meer geaccepteerd (signaalvervorming in de lange buizen die meestal uit kunststof zijn vervaardigd, en de "wachtijd" tussen de meetperiodes op één operatiekamer). Vervorming werd soms gecompenseerd door de sample flow veel hoger dan nodig te maken. In dit proefschrift werd gezocht naar mogelijke verbeteringen van deze twee ongewenste effecten.

Aangezien op een nieuwe toepassing van de massaspectrometer werd gemikt, kon het apparaat niet als een "black box" worden behandeld. Om die reden werden zijn fysicochemische basis, zijn werking, en de problemen die ontstaan door gebruik tijdens anesthesie bestudeerd en behandeld in "Part I" van het proefschrift.

De quadrupole massaspectrometer Centronic 200 MGA werd uitgetest (chapter 5). Dit instrument heeft electronische voorzieningen om de problemen, optredend tijdens anesthesie, te ondervangen. Het onderzoek wees uit dat zijn eigenschappen klinisch gebruik mogelijk maken. Het ruisniveau op het CO<sub>2</sub> signaal was echter hoger in een N<sub>2</sub>O/O<sub>2</sub> mengsel dan in lucht.

Het onderzoek naar een samplecapillair met een "minimale" signaalvervorming maakte het noodzakelijk om vooraf een mathematisch model op te stellen (chapter 6). Dan eerst was het mogelijk om de verbanden te voorspellen die bestaan tussen vervorming, transporttijd van het gas, en de sample flow enerzijds (drie factoren die verder "performance parameters" worden genoemd), en anderzijds de afmetingen van een ideale buis. In een "ideale" buis treedt geen interactie op tussen het materiaal waaruit de buis vervaardigd is en het gasmonster. In de praktijk is het wenselijk dat de drie "performance parameters" zo klein mogelijk zijn, maar transporttijd en vervorming zijn omgekeerd evenredig met de sample flow. Het model werd ontwikkeld voor twee soorten buizen: "uniforme buizen", die een uniforme diameter hebben, en "combinatiebuizen", die uit twee delen met verschillende diameters bestaan. Voorspelling van de gezochte verbanden werd vergemakkelijkt door rekenprogramma's in Fortran. Het model liet zien dat combinatiebuizen waarschijnlijk een kleinere vervorming en sneller gastransport zouden opleveren dan uniforme buizen met identieke sample flow. Als vuistregel kan worden gehanteerd dat de 10% tot 90% aanwijstijd van een uniforme tube met 5 ms per meter toeneemt. De voorspellingen van het model, met name de vervorming bij een gegeven sample flow, dienden om de resultaten te beoordelen van de selectieprocedure die werd opgezet tussen tubes van uiteenlopende materialen en afmetingen. M.a.w., er moest een samplecapillair worden gevonden dat de voorspelde vervorming bij gegeven buisafmetingen benaderde, maar dat ook nog makkelijk te hanteren viel in de praktijk.

De buizen werden getest door hun 10% tot 90% aanwijstijd en hun transporttijd te meten na stapvormige veranderingen (10 kPa) in de partiële gasspanning van  $N_2O$ ,  $O_2$ ,  $N_2$ ,  $CO_2$ , Ar, halothaan, en soms ook enfluraan en isofluraan (on en off transients). Signalen van experimenten werden meestal on-line toegevoerd aan een MINC computer met AD-converter, waarna een curve fitting programma transporttijden en aanwijstijden berekende. Sample flows werden met een bellenflowmeter gemeten (chapter 7).

De test van het standaard capillair (lengte 1.25 m) leerde dat de experimentele opstelling betrouwbare waarden opleverde: de 10% tot 90% aanwijstijd voor alle gassen was korter dan 75 ms, behalve voor

dampvormige anesthetica. Halothaan bv. vertoonde een aanwijstijd die veel langer was dan verwacht (359 ms voor de off transient) en door andere auteurs beschreven. De resultaten voor dit capillair werden verder gehanteerd als de "basisaanwijstijd" van de massaspectrometer.

Drie lengten van uniforme polyethyleen (PE) buis (9.85 m, 20 m, en 30 m) en twee combinatiebuizen van PE (4.1 + 25.4 m, en 1 + 29 m) werden uitgetest. De theoretisch voorspelde waarden konden experimenteel slechts door argon en stikstof worden benaderd: de aanwijstijd voor argon was 171 ms voor een 30 m buis, terwijl 151 ms was berekend. Het verschil wordt verklaard door het aandeel van de basisaanwijstijd in de gemeten tijd. De andere gassen hadden aanwijstijden die langer waren dan voorspeld. Deze verschillen worden veroorzaakt door interacties met het PE. De combinatiebuis vertoonde een kortere transporttijd en aanwijstijd dan de uniforme buis met vergelijkbare lengte en sample flow. De conclusie was dat het getestte PE (Portex) ongeschikt was voor gebruik als samplecapillair, omwille van de sterke interactie met halothaan.

Teflon (Talas), PVC (Talas), en stalen (Chrompack) buizen bleken eveneens onbruikbaar omwille van onaantoonbare signaalvervorming. Een 32 m glazen capillair (0.566 mm i.d.) met een sample flow van  $13 \text{ ml} \cdot \text{min}^{-1}$  evenaarde de waarden voorspeld voor een ideale buis. Glas was echter niet zonder meer geschikt voor de praktijk. Daarenboven bleek nylon gunstige eigenschappen te hebben. Daarom werd rechtstreeks gezocht naar een nylon buis die aan praktische behoeften voldeed: 30 m lengte, een maximale flow van  $50 \text{ ml} \cdot \text{min}^{-1}$ , makkelijk hanteerbaar, en "minimale" vervorming. Een nylon combinatiebuis (0.4 m met 0.25 mm i.d., en 30 m met 1.07 mm i.d.) vertoonde een lage sample flow ( $33 \text{ ml} \cdot \text{min}^{-1}$ ), een aanvaardbare transporttijd (13.37 s), en een vervorming die de theoretische grenzen benaderde: de aanwijstijden voor alle gassen waren kleiner dan 195 ms, behalve voor halothaan. Deze laatste waarneming was hoofdzakelijk toe te schrijven aan de lange basisaanwijstijd van de massaspectrometer. Deze bleek daarenboven in de loop van de studie toe te nemen. Een nylon combinatiebuis met een wat hogere flow ( $49 \text{ ml} \cdot \text{min}^{-1}$ ) werd uitgekozen voor klinisch gebruik teneinde de effecten te compenseren van de dode ruimte, die door de kleppen van het sample systeem voor

meerdere patiënten worden geïntroduceerd. De transporttijd van deze buis was 11.35 s en de aanwijstijden waren korter dan 192 ms, behalve voor de dampvormige anesthetica. Vier van deze buizen, vier electromagnetische kleppen en een stuureenheid voor de kleppen vormden een sample systeem voor sequentiële gasanalyse. Enkele illustraties van het gebruik ervan op de operatiekamer sluiten dit hoofdstuk af.

In het volgende hoofdstuk wordt de ontwikkeling beschreven van een systeem dat sequentiëel de ademhalingsgassen bij vier patiënten monstert, echter met een frequentie die veel hoger ligt dan hun ademfrequentie (chapter 8). De ademcurven werden gereconstrueerd met behulp van sample en hold circuits. Op deze manier werd de wachttijd, dit is de tijd dat geen gasanalyse voor een patient kan worden uitgevoerd, uitgesloten. Evaluatie van het frequentiespectrum van een single breath curve met behulp van snelle Fourier analyse, toonde aan dat de maximaal haalbare schakelfrequentie van het ontwikkelde systeem (1.25 Hz per patiënt) onvoldoende was om "volledige" curves van vier patienten te reconstrueren. Het systeem levert echter wel de inspiratoire en de eind-expiratoire fractionele concentratie (met een bekende onzekerheid) van alle gassen (behalve de dampvormige anesthetica) van *elke* ademhaling van *vier* patiënten, op voorwaarde dat hun ademfrequentie lager ligt dan 16 per minuut. Simultane bewaking van vier patienten is hierbij gerealiseerd.

In het laatste hoofdstuk werd over een mogelijke ontwikkeling op het gebied van lange samplecapillairen gespeculeerd (chapter 9). Theoretisch wordt aangetoond dat de aanwijstijd en transporttijd van een combinatiebuis, die uit meer dan acht delen bestaat (berekeningen werden gemaakt tot 256 delen), worden gehalveerd in vergelijking met een uniforme buis met dezelfde sample flow, op voorwaarde dat de gepaste diameters voor alle delen worden gebruikt.

## REFERENCES

- Albery, W.J., Brooks, W.N., Gibson, S.P., and Hahn, C.E.W. (1978). An electrode for  $P_{N_2O}$  and  $P_{O_2}$  analysis in blood and gas. *J. Appl. Physiol.* 45, 637-643.
- Ammann, E.C.B., and Galvin, R.D. (1968). Problems associated with the determination of carbon dioxide by infrared absorption. *J. Appl. Physiol.* 25, 333-335.
- Aris, R. (1956). On the dispersion of a solute in a fluid flowing through a tube. *Proc. R. Soc. Lond. Ser. A.* 235, 67-77.
- Attinger, E.O., Anné, A., and McDonald, D.A. (1966). Use of Fourier series for the analysis of biological systems. *Biophys. J.* 6, 291-304.
- Bargeton, D., Durand, J.Y., and Lambert, R. (1970). Stabilisation des signaux en spectrométrie de masse. *J. Physiol. (Paris)*, 62 (suppl. 1.), 117-118.
- Barnard, G.P. (1953). *Modern Mass Spectrometry*. The Institute of Physics, London.
- Beneken Kolmer, H.H., (1967). De continue polarografische meting van de zuurstofspanning in gassen. *Thesis, Nijmegen*.
- Blauth, E.W., (1965). *Dynamische Massenspektrometer*. F. Vieweg & Sohn, Braunschweig.
- Brubaker, W.M., and Tuul, J. (1964). Performance studies of a quadrupole mass filter. *Rev. Sci. Instrum.* 35, 1007-1010.
- Brunnée, C., and Voshage, H. (1964). *Massenspektrometrie*. Verlag K. Thieme KG, München.
- Buckingham, J.D., and Dennis, N.T.M. (1975). A simple medical mass spectrometer and its vacuum system requirements. *Vacuum* 25, 489-492.
- Buckingham, J.D., and Holme, A.E. (1977). Mass spectrometry for respiratory gas analysis. *Br. J. Clin. Equip.* 2, 142-148.
- Burton, G.W. (1969). Measurement of inspired and expired oxygen and carbon dioxide. *Br. J. Anaesth.* 41, 723-730.
- Bushman, J.A. (1975). The measurement of oxygen concentration in respirable gas mixtures: in *Oxygen measurements in biology and medicine* (Eds. Payne and Hill). Butterworths, London.
- Conway, C.M., Leigh, J.M., Lindop, M.J., and Webb, D.A. (1973). An evaluation of the "Rapox" rapid response paramagnetic oxygen analyser. *Br. J. Anaesth.* 45, 1191-1197.



- Cooper, E.A. (1957). Infrared analysis for the estimation of carbon dioxide in the presence of nitrous oxide. *Br. J. Anaesth.* 29, 486-490.
- Cotes (1979). *Lung Function: assessment and application in medicine*, 4th edition, Blackwell Scientific Publications, Oxford.
- Cramers, C.A., Leclercq, P.A., Lerou, J.G., and Beneken Kolmer, H.H., (1981). Mass spectrometry in monitoring anaesthetic gas mixtures using long sampling tubes: band broadening in capillary tubes caused by flow and diffusion: in *Mass spectrometry in anaesthesiology* (Eds. Vickers and Crul). Springer Verlag, Berlin.
- Crawford McAslan, T. (1976). Automated respiratory gas monitoring of critically injured patients. *Crit. Care Med.* 4, 255-260.
- Daniels, A.U., Couvillon, L.A., and Lebrizzi, J.M. (1975). Evaluation of nitrogen analyzers. *Am. Rev. Resp. Dis.* 112, 571-575.
- Davies, N.J.H., and Denison, D.M. (1979). The uses of long sampling probes in respiratory mass spectrometry. *Respir. Physiol.* 37, 335-346.
- Davis, W.O.M., and Spence, A.A. (1979). A modification of the MGA 200 mass spectrometer to enable measurement of anaesthetic gas mixtures. *Br. J. Anaesth.* 51, 987-988.
- Dawson, P.H., (Ed.), (1976). *Quadrupole Mass Spectrometry and its applications*. Elsevier Scientific Publishing Company, Amsterdam.
- Defares, J.G., Sneddon, I.N., and Wise, M.E., (1973). *An introduction to the mathematics of medicine and biology*. Amsterdam, North-Holland Publishing Company.
- Demange, J., Jacquemin, C., Varene, P., and Timbal, J. (1966). Utilization d'un spectromètre de masse sur une centrifugeuse humaine. *Med. Biol. Eng.* 4, 153-157.
- Elliott, S.E., Segger, F.J., and Osborn, J.J. (1966). A modified oxygen gauge for the rapid measurement of  $P_{O_2}$  in respiratory gases. *J. Appl. Physiol.* 21, 1672-1674.
- Fowler, K.T., (1965). The mass spectrometer in the analysis of regional lung function. *Scand. J. Resp. Dis. Suppl.* 62, 73-82.
- Fowler, K.T. (1969). The respiratory mass spectrometer. *Phys. Med. Biol.* 14, 185-199.
- Fry, D.L. (1960). Physiologic recording by modern instruments with particular reference to pressure recording. *Physiol. Rev.* 40, 753-787.

- Fuller, E.N., Schettler, P.D., and Giddings J.C. (1966). A new method for prediction of binary gas-phase diffusion coefficients. *Ind. Eng. Chem.* 58, 19-27.
- Gardenhire, L.W. (1964). Selecting sampling rates. *I.S.A. J.* 11, 59.
- Giddings, J.C. (1964). Role of column pressure drop in gas chromatographic resolution. *Anal. Chem.* 36, 741-744.
- Gielen, M.J. (1971). Body plethysmography. A comparative study of volume measurements in a constant-volume and a constant-pressure body plethysmograph. *Thesis, Nijmegen.*
- Gillbe, C.E., Heneghan, C.P., and Branthwaite, M.A. (1981). Respiratory mass spectrometry during general anaesthesia. *Br. J. Anaesth.* 53, 103-109.
- Golay, M.J. (1958). Theory of chromatography in open and coated tubular columns with round and rectangular cross-sections: in *Preprints of papers to be read at the second symposium on Gas Chromatography*, p. C13 (Ed. Desty). Butterworths, London.
- Goodwin, B. (1979). Factors influencing the accuracy of mass spectrometer measurements: in *The medical and biological application of mass spectrometry* (Eds. Payne, Bushman, and Hill). London, Academic Press.
- Gothard, J.W., Busst, C.M., Branthwaite, M.A., Davies, N.J., and Denison, D.M. (1980). Application of respiratory mass spectrometry to intensive care. *Anaesthesia* 35, 890-895.
- Graham, J.M., Salamonsen, R.F., Kay, B., Greer, W., Parkhouse, J., Stephenson, D.K. (1980). Mass spectrometry in anaesthesia. Problems for monitoring anesthetic gases and vapours. *Acta Anaesthesiol. Belg.* 4, 265-278.
- Handbook of Chemistry and Physics*, 51st edition (1970-1971), p. B-248. The Chemical Rubber Co.
- Hill, D.W., and Powell, T. (1967). Cross-sensitivity effects in non-dispersive infra-red gas analysers using condenser microphone detectors. *J. Sci. Instrum.* 44, 189-194.
- Hill, D.W., and Powell, T. (1968). *Non-dispersive infra-red gas analysis in science, medicine and industry.* Adam Hilger, London.
- Honig, R.E. (1945). Gas flow in the mass spectrometer. *J. Appl. Phys.* 16, 646-654.
- Hunter, J.A., Stacy, R.W., Hitchcock, F.A. (1949). A mass spectrometer for continuous gas analysis. *Rev. Sci. Instrum.* 20, 333-336.

- James, A.T., and Martin, A.J.P. (1952). Gas-liquid partition chromatography: the separation and micro-estimation of volatile fatty acids from formic acid to dodecanoic acid. *Biochem. J.* 50, 679-690.
- Jessop, G. (1966). Katharometers. *J. Sci. Instrum.* 43, 777-782.
- Kety, S.S. (1951). The theory and applications of the exchange of inert gas at the lung and tissues. *Pharmacol. Rev.* 3, 1-41.
- Kreuzer, F., Rogeness, G., and Bornstein, P., (1960). Continuous recording in vivo of respiratory air oxygen tension. *J. Appl. Physiol.* 15, 1157-1158.
- Levy, A. (1964). The accuracy of the bubble meter method for gas flow measurements. *J. Sci. Instrum.* 41, 449-453.
- Lilly, J.C. (1950). Physical methods of respiratory gas analysis. *Methods Med. Res.* 2, 131-138.
- Link, J., and Eyrich, K. (1982). A mass spectrometry system for respiratory monitoring of 17 anaesthetized patients. *Proceedings of VIth European Congress of Anaesthesiology*, p. 182.
- Mapleson, W.W. (1962). Physical methods of gas analysis. *Br. J. Anaesth.* 34, 631-636.
- McCray, J.A., and Cahill, T.A. (1973). *Electronic circuit analysis for scientists*. John Wiley and Sons, New York.
- McDowell, C.A. (Ed.) (1963). *Mass Spectrometry*. McGraw-Hill Book Company, New York.
- Moore, (1962). *Physical Chemistry*, 4th edition, p. 223. Longmans Green and Co., Ltd, London.
- Muysers, K., and Smidt, U., (1969). *Respirations-Massenspektrometrie*. Schattauer Verlag, Stuttgart.
- Nitta, K., and Mochizuki, M. (1969). A continuous method for measuring O<sub>2</sub> and CO<sub>2</sub>. *Jap. J. Physiol.* 19, 41-54.
- Nunn, J.F. (1977). *Applied Respiratory Physiology*. Butterworths, London.
- Ozanne, G.M., Young, W.G., Mazzei, W.J., and Severinghaus, J.W. (1981). Multipatient anesthetic mass spectrometry: Rapid analysis of data stored in long catheters. *Anesthesiology* 55, 62-70.
- Paul, W., and Raether, M. (1955). Das elektrische Massenfilter. *Z. Phys.* 140, 262-273.
- Paul, W., Reinhard, H.P., and von Zahn, U. (1958). Das elektrische Massenfilter als Massenspektrometer und Isotopentrenner. *Z. Phys.* 152, 143-182.

- Paul, W., and Steinwedel, H. (1953). Ein neues Massenspektrometer ohne Magnetfeld. *Z. Naturforsch.* 8a, 448-450.
- Pauling, L., Wood, R.E., Sturdivant, J.H., (1946). An instrument for determining the partial pressure of oxygen in a gas. *Science* 103, 338.
- Philip, J.R. (1963). The theory of dispersal during laminar flow in tubes (I). *Aust. J. Phys.* 16, 287-299.
- Ponte, J., Lerou, J., and van der Vegt, H. (1981). Development of a sampling system for multiple users of mass spectrometry in the operating theatre, in: *Mass spectrometry in anaesthesiology* (Eds Vickers and Crul). Springer Verlag, Berlin.
- Potter, W.A. (1976). Mass spectrometry for innovative techniques of respiratory care, ventilator weaning and differential ventilation in an intensive care unit. *Crit. Care Med.* 4, 235-239.
- Radford, E.P., jr. (1964). The physics of gases: in *Handbook of Physiology, Section 3: Respiration, Vol. 1*, p. 131.
- Riggs, D.S. (1970). *Control theory and physiological feedback mechanisms*. The Williams and Wilkins Co., Baltimore.
- Riker, J.B., and Habermann, B. (1976). Expired gas monitoring by mass spectrometry in a respiratory intensive care unit. *Crit. Care Med.* 4, 223-229.
- Scheid, P., Slama, H., and Piiper, J. (1971). Electronic compensation of the effects of water vapor in respiratory mass spectrometry. *J. Appl. Physiol.* 30, 258-260.
- Scurr, C., and Feldman, S. (Eds.), (1974). *Scientific Foundations of Anaesthesia*. 2nd edition, William Heinemann Medical Books Ltd, London.
- Serra, R., and Visser, B.F. (1963). Diagramme O<sub>2</sub>-CO<sub>2</sub> alvéolaire. *Poumon Coeur* 10 (bis), 1261-1272.
- Severinghaus, J.W., Weiskopf, R.B., Nishimura, M., and Bradley, A.F. (1971). Oxygen electrode errors due to polarographic reduction of halothane. *J. Appl. Phys.* 31, 640-642.
- Skilling, J.K. (1968). Pulse and frequency response, some useful relations. *Gen. Radio Exp.* 11/12, 3-10.
- Smalhout, B. (1967). *Capnografie, bij de diagnostiek, operatie en nabehandeling van neurochirurgische aandoeningen*. A. Oosthoek's uitgeversmaatschappij, Utrecht.
- Sodal, I.E., Bowman, R.R., and Filley, G.F. (1968). A fast-response oxygen analyzer with high accuracy for respiratory gas measurement. *J. Appl. Physiol.* 25 (2), 181-183.

- Sodal I.E. (1979). Mass spectrometry: Current technology and implications for anaesthesia: in *Low flow and closed system anaesthesia*, p. 167, (Eds. Aldrete, Lowe, Virtue). Grune and Stratton, London.
- Spence, A.A., and Davis, W.O.M. (1981). Mass spectrometry in anaesthesia: in *Mass spectrometry in anaesthesiology* (Eds. Vickers and Crul). Springer Verlag, Berlin.
- Stannett, V. (1968). Simple gases: in *Diffusion in polymers*, p. 41, (Eds. Crank and Park). Academic Press.
- Stott, F.D. (1957). Sonic gas analyzer for measurement of CO<sub>2</sub> in expired air. *Rev. Sci. Instrum.* 28, 914-915.
- Sykes, M.K., Vickers, M.D., and Hull, C.H. (1981). Gas and vapour analysis: in *Principles of clinical measurement*, p. 220. Blackwell Scientific Publications, Oxford.
- Tatnall, M.L., West, P.G., and Morris, P. (1978). A rapid response U.V. halothane meter. *Br. J. Anaesth.* 50, 617-621.
- Tomlin, D.H., (1966). *Fundamental Atomic Physics*. Blackie & Son Limited, London.
- Taylor, G. (1953). Dispersion of soluble matter in solvent flowing slowly through a tube. *Proc. R. Soc. Lond. Ser. A.* 219, 186-203.
- Wilson, R.S., and Laver, M.B. (1972). Oxygen analysis: Advances in methodology. *Anesthesiology* 37, 112-126.
- Wissenschaftliche Tabellen*. 7.Auflage. Ciba-Geigy, 1968 (2.Nachdruck, 1973).

## CURRICULUM VITAE

Jos Lerou was born in Brugge (Belgium) on 20th May 1949. After obtaining his secondary school certificate (Latijns-wiskundige Humaniora) at the Onze-Lieve-Vrouwecollege in Assebroek (Belgium), he enrolled to study medicine at the Catholic University of Leuven (Belgium), graduating on 30th July 1974.

He specialized in anaesthesiology under Prof. Dr J.F. Crul at the Institute of Anaesthesiology of the St. Radboud Hospital, University of Nijmegen (The Netherlands). Since 1st April 1978, he has been a staff member of the same institute.

*"For some must watch while some must sleep"*

Shakespeare (Hamlet, Prince of Denmark, Act 3, Sc. 2.)

# STELLINGEN

behorend bij het proefschrift

THE USE OF LONG SAMPLING TUBES  
IN RESPIRATORY MASS SPECTROMETRY

with special reference to the simultaneous monitoring  
of four patients during general anaesthesia

J.G.C. Lerou



## I

Lange samplebuizen, vervaardigd uit polyethyleen (Portex), zijn ongeschikt om het verloop van de fractionele halothaanconcentratie tijdens de ademhalingscyclus te meten.

Dit proefschrift

## II

Lange samplebuizen, bestaande uit de combinatie van twee buizen met verschillende, maar bepaalde inwendige diameters, zijn zowel uit theoretisch als praktisch oogpunt te verkiezen boven lange samplebuizen met een uniforme diameter.

Dit proefschrift

## III

Het is mogelijk om vier patiënten onder algemene anesthesie met behulp van één massaspectrometer zonder onderbreking te bewaken.

Dit proefschrift

## IV

Het sturen van de beademing aan de hand van de eind-expiratoire fractionele koolzuurconcentratie, zoals tijdens algemene anesthesie, wordt vergemakkelijkt door gebruik te maken van een langzame beademingsfrequentie.

## V

Bij de nasotracheale intubatie van de neonatus gaat de volgende waarneming praktisch altijd op: "wat door de neus gaat, past in de trachea".

## VI

Een operatie in de achterste schedelgroeve dient bij voorkeur bij een patiënt in liggende houding te worden verricht.

E. Gordon (1975). A basis and practice of neuroanaesthesia, p.186. Excerpta Medica, Amsterdam.

## VII

Het verdient aanbeveling dat iedere anesthesioloog-in-opleiding memoriseert dat de zuurstofvoorziening van het lichaam afhangt van hart-minuutvolume, arteriële hemoglobineconcentratie, arteriële zuurstofsaturatie, en arteriële zuurstofspanning.

## VIII

Opheffen van ongewenste opioïde effecten met behulp van naloxone aan het eind van een algemene anesthesie dient te gebeuren volgens de intraveneuze titratiemethode beschreven door Dirksen. Vóór dit antagoneren is normocarbie vereist, dienen "dampvormige anesthetica" en lachgas voldoende, dus overeenkomstig hun fysische eigenschappen, uitgewassen, en curariforme stoffen op indicatie geantagoneerd te zijn.

R. Dirksen (1980). Tijdschrift voor geneesmiddelenonderzoek, 2/80, p.610.

## IX

Bij de praeoperatieve evaluatie, het peroperatieve anesthesiebeleid, en de postoperatieve behandeling dient men er zich van bewust te zijn dat een patiënt met myotonia dystrophica lijdt aan een aandoening van meerdere orgaansystemen.

## X

In de literatuur aangegeven regels om de verse gasflow in een "low flow" anesthesiesysteem te bepalen zijn slechts vuistregels voor de gemiddelde patiënt en een technisch perfect systeem. Meting van de fractionele concentraties van de gassen en dampen die in dergelijke systemen voorkomen is derhalve noodzakelijk.

## XI

Hardlopend een vlieger oplaten is onpractisch.

## XII

In tegenstelling tot de hele en halve onwaarheden die ons dagelijks door de reclame op de mouw worden gespeld, moet toch worden geconstateerd dat het langer meegaan van vloeibaar Drecht van voordeel bleek tijdens de experimenten van tenminste twee proefschriften.

M. Gielen. Body plethysmography. A comparative study of volume measurements in a constant-volume and a constant-pressure body plethysmograph. Thesis, Nijmegen (1971), p.51.

Dit proefschrift (sectie 5.2.4).

## XIII

Een tevreden mens vergadert niet.

Onbekende Nederlandse zegswijze.

Gelezen bij Prof. Dr G.P. Hoefnagels: "Je zwam te grabbel gooien".

Nijmegen, 4 mei 1984.



